

Two-way coupled meteorology and air quality models in Asia: a systematic review and meta-analysis of impacts of aerosol feedbacks on meteorology and air quality

Chao Gao¹, Aijun Xiu^{1, *}, Xuelei Zhang^{1, *}, Qingqing Tong¹, Hongmei Zhao¹, Shichun Zhang¹, Guangyi Yang^{1, 2}, and Mengduo Zhang^{1, 2}

¹Key Laboratory of Wetland Ecology and Environment, Northeast Institute of Geography and Agroecology, Chinese Academy of Sciences, Changchun, 130102, China

²University of Chinese Academy of Sciences, Beijing, 100049, China

Correspondence to: A.J. Xiu (xiujun@iga.ac.cn) & X.L. Zhang (zhangxuelei@iga.ac.cn)

Abstract

Atmospheric aerosols can exert influence on meteorology and air quality through aerosol-radiation interactions (ARI) and aerosol-cloud interactions (ACI) and this two-way feedback has been studied by applying two-way coupled meteorology and air quality models. As one of regions with high aerosol loading in the world, Asia has attracted many researchers to investigate the aerosol effects with several two-way coupled models (WRF-Chem, WRF-CMAQ, GRAPES-CUACE, WRF-NAQPMS and GATOR-GCMOM) over the last decade. This paper attempts to offer bibliographic analysis regarding the current status of applications of two-way coupled models in Asia, related research focuses, model performances and the effects of ARI or/and ACI on meteorology and air quality. There are total 160 peer-reviewed articles published between 2010 and 2019 in Asia meeting the inclusion criteria, with more than 79 % of papers involving the WRF-Chem model. The number of relevant publications has an upward trend annually and East Asia, India, China, as well as the North China Plain are the most studied areas. The effects of ARI and both ARI and ACI induced by natural aerosols (particularly mineral dust) and anthropogenic aerosols (bulk aerosols, different chemical compositions and aerosols from different sources) are widely investigated in Asia. Through the meta-analysis of surface meteorological and air quality variables simulated by two-way coupled models, the model performance affected by aerosol feedbacks depends on different variables, simulation time lengths, selection of two-way coupled models, and study areas. Future research perspectives with respect to the development, improvement, application, and evaluation of two-way coupled meteorology and air quality models are proposed.

1 Introduction

Atmospheric pollutants can affect local weather and global climate via many mechanisms as extensively summarized in the Intergovernmental Panel on Climate Change (IPCC) reports (IPCC, 2007, 2014, 2021), and also exhibit impacts on human health and ecosystems (Lelieveld et al., 2015; Wu and Zhang, 2018). Atmospheric pollutants can modify the radiation energy balance, thus influence meteorological conditions (Gray et al., 2010; Yiğit et al., 2016). Compared to other climate agents, the short-lived and localized aerosols could induce changes in meteorology and climate through aerosol-radiation interactions (ARI, Tremback et al., 1986; Satheesh and Moorthy, 2005) and aerosol-cloud interactions (ACI, Martin and Leight, 1949; Lohmann and Feichter, 2005) or both (Sud and Walker, 1990; Haywood and Boucher, 2000). ARI (previously known as direct effect and semi-direct effect) are based on scattering and absorbing solar radiation by aerosols as well as cloud dissipation by heating (McCormick and Ludwig, 1967; Ackerman et al., 2000; Koch and Del Genio, 2010; Wilcox, 2012), and ACI (known as indirect effect) are concerned with aerosols altering albedo and lifetime of clouds (Twomey, 1977; Albrecht, 1989; Lohmann and Feichter, 2005). As our knowledge base of aerosol-radiation-cloud interactions that involve extremely complex physical and chemical processes has been expanding, accurately assessing the effects of these interactions still remains a big challenge (Rosenfeld et al., 2008, 2019; Fan et al., 2016; Kuniyal and Guleria, 2019).

The interactions between air pollutants and meteorology can be investigated by observational analyses and/or air quality models. So far, many observational studies using measurement data from a variety of sources have been conducted to analyze these interactions (Wendisch et al., 2002; Bellouin et al., 2008; Groß et al., 2013; Rosenfeld et al., 2019). Yu et al (2006) reviewed research work that adopted satellite and ground-based measurements to estimate the ARI-induced changes of radiative forcing and the associated uncertainties in the analysis. Yoon et al. (2019) analyzed the effects of aerosols on the radiative forcing based on the Aerosol Robotic Network observations and

57 demonstrated that these effects depended on aerosol types. On the other hand, since the uncertainties
58 in ARI estimations were associated with ACI (Kuniyal and Guleria, 2019), the simultaneous
59 assessments of both ARI and ACI effects were needed and had gradually been conducted via satellite
60 observations (Sekiguchi et al., 2003; Quaas et al., 2008; Illingworth et al., 2015; Kant et al., 2019).
61 In the early stages, observational studies of ACI effects were based on several cloud parameters
62 mainly derived from surface-based microwave radiometer (Kim et al., 2003; Liu et al., 2003) and
63 cloud radar (Feingold et al., 2003; Penner et al., 2004). Later on, with the further development of
64 satellite observation technology and enhanced spatial resolution of satellite measurement comparing
65 against traditional ground observations, the satellite-retrieved cloud parameters (effective cloud
66 droplet radius, liquid water path (LWP) and cloud cover) were utilized to identify the ACI effects
67 studies on cloud scale. (Goren and Rosenfeld, 2014; Rosenfeld et al., 2014). Moreover, in order to
68 clarify whether aerosols affect precipitation positively or negatively, the effects of ACI on cloud
69 properties and precipitation were widely investigated but with various answers (Andreae and
70 Rosenfeld, 2008; Rosenfeld et al., 2014; Casazza et al., 2018; Fan et al., 2018). Analyses of satellite
71 and/or ground observations revealed that increased aerosols could suppress (enhance) precipitation
72 in drier (wetter) environments (Rosenfeld, 2000; Rosenfeld et al., 2008; Li et al., 2011b; Donat et
73 al., 2016). Most recently, Rosenfeld et al. (2019) further used satellite-derived cloud information
74 (droplet concentration and updraft velocity at cloud base, LWP at cloud cores, cloud geometrical
75 thickness and cloud fraction) to single out ACI under a certain meteorological condition, and found
76 that the cloudiness change caused by aerosol in marine low-level clouds was much greater than
77 previous analyses (Sato and Suzuki, 2019). Despite the fact that aforementioned studies had
78 significantly improved our understanding of aerosol effects, many limitations still exist, such as low
79 temporal resolution of satellite data, low spatial resolution of ground monitoring sites and lack of
80 vertical distribution information of aerosol and cloud (Yu et al., 2006; Rosenfeld et al., 2014; Sato
81 and Suzuki, 2019).

82 Numerical models can also be used to study the interactions between air pollutants and
83 meteorology. Air quality models simulate physical and chemical processes in the atmosphere (ATM)
84 and are classified as offline and online models (El-Harbawi, 2013). Offline models (also known as
85 traditional air quality models) require outputs from meteorological models to subsequently drive
86 chemical models (Seaman, 2000; Byun and Schere, 2006; ENVIRON, 2008). Comparing to online
87 models, offline models usually are computationally efficient but incapable of capturing two-way
88 feedbacks between chemistry and meteorology (North et al., 2014). Online models or coupled
89 models are designed and developed to consider the two-way feedbacks and attempted to accurately
90 simulate both meteorology and air quality (Grell et al., 2005; Wong et al., 2012; Briant et al., 2017).
91 Two-way coupled models can be generally categorized as integrated and access models based on
92 whether using a coupler to exchange variables between meteorological and chemical modules
93 (Baklanov et al., 2014). As Zhang (2008) pointed out, Jacobson (1994, 1997a) and Jacobson et al.
94 (1996a) pioneered the development of a fully-coupled model named Gas, Aerosol, Transport,
95 Radiation, General Circulation, Mesoscale, and Ocean Model (GATOR-GCMOM) in order to
96 investigate all the processes related to ARI and ACI. Currently, there are three representative two-
97 way coupled meteorology and air quality models, namely the Weather Research and Forecasting-
98 Chemistry (WRF-Chem) (Grell et al., 2005), WRF coupled with Community Multiscale Air Quality
99 (CMAQ) (Wong et al., 2012) and WRF coupled with a multi-scale chemistry-transport model for
100 atmospheric composition analysis and forecast (WRF-CHIMERE) (Briant et al., 2017). The WRF-
101 Chem is an integrated model that includes various chemical modules in the meteorological model
102 (i.e., WRF) without using a coupler. For the remaining two models, which belong to access model,
103 the WRF-CMAQ uses a subroutine called *aqprep* (Wong et al., 2012) as its coupler while the WRF-
104 CHEMERE a general coupling software named Ocean Atmosphere Sea Ice Soil-Model Coupling
105 Toolkit (Craig et al. 2017). With more growing interest in coupled models and their developments,
106 applications and evaluations, two review papers thoroughly summarized the related works published
107 before 2008 (Zhang, 2008) and 2014 (Baklanov et al., 2014). Zhang (2008) overviewed the
108 developments and applications of five coupled models in the United States (US) and the treatments
109 of chemical and physical processes in these coupled models with emphasis on the ACI related
110 processes. Another paper presented a systematic review on the similarities and differences of
111 eighteen integrated or access models in Europe and discussed the descriptions of interactions
112 between meteorological and chemical processes in these models as well as the model evaluation
113 methodologies involved (Baklanov et al., 2014). Some of these coupled models can not only be used

114 to investigate the interactions between air quality and meteorology at regional scales but also at
115 global and hemispheric scales (Jacobson, 2001; Grell et al., 2011; Xing et al., 2015b; Mailler et al.,
116 2017), but large scale studies were not included in the two review papers by Zhang (2008) and
117 Baklanov et al. (2014). These reviews only focused on application and evaluation of coupled models
118 in US and Europe but there is still no systematic review targeting two-way coupled model
119 applications in Asia.

120 Compared to US and Europe, Asia has been suffering more severe air pollution in the past three
121 decades (Bollasina et al., 2011; Rohde and Muller, 2015; Gurjar et al., 2016) due to the rapid
122 industrialization, urbanization and population growth together with unfavorable meteorological
123 conditions (Jeong and Park, 2017; Li et al., 2017a; Lelieveld et al., 2018). Then, the interactions
124 between atmospheric pollution and meteorology in Asia, which have received a lot of attention from
125 scientific community, are investigated using extensive observations and a certain number of
126 numerical simulations (Wang et al., 2010; Li et al., 2016; Nguyen et al., 2019a). Based on airborne,
127 ground-based, and satellite-based observations, multiple important experiments have been carried
128 out to analyze properties of radiation, cloud and aerosols in Asia, as briefly reviewed by Lin et al.
129 (2014b). Recent observational studies confirmed that increasing aerosol loadings play important
130 roles in radiation budget (Eck et al., 2018; Benas et al., 2020), cloud properties (Dahutia et al., 2019;
131 Yang et al., 2019), precipitation intensity along with vertical distributions of precipitation types
132 (Guo et al., 2014, 2018). According to previous observational studies in Southeast Asia (SEA), Tsay
133 et al. (2013) and Lin et al. (2014b) comprehensively summarized the spatiotemporal characteristics
134 of biomass burning (BB) aerosols and clouds as well as their interactions. Li et al. (2016) analyzed
135 how ARI or ACI influenced climate/meteorology in Asia utilizing observations and climate models.
136 With regard to the impacts of aerosols on cloud, precipitation and climate in East Asia (EA), a
137 detailed review of observations and modeling simulations has also been presented by Li et al.
138 (2019c). Since the 2000s, substantial progresses have been made in the climate-air pollution
139 interactions in Asia based on regional climate models simulations, which have been summarized by
140 Li et al. (2016). Moreover, starting from year of 2010, with the development and availability of two-
141 way coupled meteorology and air quality models, more and more modeling studies have been
142 conducted to explore the ARI or/and ACI effects in Asia (Wang et al., 2010, 2014a; Sekiguchi et al.,
143 2018; Nguyen et al., 2019a). In recent studies, a series of WRF-Chem and WRF-CMAQ simulations
144 were performed to assess the consequences of ARI on radiative forcing, planetary boundary layer
145 height (PBLH), precipitation, and fine particulate matter (PM_{2.5}) and ozone concentrations (Wang
146 et al., 2014a; Huang et al., 2016; Sekiguchi et al., 2018; Nguyen et al., 2019b). Different from current
147 released version of WRF-CMAQ model (based on WRF version 4.3 and CMAQ version 5.3.3) that
148 only includes ARI, WRF-Chem with ACI (starting from WRF-Chem version 3.0, Chapman et al.,
149 2009) has been implemented for analyzing the complicated aerosol effects that lead to variations of
150 cloud properties, precipitations and PM_{2.5} concentrations (Zhao et al., 2017; Liu et al., 2018c; Park
151 et al., 2018; Bai et al., 2020). To quantify the individual or joint effects of ARI or/and ACI on
152 meteorological variables and pollutants concentrations, several modeling studies have been
153 performed in Asia (Zhang et al., 2015a, 2018; Ma et al., 2016; Chen et al., 2019a). In addition, model
154 comparisons (including offline and online models) targeting EA have been carried out recently under
155 the Model Inter-Comparison Study for Asia (MICS-Asia) phase III (Gao et al., 2018b; Chen et al.,
156 2019b; Li et al., 2019a). As mentioned above, even though there are already several reviews
157 regarding the observational studies of ARI or/and ACI (Tsay et al., 2013; Lin et al., 2014b; Li et al.,
158 2016, 2019c) it is necessary to conduct a systematic review in Asia focusing on applications of two-
159 way coupled meteorology and air quality models as well as simulated variations of meteorology and
160 air quality induced by aerosol effects.

161 This paper is constructed as follows: Section 2 describes the methodology for literature
162 searching, paper inclusion, and analysis; Section 3 summarizes the basic information about
163 publications as well as developments and applications of coupled models in Asia and Section 4
164 provides the recent overviews of their research points. Sections 5 to 6 present systematic review and
165 meta-analysis of the effects of aerosol feedbacks on model performance, meteorology and air quality
166 in Asia. The summary and perspective are provided in Section 7.

167

168 **2 Methodology**

169 **2.1 Criteria and synthesis**

170 Since 2010, in Asia, regional studies of aerosol effects on meteorology and air quality based

171 on coupled models have been increasing gradually, therefore in this study we performed a systematic
172 search of literatures to identify relevant studies from January 1, 2010 to December 31, 2019. In
173 order to find all the relevant papers in English, Chinese, Japanese and Korean, we deployed several
174 science-based search engines, including Google Scholar, the Web of Science, the China National
175 Knowledge Infrastructure, the Japan Information Platform for S&T Innovation, the Korean Studies
176 Information Service System. The different keywords and their combinations for paper searching are
177 as follows: (1) model-related keywords including “coupled model”, “two-way”, “WRF”, “NU-
178 WRF”, “WRF-Chem”, “CMAQ”, “WRF-CMAQ”, “CAMx”, “CHIMERE”, “WRF-CHIMERE”
179 and “GATOR-GCMOM”; (2) effect-related keywords including “aerosol radiation interaction”,
180 “ARI”, “aerosol cloud interaction”, “ACI”, “aerosol effect” and “aerosol feedback”; (3) air
181 pollution-related keywords including “air quality”, “aerosol”, “PM2.5”, “O3”, “CO”, “SO2”,
182 “NO2”, “dust”, “BC”, “black carbon”, “blown carbon”, “carbonaceous”, “primary pollutants”; (4)
183 meteorology-related keywords including “meteorology”, “radiation”, “wind”, “temperature”,
184 “specific humidity”, “relative humidity”, “planetary boundary layer”, “cloud” and “precipitation”;
185 (5) region-related keywords including “Asia”, “East Asia”, “Northeast Asia”, “South Asia”,
186 “Southeast Asia”, “Far East”, “China”, “India”, “Japan”, “Korea”, “Singapore”, “Thailand”,
187 “Malaysia”, “Nepal”, “North China Plain”, “Yangtze River Delta”, “Pearl River Delta”, “middle
188 reaches of the Yangtze River”, “Sichuan Basin”, “Guanzhong Plain”, “Northeast China”,
189 “Northwest China”, “East China”, “Tibet Plateau”, “Taiwan”, “northern Indian”, “southern Indian”,
190 “Gangetic Basin”, “Kathmandu Valley”.

191 After applying the search engines and the keywords combinations mentioned above, we found
192 946 relevant papers. In order to identify which paper should be included or excluded in this paper,
193 following criteria were applied: (1) duplicate literatures were deleted; (2) studies of using coupled
194 models in Asia with aerosol feedbacks turned on were included, and observational studies of aerosol
195 effects were excluded; (3) publications involving coupled climate model were excluded. According
196 to these criteria, not only regional studies, but also studies using the coupled models at global or
197 hemispheric scales involving Asia or its subregions were included. Then, we carefully examined all
198 the included papers and further checked the listed reference in each paper to make sure that no
199 related paper was neglected. A flowchart that illustrated the detailed procedures applied for article
200 identification is presented in Appendix Figure A1 (Note: Although the deadline for literature
201 searching is 2019, any literature published in 2020 is also included.). There was a total of 160
202 publications included in our study.

204 2.2 Analysis method

205 To summarize the current status of coupled models applied in Asia and quantitatively analyze
206 the effects of aerosol feedbacks on model performance as well as meteorology and air quality, we
207 carried out a series of analyses based on data extracted from the selected papers. We firstly compiled
208 the publication information of the included papers as well as the information regarding model name,
209 simulated time period, study region, simulation design, and aerosol effects. Secondly, we
210 summarized the important findings of two-way coupled model applications in Asia according to
211 different aerosol sources and components to clearly acquire what are the major research focuses in
212 past studies. Finally, we gathered all the simulated results of meteorological and air quality variables
213 with/without aerosol effects and their statistical indices (SI). For questionable results, the quality
214 assurance was conducted after personal communications with original authors to decide whether
215 they were deleted and/or corrected. All the extracted publication and statistical information were
216 exported into an Excel file, which was provided in Table S1. Moreover, we performed quantitative
217 analyses of the effects of aerosol feedbacks through following steps. (1) We discussed whether
218 meteorological and air quality variables were overestimated or underestimated based on their SI.
219 Then, variations of the SI of these variables were further analyzed in detail with/without turning on ARI
220 or/and ACI in two-way coupled models. (2) We investigated the SI of simulation results at different
221 simulation time lengths and spatial resolutions in coupled models. (3) More detailed inter-model
222 comparisons of model performance based on the compiled SI among different coupled models are
223 conducted. (4) Differences in simulation results with/without aerosol feedbacks were grouped by study
224 regions and time scales (yearly, seasonal, monthly, daily and hourly). Toward a better understanding
225 of the complicated interactions between air quality and meteorology in Asia, the results sections in
226 this paper are organized following above analysis methods (1) - (3) and represented in Section 5,
227 and the results following method (4) were represented in Section 6. In addition, Excel and Python

228 were used to conduct data processing and plotting in this study.

229

230 3 Basic overview

231 3.1 Summary of applications of coupled models in Asia

232 A total of 160 articles were selected according to the inclusion criteria, and their basic
233 information was compiled in Table 1. In Asia, five two-way coupled models are applied to study the
234 ARI and ACI effects. These include GATOR-GCMOM, two commonly used models, i.e., WRF-
235 Chem and WRF-CMAQ, and two locally developed models, i.e., the global-regional assimilation
236 and prediction system coupled with the Chinese Unified Atmospheric Chemistry Environment
237 forecasting system (GRAPES-CUACE) and WRF coupled with nested air-quality prediction
238 modeling system (WRF-NAQPMS). 127 out of total 160 papers involved the applications of WRF-
239 Chem in Asia since its two-way coupled version was publicly available in 2006 (Fast et al., 2006).
240 WRF-CMAQ was applied in only 16 studies due to its later initial release in 2012 (Wong et al.,
241 2012). GRAPES-CUACE was developed by the China Meteorological Administration and
242 introduced in details in Zhou et al. (2008, 2012, 2016), then firstly utilized in Wang et al. (2010) to
243 estimate impacts of aerosol feedbacks on meteorology and dust cycle in EA. The coupled version
244 of WRF-NAQPMS was developed by the Institute of Atmospheric Physics, Chinese Academy of
245 Sciences and could improve the prediction accuracy of haze pollution in the North China Plain (NCP)
246 (Wang et al., 2014c). Note that GRAPES-CUACE and WRF-NAQPMS were only applied in China.
247 There were only three published papers about the applications of GATOR-GCMOM in Northeast
248 Asia (NEA), NCP and India. In the included papers, 93, 33, 31 studies targeted various areas in
249 China, EA and India, respectively. There were 79 papers regarding effects of ARI (7 health), 63 both
250 ARI and ACI (1 health) and 18 ACI. ACI studies were much less than ARI related ones, which
251 indicated that ACI related studies need to be paid with more attention in the future. Considering that
252 the choices of cloud microphysics and radiation schemes can affect coupled models' results (Baró
253 et al., 2015; Jimenez et al., 2016), these schemes used in the selected studies were also summarized
254 in Table 1. This table presents a concise overview of coupled models' applications in Asia with the
255 purpose of providing basic information regarding models, study periods and areas, aerosol effects,
256 scheme selections, and reference. More complete information is summarized Table S1 including
257 model version, horizontal resolution, vertical layer, aerosol and gas phase chemical mechanisms,
258 photolysis rate, PBL, land surface, surface layer, cumulus, urban canopy schemes, meteorological
259 initial and boundary conditions (ICs and BCs), chemical ICs and BCs, spin-up time, and
260 anthropogenic natural emissions.

261 It should be noted that in Table 1 there were four model inter-comparison studies that aimed at
262 evaluating model performance, identifying error sources and uncertainties, and providing optimal
263 model setups. By comparing simulations from two coupled models (WRF-Chem and Spectral
264 Radiation-Transport Model for Aerosol Species) (Takemura et al., 2003) in India (Govardhan et al.,
265 2016), it was found that the spatial distributions of various aerosol species (black carbon (BC),
266 mineral dust and sea salt) were similar with the two models. Based on the intercomparisons of WRF-
267 Chem simulations in different areas, Yang et al. (2017) revealed that aerosol feedbacks could
268 enhance PM_{2.5} concentrations in the Indo-Gangetic Plain but suppress the concentrations in the
269 Tibetan Plateau (TP). Targeting China and India, Gao et al. (2018c) also applied the WRF-Chem
270 model to quantify the contributions of different emission sectors to aerosol radiative forcings,
271 suggesting that reducing the uncertainties in emission inventories were critical, especially for India.
272 Moreover, for the NCP region, Gao et al. (2018b) presented a comparison study with multiple online
273 models under the MICS-Asia Phase III and pointed out noticeable discrepancies in the simulated
274 secondary inorganic aerosols under heavy haze conditions and the importance of accurate wind
275 speed at 10 meters above surface (WS10) predictions by these models. Comprehensive comparative
276 studies for Asia have been emerging lately but are still limited, comparing to those for North
277 America and Europe, such as the Air Quality Model Evaluation International Initiative Phase II
278 (Brunner et al., 2015; Campbell et al., 2015; Im et al., 2015a, b; Kong et al., 2015; Makar et al.,
279 2015a, b; Wang et al., 2015b; Forkel et al., 2016).

280

281 Table 1. Basic information of coupled model applications in Asia during 2010-2019.

No.	Model	Study period	Region	Aerosol effect	Short/long-wave radiation scheme	Microphysics scheme	Reference
1	WRF-Chem	2013	India	ARI	Dudhia/RRTM	Thompson	Singh et al. (2020)*

2	WRF-Chem	12/2015	India	ARI	Goddard/RRTM	Lin	Bharali et al. (2019)
3	WRF-Chem	10/13/2016 to 11/20/2016	India	ARI	RRTMG	†	Shahid et al. (2019)
4	WRF-Chem	12/27/2017 to 12/30/2017	NCP	ARI	RRTMG	Lin	Wang et al. (2019a)
5	WRF-Chem	12/05/2015 to 01/04/2016	NCP	ARI	Goddard	WSM 6-class graupel	Wu et al. (2019a)
6	WRF-Chem	12/05/2015 to 01/04/2016	NCP	ARI	Goddard	WSM 6-class graupel	Wu et al. (2019b)
7	WRF-Chem	06/01/2006 to 12/31/2011	NWC	ARI	RRTMG	Morrison	Yuan et al. (2019)
8	WRF-Chem	07/2016, 10/2016, 01/2017, 04/2017	NCP	ARI	Goddard/RRTM	Lin	Zhang et al. (2019)
9	WRF-Chem	02/17/2014 to 02/26/2014, 10/21/2014 to 10/25/2014, 11/05/2014 to 11/11/2014, 12/18/2015 to 12/24/2015	NCP	ARI	RRTMG	Morrison	Zhou et al. (2019)
10	WRF-Chem	03/15/2012 to 03/25/2012	WA	ARI	RRTMG	Morrison	Bran et al. (2018)
11	WRF-Chem	2013	China & India	ARI	RRTMG	Lin	Gao et al. (2018bc)
12	WRF-Chem	05/01/2007 to 05/07/2007	CA	ARI	RRTM	Lin	Li and Sokolik (2018)
13	WRF-Chem	06/02/2012 to 06/15/2012	YRD	ARI	RRTMG	Lin	Li et al. (2018b)
14	WRF-Chem	12/15/2016 to 12/21/2016	NCP	ARI	RRTMG	Morrison	Liu et al. (2018b)
15	WRF-Chem	11/30/2016 to 12/04/2016	NCP	ARI	RRTMG	Lin	Miao et al. (2018)
16	WRF-Chem	2010	India	ARI	RRTMG	Morrison	Soni et al. (2018)
17	WRF-Chem	01/01/2013 to 01/31/2013	NCP	ARI	Goddard/RRTM	Lin	Wang et al. (2018c)
18	WRF-Chem	12/2013	EC	ARI	RRTMG	Lin	Wang et al. (2018d)
19	WRF-Chem	2013	TP	ARI	RRTMG	Morrison	Yang et al. (2018)
20	WRF-Chem	03/11/2015 to 03/26/2015	EA	ARI	RRTMG	Lin	Zhou et al. (2018)
21	WRF-Chem	01/2013	EC	ARI	RRTMG	Lin	Gao et al. (2017b)
22	WRF-Chem	10/15/2015 to 10/17/2015	YRD	ARI	Goddard/RRTM	Lin	Li et al. (2017b)
23	WRF-Chem	03/16/2014 to 03/18/2014	YRD	ARI	RRTMG	Lin	Li et al. (2017c)
24	WRF-Chem	02/21/2014 to 02/27/2014	NCP	ARI	RRTMG	Lin	Qiu et al. (2017)
25	WRF-Chem	07/21/2012	NCP	ARI	RRTMG	Lin	Yang and Liu (2017a)
26	WRF-Chem	07/21/2012	NCP	ARI	RRTMG	Lin	Yang and Liu (2017b)
27	WRF-Chem	05/30/2013 to 06/27/2013	EC	ARI	RRTMG	Lin	Yao et al. (2017)
28	WRF-Chem	11/15/2013 to 12/30/2013	SEC	ARI	RRTMG	Lin	Zhan et al. (2017)
29	WRF-Chem	03/2012	India	ARI	RRTMG	Thompson	Feng et al. (2016)
30	WRF-Chem	1960-2010	NCP	ARI	Goddard/RRTM	Lin	Gao et al. (2016b)
31	WRF-Chem	04/2011	NCP	ARI	RRTMG	Single-Moment 5-class	Liu et al. (2016a)
32	WRF-Chem	01/2008, 04/2008, 07/2008, 10/2008	EA	ARI	Goddard/RRTM	Lin	Liu et al. (2016b)
33	WRF-Chem	09/21/2011 to 09/23/2011	NCP	ARI	RRTMG	Lin	Miao et al. (2016)
34	WRF-Chem	03/2005	EA	ARI	Goddard/RRTM	Morrison	Wang et al. (2016)
35	WRF-Chem	06/23/2008 to 07/20/2008	NWC	ARI	RRTMG	Morrison	Yang et al. (2016)
36	WRF-Chem	01/2007, 04/2007, 07/2007, 10/2007	EA	ARI	RRTM	Lin	Zhong et al. (2016)
37	WRF-Chem	05/2011, 10/2011	India	ARI	RRTMG	Thompson	Govardhan et al. (2015)
38	WRF-Chem	2006	China	ARI	RRTMG	Lin	Huang et al. (2015)
39	WRF-Chem	2007 to 2011	EA	ARI	Goddard/RRTM	Lin	Chen et al. (2014)
40	WRF-Chem	11/2007 to 12/2008	EA	ARI	RRTMG	Lin	Gao et al. (2014)
41	WRF-Chem	10/2006	SEA	ARI	RRTM	Lin	Ge et al. (2014)
42	WRF-Chem	04/17/2010 to 04/22/2010	India	ARI	RRTM	Thompson	Kumar et al. (2014)
43	WRF-Chem	01/11/2013 to 01/14/2013	NCP	ARI	Goddard/RRTM	Lin	Li and Liao (2014)
44	WRF-Chem	03/15/2008 to 03/18/2008	EA	ARI	RRTMG	Morrison	Lin et al. (2014a)
45	WRF-Chem	07/21/2006 to 07/30/2006	NWC	ARI	RRTMG	Morrison	Chen et al. (2013)

46	WRF-Chem	05/12/2009 to 05/22/2009	India	ARI	Goddard/RRTM	Milbrandt-Yau	Dipu et al. (2013)
47	WRF-Chem	2008	India	ARI	Goddard/RRTM	Thompson	Kumar et al. (2012a)
48	WRF-Chem	2008	India	ARI	Goddard/RRTM	Thompson	Kumar et al. (2012b)
49	WRF-Chem	1999	India	ARI	Goddard/*	Lin	Seethala et al. (2011)
50	WRF-Chem	2006	China	ARI	†	†	Zhuang et al. (2011)
51	WRF-Chem	12/14/2013 to 12/16/2013	PRD	ARI & ACI	RRTMG	Morrison	Liu et al. (2020)*
52	WRF-Chem	11/30/2009 to 12/01//2009	NCP	ARI & ACI	Goddard/RRTM	Morrison	Jia et al. (2019)
53	WRF-Chem	11/25/2013 to 12/26/2013	EC	ARI & ACI	RRTMG	Lin	Wang et al. (2019b)
54	WRF-Chem	01/2014	China	ARI & ACI	RRTMG	Morrison	Archer-Nicholls et al. (2019)
55	WRF-Chem	12/01/2016 to 12/09/2016, 12/19/2016 to 12/24/2016	YRD	ARI & ACI	RRTMG	Lin	Li et al. (2019b)
56	WRF-Chem	05/06/2013 to 20/06/2013 & 24/08/2014 to 08/09/2014	India	ARI & ACI	RRTM	Lin	Kedia et al. (2019a)
57	WRF-Chem	06/2010 to 09/2010	India	ARI & ACI	RRTM	Lin, Morrison, Thompson	Kedia et al. (2019b)
58	WRF-Chem	04/2013	PRD	ARI & ACI	RRTMG	Lin	Huang et al. (2019)
59	WRF-Chem	11/30/2013 to 12/10/2013	EC	ARI & ACI	RRTMG	Morrison	Ding et al. (2019)
60	WRF-Chem	12/01/2015	NCP	ARI & ACI	RRTMG	Lin	Chen et al. (2019a)
61	WRF-Chem	04/12/2015 to 27/12/2015	EA	ARI & ACI	Goddard	WSM 6-class graupel	An et al. (2019)
62	WRF-Chem	06/2015 to 02/2016	MRYR	ARI & ACI	Goddard/RRTM	WSM 6-class graupel	Liu et al. (2018a)
63	WRF-Chem	06/2008, 06/2009, 06/2010, 06/2011, 06,2012	PRD	ARI & ACI	RRTMG	Morrison	Liu et al. (2018c)
64	WRF-Chem	01/2014, 04/2014, 07/2014, 10/2014	China	ARI & ACI	RRTMG	Lin	Zhang et al. (2018)
65	WRF-Chem	10/01/2015 to 10/26/2015	YRD	ARI & ACI	RRTMG	Lin	Gao et al. (2018a)
66	WRF-Chem	2001, 2006, 2011	EA	ARI & ACI	RRTMG	Morrison	Zhang et al. (2017)
67	WRF-Chem	06/01/2011 to 06/06/2011	EC	ARI & ACI	Goddard/RRTM	Lin	Wu et al. (2017)
68	WRF-Chem	11/27/2013 to 12/12/2013	YRD	ARI & ACI	Goddard/RRTM	Single-Moment 5-class	Sun et al. (2017)
69	WRF-Chem	2005 & 2009	YRD	ARI & ACI	RRTMG	Morrison	Zhong et al. (2017)
70	WRF-Chem	01/2013	NCP	ARI & ACI	Goddard/RRTM	Lin	Gao et al. (2017a)
71	WRF-Chem	11/05/2014 to 11/11/2014	NCP	ARI & ACI	Goddard/RRTM	Lin	Gao et al. (2017c)
72	WRF-Chem	01/2010, 07/2010	China	ARI & ACI	†	†	Ma and Wen (2017)
73	WRF-Chem	06/01/2008 to 07/05/2008	India	ARI & ACI	†	†	Lau et al. (2017)
74	WRF-Chem	01/2013	NCP	ARI & ACI	Goddard/RRTM	Morrison	Kajino et al. (2017)
75	WRF-Chem	03/01/2009 to 03/31/2009	TP & India	ARI & ACI	RRTMG	Morrison	Yang et al. (2017)
76	WRF-Chem	2001, 2006, 2011	EA	ARI & ACI	RRTMG	Morrison	He et al. (2017)
77	WRF-Chem	05/2008 to 08/2008	YRD	ARI & ACI	†	†	Campbell et al. (2017)
78	WRF-Chem	01/2006, 04/2006, 07/2006, 10/2006	China	ARI & ACI	Goddard/RRTM	Lin	Ma et al. (2016)
79	WRF-Chem	01/2005, 04/2005, 07/2005, 10/2005	EC	ARI & ACI	Goddard/RRTM	Lin	Zhang et al. (2016a)
80	WRF-Chem	01/2005, 04/2005, 07/2005, 10/2005	EC	ARI & ACI	Goddard/RRTM	Lin	Zhang et al. (2016b)
81	WRF-Chem	12/07/2013 to 12/09/2013	EC	ARI & ACI	Goddard/RRTM	Morrison	Zhang et al. (2016c)
82	WRF-Chem	06/2012	EC	ARI & ACI	RRTMG	Lin	Huang et al. (2016)
83	WRF-Chem	01/2010, 07/2010	YRD	ARI & ACI	Goddard/RRTM	Lin	Xie et al. (2016)
84	WRF-Chem	11/12/2012 to 11/16/2012, 11/02/2013 to 11/06/2013	India	ARI & ACI	Goddard/RRTM	Lin	Srinivas et al. (2016)
85	WRF-Chem	07/2010	India	ARI & ACI	RRTMG	Lin	Kedia et al. (2016)
86	WRF-Chem	05/20/2008 to 08/31/2015	India	ARI & ACI	Goddard/RRTM	Lin	Jin et al. (2016a)
87	WRF-Chem	05/20/2008 to 08/31/2015	India	ARI & ACI	Goddard/RRTM	Lin	Jin et al. (2016b)
88	WRF-Chem	01/2010	NCP	ARI & ACI	Goddard/RRTM	Lin	Gao et al. (2016a)
89	WRF-Chem	01/05/2008 to 01/09/2008	NCP	ARI & ACI	RRTMG	Lin	Gao et al. (2016c)

90	WRF-Chem	12/2013	EC	ARI & ACI	RRTMG	Lin	Ding et al. (2016)
91	WRF-Chem	02/15/2013 to 02/17/2013	NCP	ARI & ACI	Goddard/RRTM	†	Yang et al. (2015)
92	WRF-Chem	01/2010, 04/2010, 07/2010, 10/2010	NCP	ARI & ACI	Goddard/RRTM	Lin	Shen et al. (2015)
93	WRF-Chem	2006 & 2011	EA	ARI & ACI	RRTMG	Morrison	Zhang et al. (2015d)
94	WRF-Chem	2006 & 2011	EA	ARI & ACI	RRTMG	Morrison	Chen et al. (2015b)
95	WRF-Chem	06/27/2008 to 06/28/2008	NCP	ARI & ACI	RRTM	Lin	Zhong et al. (2015)
96	WRF-Chem	05/20/2008 to 08/31/2015	India	ARI & ACI	Goddard/RRTM	Lin	Jin et al. (2015)
97	WRF-Chem	03/2005, 04/2005, 05/2005	India	ARI & ACI	Goddard/RRTM	Thompson	Jena et al. (2015)
98	WRF-Chem	01/02/2013 to 01/26/2013	NCP	ARI & ACI	RRTMG	Morrison	Gao et al. (2015b)
99	WRF-Chem	07/08/2013 to 07/09/2013	SWC	ARI & ACI	RRTMG	†	Fan et al. (2015)
100	WRF-Chem	01/2010, 04/2010, 07/2010, 10/2010	NCP	ARI & ACI	Goddard/RRTM	Lin	Chen et al. (2015a)
101	WRF-Chem	01/2013	EC	ARI & ACI	Goddard/RRTM	Lin	Zhang et al. (2015a)
102	WRF-Chem	2006 & 2007	EA	ARI & ACI	Goddard/†	Lin	Wu et al. (2013)
103	WRF-Chem	09/27/2010 to 10/22/2010	India	ARI & ACI	Goddard/RRTM	Lin	Beig et al. (2013)
104	WRF-Chem	12/1/2009	NCP	ARI & ACI	Goddard/RRTM	Lin	Jia and Guo, (2012)
105	WRF-Chem	01/2001, 07/2001	EA	ARI & ACI	Goddard/RRTM	Lin	Zhang et al. (2012)
106	WRF-Chem	11/10/2007 to 01/01/2008	China	ARI & ACI	RRTMG	Lin	Gao et al. (2012)
107	WRF-Chem	06/18/2018 to 06/19/2018	MRYR	ACI	Goddard/RRTM	†	Bai et al. (2020)*
108	WRF-Chem	06/07/2017 to 06/12/2017	YRD	ACI	RRTMG	Morrison	Liu et al. (2019)
109	WRF-Chem	03/2010 to 05/2010	EA	ACI	RRTMG	Morrison	Wang et al. (2018b)
110	WRF-Chem	03/09/2012 to 04/30/2012	EA	ACI	RRTMG	Thompson	Su and Fung (2018a)
111	WRF-Chem	03/09/2012 to 04/30/2012	EA	ACI	RRTMG	Thompson	Su and Fung (2018b)
112	WRF-Chem	05/18/2015 to 06/13/2015	NEA	ACI	RRTMG	Morrison	Park et al. (2018)
113	WRF-Chem	08/2008	EC	ACI	RRTMG	Lin	Gao and Zhang (2018)
114	WRF-Chem	10/03/2013 to 10/07/2013	SEC	ACI	RRTMG	Morrison	Shen et al. (2017)
115	WRF-Chem	01/2013, 07/2013	China	ACI	Fu-Liou-Gu	Morrison	Zhao et al. (2017)
116	WRF-Chem	06/04/2004 to 07/10/2004	India	ACI	Goddard	Lin	Bhattacharya et al. (2017)
117	WRF-Chem	09/20/2013 to 09/23/2013	PRD	ACI	RRTMG	Lin	Jiang et al. (2016)
118	WRF-Chem	2005 & 2010	EA	ACI	RRTMG	Morrison	Zhang et al. (2015c)
119	WRF-Chem	08/20/2009 to 08/29/2008	India	ACI	Goddard/RRTM	Morrison	Sarangi et al. (2015)
120	WRF-Chem	01/2001, 04/2001, 07/2001, 10/2001, 01/2005, 04/2005, 07/2005, 10/2005, 01/2008, 04/2008, 07/2008, 10/2008	EA	ACI	†	†	Zhang et al. (2014b)
121	WRF-Chem	07/2008	EC	ACI	RRTMG	Morrison	Lin et al. (2014a)
122	WRF-Chem	1980 to 2010	SEC	ACI	†	†	Bennartz et al. (2011)
123	WRF-Chem	2008 & 2050	China	ARI (Health)	†	†	Zhong et al. (2019)
124	WRF-Chem	2014	India	ARI (Health)	RRTM	Thompson	Conibear et al. (2018a)
125	WRF-Chem	2015 & 2050	India	ARI (Health)	RRTM	Thompson	Conibear et al. (2018b)
126	WRF-Chem	2011	India	ARI (Health)	Goddard/RRTM	Thompson	Ghude et al. (2016)
127	WRF-Chem	2013	NCP	ARI (Health)	RRTMG	†	Gao et al. (2015a)
128	WRF-CMAQ	03/2006 & 04/2006 to 03/2010 & 04/2010	EA	ARI	†	†	Dong et al. (2019)
129	WRF-CMAQ	04/10/2016 to 06/19/2016	NEA	ARI	RRTMG	Single-Moment 3-class	Jung et al. (2019)
130	WRF-CMAQ	2014	EA	ARI	RRTMG	Morrison	Nguyen et al. (2019a)
131	WRF-CMAQ	2014	SEA	ARI	RRTMG	Morrison	Nguyen et al. (2019b)
132	WRF-CMAQ	02/2015	NEA	ARI	RRTMG	Single-Moment 5-class	Yoo et al. (2019)
133	WRF-CMAQ	01/2014, 02/2014, 03/2014	EA	ARI	RRTMG	Morrison	Sekiguchi et al. (2018)

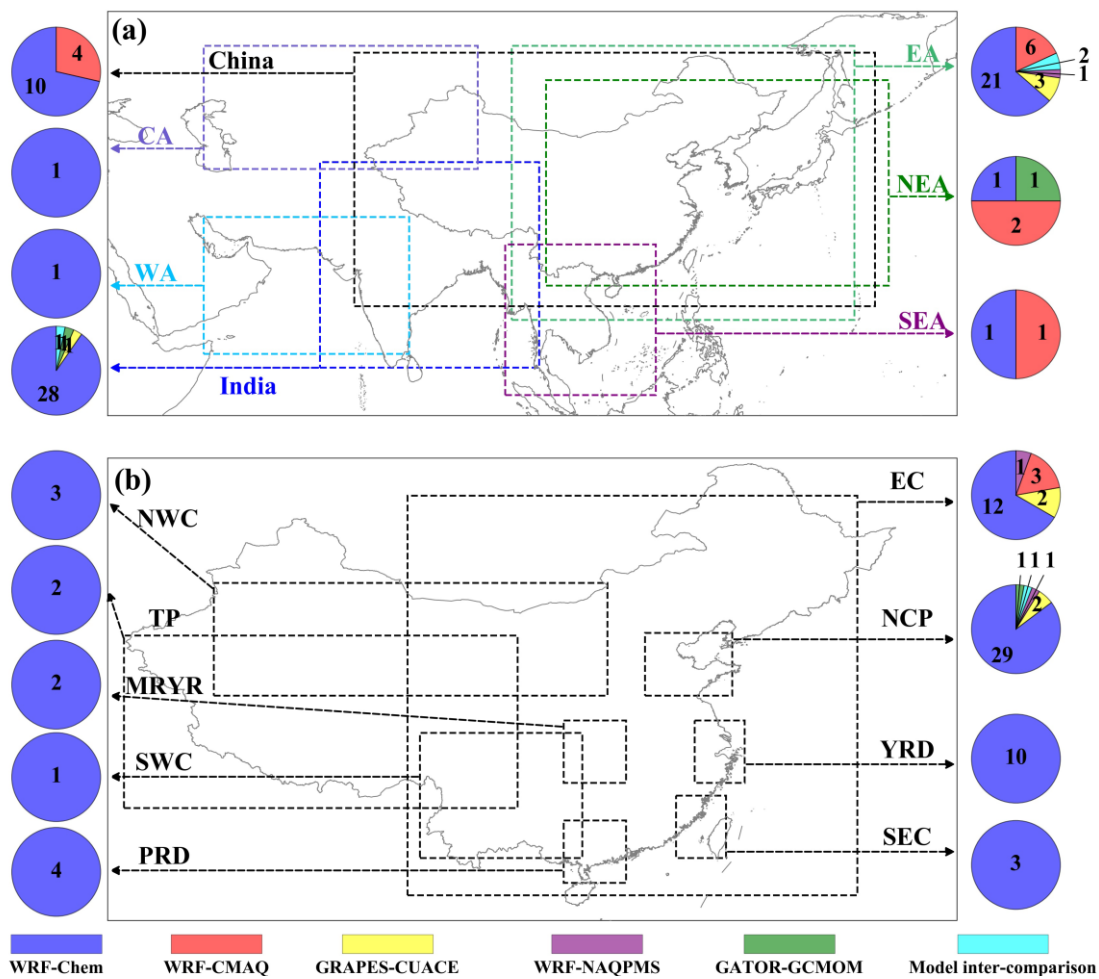
134	WRF-CMAQ	2006 to 2010, 2013	EA	ARI	RRTMG	Morrison	Hong et al. (2017)
135	WRF-CMAQ	01/2013, 07/2013	China	ARI	RRTMG	Morrison	Xing et al. (2017)
136	WRF-CMAQ	1990 to 2010	EA	ARI	RRTMG	Morrison	Xing et al. (2016)
137	WRF-CMAQ	1990 to 2010	EC	ARI	RRTMG	Morrison	Xing et al. (2015a)
138	WRF-CMAQ	1990 to 2010	EC	ARI	RRTMG	Morrison	Xing et al. (2015b)
139	WRF-CMAQ	1990 to 2010	EC	ARI	RRTMG	Morrison	Xing et al. (2015c)
140	WRF-CMAQ	01/2013	China	ARI	RRTMG	Morrison	Wang et al. (2014a)
141	WRF-CMAQ	01/2013, 04/2013, 07/2013, 10/2013	China	ACI	RRTMG	Morrison	Chang (2018)
142	WRF-CMAQ	2050	China	ARI (Health)	RRTMG	Morrison	Hong et al. (2019)
143	WRF-CMAQ	1990 to 2010	EA & India	ARI (Health)	RRTMG	Morrison	Wang et al. (2017)
144	GRAPES-CUACE	12/15/2016 to 12/24/2016	NCP	ARI	Goddard	†	Wang et al. (2018a)
145	GRAPES-CUACE	07/07/2008 to 07/11/2008	EC	ARI	CLIRAD	†	Wang et al. (2015a)
146	GRAPES-CUACE	04/26/2006	EA	ARI	Goddard/†	†	Wang and Niu (2013)
147	GRAPES-CUACE	04/26/2006	EA	ARI	Goddard/†	†	Wang et al. (2013)
148	GRAPES-CUACE	07/13/2008 to 07/31/2008	NCP	ARI	†	†	Zhou et al. (2012)
149	GRAPES-CUACE	04/26/2006	EA	ARI	Goddard/†	†	Wang et al. (2010)
150	GRAPES-CUACE	01/2013	EC	ACI	†	Single-Moment 6-class	Zhou et al. (2016)
151	WRF-NAQPMS	2013	EA	ARI	†	†	Li et al. (2018a)
152	WRF-NAQPMS	09/27/2013 to 10/01/2013	NCP	ARI	Goddard/RRTM	Lin	Wang et al. (2014b)
153	WRF-NAQPMS	01/01/2013	EC	ARI	Goddard/RRTM	Lin	Wang et al. (2014c)
154	GATOR-GCMOM	2000 & 2009	NEA	ARI & ACI	†	†	Ten Hoeve and Jacobson, 2012
155	GATOR-GCMOM	2002 & 2009	India	ARI & ACI	†	†	Jacobson et al. (2019)
156	GATOR-GCMOM	2000 & 2009	NCP	ARI & ACI	†	†	Jacobson et al. (2015)
157	Multi-model comparison	†	EA	ARI & ACI	†	†	Chen et al. (2019b)
158	Multi-model comparison	2010	EA	ARI & ACI	†	†	Li et al., (2019a)
159	Multi-model comparison	01/2010	NCP	ARI & ACI	†	†	Gao et al. (2018b)
160	Multi-model comparison	05/2011	India	ARI & ACI	†	†	Govardhan et al. (2016)

†: Unclear; *: A preprint version of this study was available online on October 31, 2019, and was formally published on January 1, 2020. (EA: East Asia, NEA: Northeast Asia, SEA: Southeast Asia, EC: East China, NCP: North China Plain, YRD: Yangtze River Delta, SEC: Southeast China, NWC: Northwest China, TP: Tibetan Plateau, MRYR: middle reaches of the Yangtze River, SWC: Southwest China; PRD: Pearl River Delta).

3.2 Spatiotemporal distribution of publications

To gain an overall understanding of applications of coupled models in Asia, the spatial distributions of study areas of the selected literatures and the temporal variations of the annual publication numbers were extracted from Table 1 and summarized. Figure 1 illustrates the spatial distributions of study regions as well as the number of papers involving coupled models in Asia (Fig. 1a) and China (Fig. 1b). In this figure, the color and number in the pie charts represent individual (WRF-Chem, WRF-CMAQ, GRAPES-CUACE, WRF-NAQPMS, and GATOR-GCMOM) or multiple coupled models and the quantity of corresponding articles, respectively. At subregional scales, most studies targeted EA where high anthropogenic aerosol loading occurred in recent decades, mainly using WRF-Chem and WRF-CMAQ (Fig. 1a). For other subregions, such as NEA, SEA, Central Asia (CA), and West Asia (WA), there were rather limited research activities taking into account aerosol feedbacks with two-way coupled models. National scale applications of two-way coupled models targeted mostly modeling domains covering India and China but much less work were carried out in other countries, such as Japan and Korea, where air pollution levels are much lower. With respect to various areas in China (Fig. 1b), the research activities concentrated mostly in NCP and secondly in the East China (EC), then in the Yangtze River Delta (YRD) and Pearl River Delta (PRD) areas. WRF-Chem was the most popular model applied in all areas, but

304 there were a few applications of GPRAPES-CUACE and WRF-NAQPMS in EC and NCP.
 305 Figure 2 depicts the temporal variations of research activities with two-way coupled models in
 306 Asia over the period of 2010 to 2019. The total number of papers related to two-way coupled models
 307 had an obvious upward trend in the past decade. Prior to 2014, applications of two-way coupled
 308 models in Asia were scarce, with about 1 to 6 publications per year. A noticeable increase of research
 309 activities emerged starting from 2014 and the growth was rapid from 2014 to 2016, at a rate of 7-9
 310 more papers per year, especially in China. It could be related to the Action Plan on Prevention and
 311 Control of Atmospheric Pollution (2013-2017) implemented by the Chinese government. The
 312 growth was rather flat during 2016-2018 before reaching a peak of 31 articles in 2019. In addition,
 313 the pie charts in Fig. 2 indicates that modeling activities had been picking up with a diversified
 314 pattern in study domain from 2010 to 2019. The modeling domains extended from EA to China and
 315 India and then several subregions in Asia and various areas in China. For EA and India, investigations of aerosol feedbacks based on two-way coupled models rose from 1-2 papers per year during 2010-2013 to 4-8 during 2014-2019. Since 2014, most model simulations were carried out towards areas with severe air pollution in China, especially the NCP area where attracted 5-7 publications per year.



321
 322
 323 Figure 1. The spatial distributions of study domains as well as the two-way coupled modeling publication numbers
 324 in different subregions or countries of Asia (a) and areas of China (b). (EA: East Asia, NEA: Northeast Asia, SEA:
 325 Southeast Asia, EC: East China, NCP: North China Plain, YRD: Yangtze River Delta, SEC: Southeast China, NWC:
 326 Northwest China, TP: Tibetan Plateau, MRYS: middle reaches of the Yangtze River, SWC: Southwest China; PRD:
 327 Pearl River Delta).

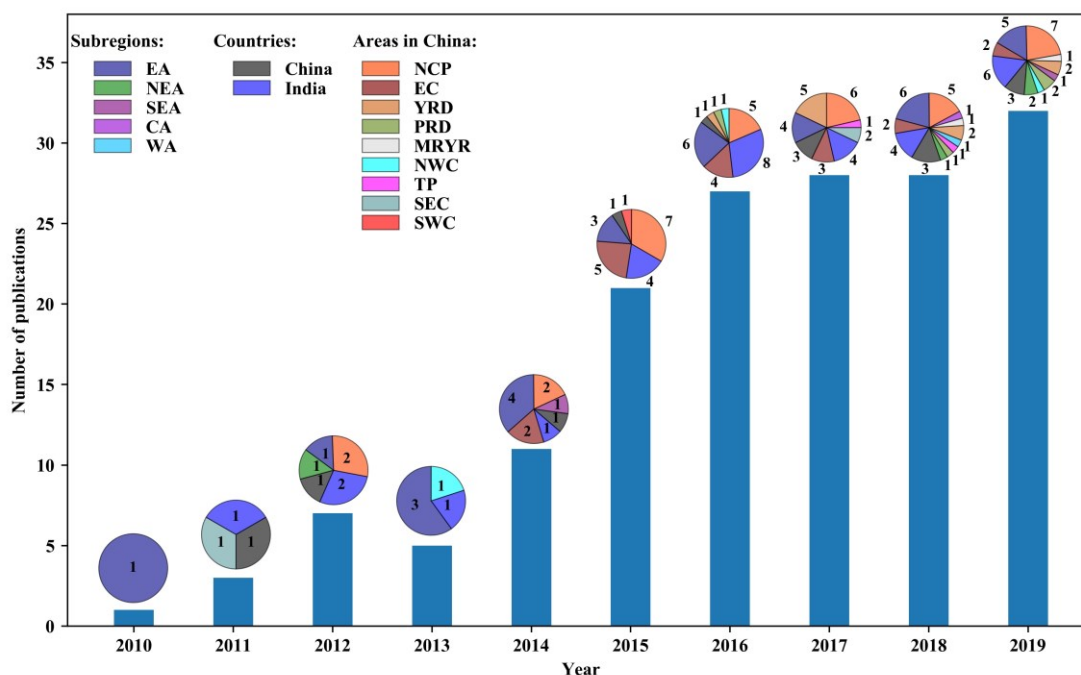


Figure 2. The temporal variations of study activities adopting two-way coupled models in Asia during 2010-2019. (EA: East Asia, NEA: Northeast Asia, SEA: Southeast Asia, EC: East China, NCP: North China Plain, YRD: Yangtze River Delta, SEC: Southeast China, NWC: Northwest China, TP: Tibetan Plateau, MRYS: middle reaches of the Yangtze River, SWC: Southwest China; PRD: Pearl River Delta).

3.3 Summary of modeling methodologies

The physiochemical processes involved with ARI and ACI are sophisticated in actual conditions of atmospheric environment but their representations in two-way coupled models can be rather different. Also, simulation results depend on how these models are configured and set up. Therefore, the treatments of aerosol and cloud microphysics, and aerosol-radiation-cloud interactions in WRF-Chem, WRF-CMAQ, GRAPES-CUACE, WRF-NAQPMS and GATOR-GCMOM applied in Asia, as well as the various aspects of how the modeling studies being set up in the selected papers are summarized in Tables 2-5, respectively, and outlined in this section.

Aerosol microphysics processes consist of particle nucleation, coagulation, condensation/evaporation, gas/particle mass transfer, inorganic aerosol thermodynamic equilibrium, aqueous chemistry and formation of secondary organic aerosol (SOA). Their representations in a variety of aerosol mechanisms offered in the five two-way coupled models applied in Asia and relevant references are compiled in Table 2. Note that the GOCART scheme in WRF-Chem is based on a bulk aerosol mechanism that is not able to consider the details of these microphysics processes. The binary homogeneous nucleation schemes with/out hydration developed by different authors are applied in the five coupled models for simulating the new particle formation and GATOR-GCMOM also adopts the ternary nucleation parameterization scheme for H₂SO₄, NH₃ and H₂O vapors. All the five coupled models calculate the aerosol-aerosol coagulation rate coefficients based the Brownian coagulation theory, with certain enhancements in GATOR-GCMOM as stated in details by Jacobson (1999). The dynamic condensation/evaporation approaches of inorganic gases (e.g., H₂SO₄, NH₃, HNO₃, and HCl) and organic gases (VOCs) based on the Fuchs-Sutugin expression are implemented in various aerosol mechanisms offered by WRF-Chem, WRF-CMAQ, GRAPES-CUACE, and WRF-NAQPMS, while GATOR-GCMOM deploys the condensation/evaporation approach in which several terms of processes are factored in the 3-D equations of discrete size-resolved aerosol growth (Jacobson, 2012a). The mass transfer between gaseous and aerosol particles are treated via two typical methods (i.e., bulk equilibrium and kinetic) in most coupled models, and the hybrid and Henry's law equilibrium methods are also applied in the MADRID (WRF-Chem) and the 6th/7th generation CMAQ aerosol modules (AERO6/AERO7) (WRF-CMAQ), respectively. Different versions of the ISORROPIA module, the Model for an Aerosol Reacting System-version A (MARS-A), the Multicomponent Equilibrium Solver for Aerosols with the Multicomponent Taylor Expansion Method (MESA-MTEM), and the EQUilibrium SOLVER version 2 (EQUISOLV

365 II) modules are implemented for computing the inorganic aerosol thermodynamic equilibrium in
 366 these two-way coupled models. For aqueous chemistry, the bulk aqueous chemistry scheme and
 367 variations of the CMAQ's standard aqueous chemistry module (AQCHEM) are the most applied,
 368 and the CBM-IV aqueous chemistry scheme, the Regional Acid Deposition Model (RADM)
 369 aqueous chemistry module, and the size-resolved aqueous chemistry module are utilized as well.
 370 Multiple approaches have been incorporated into the five coupled models for calculating the SOA
 371 formation and include the volatility basis set (VBS) approach, approaches considering reversible
 372 absorption or combined absorption and dissolution, fixed or bulk two-product yield approaches, and
 373 the approach of time-dependent organics condensation/evaporation with considering vapor pressure.
 374

375 Table 2. Treatments of aerosol microphysics processes in two-way coupled models (WRF-Chem, WRF-CMAQ,
 376 GRAPES-CUACE, WRF-NAQPMS and GATOR-GCMOM) applied in Asia.

	WRF-Chem			WRF-CMAQ						GRAPES-CUACE	WRF-NAQPMS	GATOR-GCMOM
	GOCART	MADE/SORGAM	AEROS	MAM3/MAM7	MOSAIC	MADRID	AEROS	AERO6	AERO7	CUACE [※]	AEROS	GATOR2012 [*]
New particle formation/with hydration	None	H ₂ SO ₄ -H ₂ O binary homogeneous nucleation (Kulmala et al., 1998)/Yes	H ₂ SO ₄ -H ₂ O binary homogeneous nucleation (Kulmala et al., 1998)/Yes	H ₂ SO ₄ -H ₂ O binary homogeneous nucleation (Vehkamäki et al., 2002)/Yes	H ₂ SO ₄ -H ₂ O binary homogeneous nucleation (Wexler, et al., 1994)/Yes	H ₂ SO ₄ -H ₂ O binary homogeneous nucleation (McMurry and Friedlander, 1979)/Unclear	H ₂ SO ₄ -H ₂ O binary homogeneous nucleation (Kulmala et al., 1998)/Yes	H ₂ SO ₄ -H ₂ O binary homogeneous nucleation (Vehkamäki et al., 2002)/Yes	H ₂ SO ₄ -H ₂ O binary homogeneous nucleation (Vehkamäki et al., 2002)/Yes	H ₂ SO ₄ -H ₂ O binary homogeneous nucleation (Kulmala et al., 1998)/Yes	H ₂ SO ₄ -H ₂ O binary homogeneous nucleation (Yu, 2006)/Yes	H ₂ SO ₄ -H ₂ O binary homogeneous nucleation (Vehkamäki et al., 2002)/Yes; H ₂ SO ₄ -NH ₃ -H ₂ O ternary homogeneous nucleation (Napari et al., 2002)/Yes
Coagulation	None	Brownian motion (Binkowski and Shankar, 1995)	Brownian motion (Binkowski and Roselle, 2003)	Brownian motion (Whitby, 1978)	Brownian motion (Jacobson et al., 1994)	Brownian motion (Jacobson et al., 1994)	Brownian motion (Binkowski and Roselle, 2003)	Brownian motion (Binkowski and Roselle, 2003)	Brownian motion (Binkowski and Roselle, 2003)	Brownian motion (Jacobson et al., 1994)	Brownian motion (Jacobson et al., 1994; Chen et al., 2017d)	Brownian motion, Brownian diffusion enhancement, turbulent shear, turbulent inertial motion, gravitational settling, Van der Waals forces, viscous forces, fractal geometry (Jacobson, 2003)
Condensation/Evaporation	None	Dynamical condensation/evaporation of H ₂ SO ₄ vapor and VOCs based on Fuchs-Sutugin expression (Binkowski and Shankar, 1995)	Dynamical condensation/evaporation of H ₂ SO ₄ vapor and VOCs based on Fuchs-Sutugin expression (Binkowski and Shankar, 1995); Condensation/evaporation of volatile inorganic gases to/from the gas-phase concentrations of coarse particle surfaces using ISORROPIA in reverse mode (CMAQ User's Guide)	Dynamical condensation of H ₂ SO ₄ vapor, NH ₃ (7 modes) and semi-volatile organics; Condensation/evaporation of SOA gas (Liu et al., 2012)	Dynamical condensation/evaporation of H ₂ SO ₄ vapor, methanesulfonic acid, HNO ₃ , HCl and NH ₃ with adaptive step time-split Euler approach (Zaveri et al., 2008)	Dynamical condensation/evaporation of semi-volatile species for analytical predictor of condensation with moving-center approach (Zhang et al., 2010)	Dynamical condensation/evaporation of H ₂ SO ₄ vapor and VOCs based on Fuchs-Sutugin expression (Binkowski and Shankar, 1995); Condensation/evaporation of volatile inorganic gases to/from the gas-phase concentrations of coarse particle surfaces using ISORROPIA in reverse mode (CMAQ User's Guide)	Same as in AERO5	Same as in AERO5	Dynamical condensation/evaporation of H ₂ SO ₄ vapor and gaseous precursors based on modified Fuchs-Sutugin expression (Jacobson, et al., 1994; Gong et al., 2003a)	Condensation/evaporation of H ₂ SO ₄ with advanced particle microphysics approach (Li et al., 2018a; Yu and Luo, 2009; Chen et al., 2019c; Yu, 2006)	Dynamical condensation of H ₂ O and involatile species with Analytical Predictor of Nucleation, Condensation, and Dissolution scheme (Jacobson, 2002); Evaporation of a volatile component over a single particle (Jacobson and Turco, 1995)
Gas/particle mass transfer	None	1. Bulk equilibrium approach for HNO ₃ and NH ₃ (Zhang et al., 2005) 2. Kinetic approach for H ₂ SO ₄ (Zhang et al., 2016d)	Kinetic approach for all species (Foley et al., 2010)	Bulk equilibrium approach for (NH ₄) ₂ SO ₄ (He and Zhang, 2014)	Kinetic approach for all species (Zaveri et al., 2008)	1. Bulk equilibrium approach for HNO ₃ and NH ₃ (Zhang et al., 2010) 2. Kinetic approach for all species (Zhang et al., 2010) 3. Hybrid approach (Zhang et al., 2010)	Kinetic approach for all species (Foley et al., 2010)	1. Henry's law equilibrium (Foley et al., 2017) 2. Kinetic approach for all species (Foley et al., 2017)	Same as in AERO6	Kinetic approach for all species (Zhou et al., 2021)	Kinetic for all species (Chen et al., 2021)	Kinetic approach for all species (Jacobson, 1999)
Inorganic aerosol thermodynamic equilibrium	None	MARS-A (Binkowski and Shankar, 1995)	ISORROPIA (Byun and Kenneth, 2006)	ISORROPIA II (He and Zhang, 2014)	MESA-MTEM (Zaveri et al., 2008)	ISORROPIA (Zhang et al., 2010)	ISORROPIA (Byun and Kenneth, 2006)	ISORROPIA II (Appel et al., 2013)	ISORROPIA II (Appel et al., 2013)	ISSORROPIA (Zhou et al., 2012)	ISSORROPIA (Li et al., 2011)	EQUISOLV II (Jacobson, 1999)
Aqueous chemistry	None	Bulk cloud-chemistry scheme (Fahey and Pandis, 2001; Zhang et al., 2015b)	AQCHEM (Fahey et al., 2017)	Based on algorithm developed by Barth et al. (2000) (He and Zhang, 2014)	Same as in MADE/SORGAM (Fahey and Pandis, 2001; Chapman et al., 2009)	Same as in MADE/SORGAM (Fahey and Pandis, 2001; Zhang et al., 2004)	1. AQCHEM 2. AQCHEM-KMT (Fahey et al., 2017)	1. AQCHEM-KMT 2. AQCHEM-KMTI (Fahey et al., 2017)	1. AQCHEM-KMT 2. AQCHEM-KMTI (Fahey et al., 2017)	Based on aqueous chemistry in CBM-IV mechanism by Gery et al. (1989)	Based on the RADM mechanism used in CMAQ v4.6 (AEROS) (Li et al., 2011a)	Bulk or size-resolved cloud-chemistry module (GATOR2012)
SOA formation	None	1. Reversible absorption of 8 classes volatile organic compounds (VOCs) based on Caltech smog-chamber data (Odum et	Combined absorption and dissolution approaches for 9 parent VOCs and 32 SOA species (Carlton, et al., 2010)	Treatment of SOA from fixed mass yields for anthropogenic and biogenic precursor VOCs (Liu et al., 2012)	1. Based on ambient ageing measurement of organic aerosols by Hodzic and Jimenez (2011) 2. Based on volatility basis set approach	1. Absorptive approach for 14 parent VOCs and 38 SOA species 2. Combined absorption and	Combined absorption and dissolution approaches for 9 parent VOCs and 32 SOA species (Carlton, et al., 2010)	On the basis of SOA scheme in AEROS5, adding parameterization of in-cloud SOA formation from biogenic VOCs (Foley et al., 2017)	On the basis of SOA scheme in AEROS5/6, updated parameterization of monoterpene SOA yielded from photooxidation	Reversible absorption of 8 classes VOCs based on Caltech smog-chamber data (Zhou et al., 2012)	Bulk two-product yield parameterization (Fu et al., 2016; Odum et al., 1997)	Using Henry's Law to determine vapor pressure of organics and perform either time-dependent condensation or evaporation calculations.

al., 1997;
Griffin et al.,
1999)
2. Based on
volatility basis
set approach
(Ahmadov et
al., 2012)

(Knote et al.,
2014)

dissolution
approaches
for 42
hydrophilic
and
hydrophobic
VOCs
(Zhang et al.,
2004)

(Foley et al.,
2021)

(Jacobson, 2002)

377 *CUACE is the aerosol mechanism implemented in the GRAPES-CUACE model (Zhou et al., 2012).

378 *GATOR2012 is the aerosol mechanism implemented in the GATOR-GCMOM model (Jacobson et al., 2012b).

379

380 In addition to aerosol microphysics processes, the cloud properties included in cloud
381 microphysics schemes and the treatment of aerosol-cloud processes in the five two-way coupled
382 models are different in terms of hydrometeor classes, cloud droplet size distribution, aerosol water
383 uptake, in-/below-cloud scavenging, hydrometeor-aerosol coagulations, and sedimentation of
384 aerosols and cloud droplets (Table 3). Among the microphysics schemes implemented in the five
385 coupled models, mass concentrations of different hydrometeors (including cloud water, rain, ice,
386 snow or graupel) are included but their number concentrations are only considered if the cloud
387 microphysics schemes are two-moment or three-moment. The single modal approach with either
388 lognormal or gamma distribution and the sectional approach with discrete size distributions for
389 cloud droplets are applied in different microphysics schemes. Based on the Mie theory, WRF-Chem,
390 WRF-CMAQ, GRAPES-CUACE, WRF-NAQPMS and GATOR-GCMOM calculate cloud
391 radiative properties (including extinction/scattering/absorption coefficient, single scattering albedo
392 and asymmetry factor of liquid and ice clouds) in their radiation schemes (e.g., RRTMG,
393 GODDARD, GATOR2012). In atmosphere, the hygroscopic growth of aerosols due to water uptake
394 is parameterized based on the Köhler or Zdanovskii-Stokes-Robinson theory and the hysteresis
395 effects depending on the deliquescence and crystallization RH are taken into account in the five
396 coupled models. The removal processes of aerosol particles include wet removal and sedimentation.
397 Aerosol particles in accumulation and coarse modes can act as CCN or IN via activations in cloud,
398 which can further develop to different types of hydrometeors (cloud water, rain, ice, snow and
399 graupel), and then gradually form precipitations. These processes are named as in-cloud scavenging
400 or rainout. The aerosol particles below cloud base also can be coagulated with the falling
401 hydrometeors, which are known as below-cloud scavenging or wash out. Both representations of
402 in- and below-cloud scavenging processes are based on scavenging rate approach in aerosol
403 mechanisms of WRF-Chem, WRF-CMAQ, GRAPES-CUACE and WRF-NAQPMS except
404 GATOR-GCMOM. Size-resolved sedimentation of aerosols are computed from one model layer to
405 layers below down to the surface layer using settling velocity in most coupled models and the
406 MOSAIC aerosol mechanism in WRF-Chem only considers the sedimentation in the lowest model
407 level (Marelle et al., 2017).

408

409 Table 3. Compilation of cloud properties and aerosol-cloud processes in two-way coupled models (WRF-Chem,
410 WRF-CMAQ, GRAPES-CUACE, WRF-NAQPMS and GATOR-GCMOM) applied in Asia.

	WRF-Chem	WRF-CMAQ	GRAPES-CUACE	WRF-NAQPMS	GATOR-GCMOM
Hydrometeor (Cloud microphysics scheme)	Mass concentrations: Cloud water, rain, ice, snow and graupel (Morrison, Lin, Thompson, WSM 6 class and Milbrandt-Yau) Cloud water, rain, ice and snow (WSM 5 class) Number concentrations: Rain, ice, snow and graupel (Morrison and Milbrandt-Yau) Rain and ice (Thompson) None (Lin, WSM 5 class and WSM 6 class)	Mass concentrations: Cloud water, rain, ice, snow and graupel (Morrison) Cloud water, rain, ice and snow (WSM 5 class) Cloud water and rain (WSM 3 class) Number concentrations: Rain, ice, snow and graupel (Morrison) None (WSM 3 class and WSM 5 class)	Mass concentrations: Cloud water, rain, ice, snow and graupel (WSM 6 class) Number concentrations: None (WSM 6 class)	Mass concentrations Cloud water, rain, ice, snow and graupel (Lin) Number concentrations: None (Lin)	Mass concentrations: Cloud water, ice and graupel (GATOR2012) Number concentrations: Cloud water, ice and graupel (GATOR2012)
Cloud droplet size distribution (Cloud microphysics scheme)	1. Single, modal approach with lognormal distribution (Morrison and Lin) 2. Gamma distribution (Thompson, WSM 5 class and WSM 6 class)	1. Single, modal approach with lognormal distribution (Morrison) 2. Gamma distribution (WSM 3 class and WSM 5 class)	Gamma distribution (WSM 6 class)	Single, modal approach with lognormal distribution (Lin)	Sectional approach with multiple size distributions (GATOR2012') (Jacobson, et al., 2007)
Cloud radiative properties (Radiation scheme)	Extinction coefficient, single scattering albedo and asymmetry factor of liquid and ice clouds based on Mie scattering theory (RRTMG SW) Absorption coefficient of liquid and ice clouds using constant values (RRTMG LW) Extinction coefficient, single scattering albedo and asymmetry factor of liquid and ice clouds from lookup tables (Goddard SW and LW)	Extinction coefficient, single scattering albedo and asymmetry factor of liquid and ice clouds based on Mie scattering theory (RRTMG SW) Absorption coefficient of liquid and ice clouds using constant values (RRTMG LW)	Extinction coefficient, single scattering albedo and asymmetry factor of liquid and ice clouds using lookup tables (Goddard SW) Extinction coefficient, single scattering albedo and asymmetry factor of liquid and ice clouds from lookup tables (Goddard LW)	Extinction coefficient, single scattering albedo and asymmetry factor of liquid and ice clouds using lookup tables (Goddard SW) Clear sky optical depth from lookup table (RRTM LW)	Integrating spectral optical properties over each size bin of each hydrometeor particle size distribution (Toon SW and LW) (Jacobson and Jadhav, 2018)
Aerosol water uptake	Equilibrium with RH based on Köhler theory, and hysteresis is treated (Ghan and Zaveri, 2007)	The empirical equations of deliquescence and crystallization RH developed by Martin et al (2003), and hysteresis is treated (CMAQ source code)	Equilibrium with the mutual deliquescence and crystallization RH using the Zdanovskii-Stokes-Robinson equation, and hysteresis is treated (Personal communication)	Equilibrium with the mutual deliquescence and crystallization RH using the Zdanovskii-Stokes-Robinson equation, and hysteresis is treated (Nenes et al., 1998; Li et al., 2011)	Size-resolved equilibrium with the mutual deliquescence and crystallization RH using the Zdanovskii-Stokes-Robinson equation, and hysteresis is treated (Jacobson et al., 1996b)
In-cloud scavenging (Aerosol mechanism)	Scavenging via nucleation, Brownian diffusion, collection and autoconversion in both grid-scale and sub-grid clouds with a first-order removal rate (MADE/SORGAM, MOSAIC, MAM3 and MAM7) (Easter et al., 2004)	Scavenging of interstitial aerosol in the Aitken mode and nucleation scavenging of aerosol in the accumulation and coarse modes by the cloud droplets in both grid-scale and sub-grid clouds (AEROS, AERO6 and AERO7) (Binkowski and Roselle, 2004; Fahey et al., 2017)	Algorithm of rainout removal tendency by Giorgi and Chameides (1986)	Employing a scavenging coefficient approach based on relationships described by Seinfeld and Pandis (1998), only hydrophilic particles can be scavenged (Chen et al., 2017d)	Size-resolved aerosol activation; nucleation scavenging and autoconversion for size-resolved cloud droplets (GATOR2012) (Jacobson, 2003)

Below-cloud scavenging (Aerosol mechanism)	Scavenged aerosols are instantly removed by interception and impaction but not resuspended by evaporating rain (MADE/SORGAM, MOSAIC, MAM3 and MAM7) (Slinn, 1984; Easter et al., 2004)	All aqueous species are scavenged from the cloud top to the ground in both grid-scale and sub-grid clouds (AEROS, AERO6 and AERO7) (CMAQ User's Guide; Fahey et al., 2017)	Aerosol particles between sizes ranging from 0.5 to 1 μm radius are instantly removed with considering cloud fraction, and scavenged rate depends on aerosol and hydrometeor sizes (Slinn, 1984; Gong et al., 2003a)	Employing a scavenging coefficient approach based on relationships described by Seinfeld and Pandis (1998), considering accretion of in-cloud droplets particles into precipitation and impaction of ambient particles into precipitation	Discrete size-resolved coagulation between hydrometeors and aerosol particles (aerosol-liquid, aerosol-ice and aerosol-graupel) (GATOR2012) (Jacobson, 2003)
Sedimentation of aerosols (Aerosol mechanism)	Sedimentation with considering mass and number concentrations of aerosols at surface (MOSAIC) (Marelle et al., 2017)	Only considering gravitational sedimentation for aerosols (AEROS, AERO6 and AERO7)	Size-resolved sedimentation of aerosol particles above surface layer is computed with the settling velocity (CUACE) (Gong et al., 2003)	Using size-resolved sedimentation velocity to simulate sedimentation of aerosols (AEROS)	Sedimentation of size-resolved aerosols is computed from one model layer to layers below down to the surface, and the sedimentation velocities are calculated by two-step iterative method (GATOR2012) (Beard, 1976; Jacobson, 1997b, 2003)

411 * GATOR2012 refers to either the aerosol or cloud microphysics scheme used in Jacobson (2012b).

412

413 Table 4 further lists various aspects with regards to how ARI and ACI being calculated in the
414 five two-way coupled models (WRF-Chem, WRF-CMAQ, GRAPES-CUACE, WRF-NAQPMS,
415 and GATOR-GCMOM) applied in Asia. Note that the information in this table was extracted from
416 the latest released version of WRF-Chem (version 4.3.3) and WRF-CMAQ (based on WRF v4.3
417 and CMAQ v5.3.3) as well as relevant references for GRAPES-CUACE (Wang et al., 2015), WRF-
418 NAQPMS (Wang et al., 2014) and GATOR-GCMOM (Jacobson et al., 2012). These models all use
419 the Mie theory to compute ARI effects but differ in representations of aerosol optical properties and
420 radiation schemes. To simplify the calculation, aerosol species simulated by the chemistry
421 module/model are put into different groups (Table 4) and the refractive indices of these groups are
422 directly from the Optical Properties of Aerosols and Clouds (OPAC) database (Hess et al., 1998) in
423 WRF-Chem and WRF-CMAQ (Table B6 in Appendix B). In WRF-Chem, the aerosol optical
424 properties (AOD, extinction/scattering/absorption coefficient, single scattering albedo and
425 asymmetry factor) are calculated in terms of four spectral intervals (listed in Table B6 in Appendix
426 B) and then inter/extrapolated to 11 (14) SW intervals defined in the GODDARD (RRTMG) scheme.
427 For SW and LW radiation in both WRF-CMAQ and WRF-Chem, these optical parameters are
428 computed at each of corresponding spectral intervals in the RRTMG scheme. The aerosol optical
429 property for LW radiation is considered only at 5 thermal windows (listed in Table B6) in WRF-
430 CMAQ. No detailed information regarding how aerosol optical property and relevant parameters
431 being calculated in GRAPES-CUACE and WRF-NAQPMS can be found from the relevant
432 references.

433 With respect to ACI effects, the simulated aerosol characteristics (such as mass, size
434 distribution and species) are utilized for the calculation of cloud droplet activation and aerosol
435 resuspension based on the Köhler theory (Abdul-Razzak and Ghan, 2002) in several (one)
436 microphysics schemes (scheme) in WRF-Chem (GRAPES-CUACE). GATOR-GCMOM is the first
437 two-way coupled model adding IN activation processes including heterogeneous and homogeneous
438 freezing (Jacobson et al., 2003). None of the other four two-way coupled models considers the IN
439 formation processes (including immersion freezing, deposition freezing, contact freezing, and
440 condensation freezing) but they have been included in some specific versions of WRF-Chem (Keita
441 et al., 2020; Lee et al., 2020), which are not yet in the latest release version 4.3.3 of WRF-Chem.

442

443 Table 4. Summary of relevant information regarding calculations of aerosol-radiation interactions (ARI) and aerosol-
444 cloud interactions (ACI) in two-way coupled models (WRF-Chem, WRF-CMAQ, GRAPES-CUACE, WRF-
445 NAQPMS and GATOR-GCMOM) applied in Asia.

Model	ARI			ACI			
	Aerosol species groups	Aerosol size distribution (Aerosol mechanism)	Mixing state [‡]	SW scheme (# of spectral intervals)	LW scheme (# of spectral intervals)	CCN (Microphysics scheme)	IN (Microphysics scheme)
WRF-Chem	1. Water 2. Dust 3. BC 4. OC 5. Sea-salt 6. Sulfate	1. Bulk (GOCART) 2. Modal (MADE/SORGAM, AEROS, MAM3 and MAM7) 3. Sectional (MOSAIC (4bins and 8 bins) and MADRID (8bins))	Internal mixing (Volume averaging, Core-shell, and Maxwell-Garnett)	1. Goddard (11) 2. RRTMG (14)	RRTMG (16)	Activation under a certain supersaturation in an air parcel based on Köhler theory (Morrison, Lin, Thompson, WSM 6/5/3 class and Milbrandt-Yau)	Ice heterogeneous nucleation of mineral dust aerosols in based on classical nucleation theory (Milbrandt-Yau and Morrison) [†]
WRF-CMAQ	1. Water 2. Water-soluble 3. BC 4. Insoluble 5. Sea-salt	Modal (AEROS, AERO6 and AERO7)	Internal mixing (Core-shell)	RRTMG (14)	RRTMG (16)	None	None
GRAPES-CUACE	1. Nitrate 2. Dust 3. BC 4. OC 5. Sea-salt 6. Sulfate 7. Ammonium	Sectional (CUACE (12 bins))	External mixing	Goddard (11)	Goddard (10)	Activation under a certain supersaturation in an air parcel based on Köhler theory (WSM 6-class)	None
WRF-NAQPMS	1. Nitrate 2. Dust 3. BC 4. OC 5. Sea-salt 6. Sulfate	Modal (AEROS)	External mixing	Goddard (11)	RRTM (16)	Activation under a certain supersaturation in an air parcel based on Köhler theory (Lin)	None

7. Ammonium
8. Other primary particles

GATOR-GCMOM	1. Water 2. Dust 3. BC 4. HCO ₃ 5. SOA 6. Sulfate ... 42. MgCO ₃ (s)	Sectional (GATOR2012* (17-30 bins))	Internal mixing (Core-shell [†])	Toon* (318)	Toon* (376)	Activation under a certain supersaturation in an air parcel based on Köhler theory (GATOR2012 [‡])	Ice heterogeneous and homogeneous nucleation (GATOR2012 [*])
-------------	---	--	---	-------------	-------------	--	--

446 ‡ Specific version of WRF-Chem, WRF-NAQPMS and GATOR-GCMOM have the ability of simulating aerosol aging (Zhang et al., 2014a;
447 Chen et al., 2017d; Li et al., 2018a; Jacobson, 2012b).

448 † Some specific versions of WRF-Chem consider IN (Keita et al., 2020; Lee et al., 2020).

449 *The short- and long-wave radiation calculations in GATOR-GCMOM are based on the algorithm of Toon et al. (1989).

450 * GATOR2012 refers to either the aerosol or cloud microphysics scheme used in Jacobson (2012b).

451

452 How accurately ARI and ACI are simulated also rely on the representation of aerosol
453 composition and size distribution in two-way coupled models. Table 5 presents the treatments of
454 aerosol compositions and size distributions in the five two-way coupled models applied in Asia. As
455 shown in Tables 4 and 5, GATOR-GCMOM considered more detailed aerosol species groups as
456 high as 42 kinds, and others coupled models different numbers of species groups (such as 6, 5, 7, 8
457 aerosol species groups in WRF-Chem, CMAQ, NAQPMS and CUACE, respectively). Three typical
458 representation approaches of size distribution (bulk, modal and sectional methods) are adopted by
459 the five two-way coupled models and WRF-Chem offers all the three approaches, but other models
460 only support one specific option. The Global Ozone Chemistry Aerosol Radiation and Transport
461 (GOCART) model (Ginoux et al., 2001) in WRF-Chem is the only one that is based on a
462 combination of bulk (for water, BC, OC, and sulfate aerosols) and sectional (for dust and sea salt
463 aerosols) approaches. The widely used modal and sectional approaches in five coupled models and
464 their detailed numerical settings of aerosol size distribution (namely, geometric diameter and
465 standard deviation for modal approach or bin ranges for sectional method) are listed in Table 5.
466 Regarding the modal method, same parameter values for Aitken and accumulation modes and
467 geometric diameters for coarse mode in the latest version of WRF-Chem (v4.3.3) and older version
468 of WRF-CMAQ (before v5.2) are set as default, except the standard deviations for coarse mode are
469 slightly different. In the official version of WRF-CMAQ released after v5.2, there are some
470 modifications to the default setting of geometric diameters in Aitken, accumulation and coarse
471 modes, from 0.01 to 0.015 μm, 0.07 to 0.08 μm and 1.0 to 0.6 μm, respectively. For the GRAPES-
472 CUACE model, the parameters of size distribution for certain aerosol species in the accumulation
473 mode were updated from its older version (Zhou et al., 2012) to newer one (Zhang et al., 2021).
474 With respect to the sectional approach, 4 or 8 (from 0.039 to 10 μm), 12 (from 0.005 to 20.48 μm)
475 and 14 (from 0.002 to 50 μm) particle size bins are defined in WRF-Chem, CUACE and GATOR-
476 GCMOM, respectively.

477

478 Table 5. Summary of numerical representations of aerosol size distribution and composition in two-way coupled
479 models (WRF-Chem, WRF-CMAQ, GRAPES-CUACE, WRF-NAQPMS and GATOR-GCMOM) applied in Asia.

Model	Aerosol mechanism	Modal approach						Compositions	Reference
		Aitken		Accumulation		Coarse			
		Geometric diameters (μm)	Standard deviations (μm)	Geometric diameters (μm)	Standard deviations (μm)	Geometric diameters (μm)	Standard deviations (μm)		
WRF-Chem v4.3.3	MADE/ SORGAM	0.010	1.7	0.07	2.0	1.0	2.5	Water, BC, OC, and sulfate, dust and sea salt	WRF-Chem codes [®]
WRF- Chem ^A	MAM3	0.013 (Sulfate and secondary OM)	1.6 (Sulfate and secondary OM)	0.068 (Sulfate, secondary OM, primary OM, BC, dust and sea salt)	1.8 (Sulfate, secondary OM, primary OM, BC, dust and sea salt)	2.0 (Sea salt), 1.0 (Dust)	1.8 (Sea salt and dust)	Sulfate, methane sulfonic acid (MSA), OM, BC, sea salt and dust	Easter et al. (2004) Liu et al. (2012)
WRF- Chem ^A	MAM7	0.013 (Sulfate and secondary OM and BC)	1.6 (Sulfate, OM and BC)	0.068 (Sulfate and BC) 0.068 (Primary OM) 0.2 (Sea salt) 0.11 (Dust)	1.8 (Sulfate and BC) 1.6 (Primary OM) 1.8 (Sea salt) 1.8 (Dust)	2.0 (Sea salt) 1.0 (Dust)	2.0 (Sea salt) 1.8 (Dust)	Sulfate, methane sulfonic acid (MSA), OM, BC, sea salt and dust	Easter et al. (2004) Liu et al. (2012)
WRF- CMAQ	AEROS	0.010	1.7	0.07	2.0	1.0	2.2	Water, water- soluble BC,	CMAQ codes [*]

(before CMAQ v5.2)									insoluble, sea salt	
WRF-CMAQ (after CMAQ v5.2)	AERO6 and AERO7	0.015	1.7	0.08	2.0	0.60		2.2	Water, water-soluble BC, insoluble, sea salt	CMAQ codes [‡]
WRF-NAQPMS	AERO5	0.052	1.9	0.146	1.8	0.80		1.9	Nitrate, dust, BC, OC, sea-salt, sulfate, ammonium, other primary particles	Wang et al. (2014)
GRAPES-CUACE	CUACE	0.10 (BC and OC)	1.7 (BC and OC)	0.25 (Sulfate and nitrate)	1.7 (Sulfate and nitrate)	3.0 (Dust)		1.7 (Dust)	Nitrate, dust, BC, OC, sea-salt, sulfate, ammonium [‡]	Zhou et al. (2012)
GRAPES-CUACE	CUACE	Unclear	Unclear	0.37 (BC and OC)	0.42 (BC and OC)	Unclear		Unclear	Nitrate, dust, BC, OC, sea-salt, sulfate, ammonium [‡]	Zhang et al. (2021)
WRF-Chem v4.3.3	MOSAIC	Sectional approach 0.039-0.156, 0.156-0.625, 0.625-2.5, 2.5-10.0 μm (4 bins) 0.039-0.078, 0.078-0.156, 0.156-0.312, 0.312-0.625, 0.625-1.25, 1.25-2.5, 2.5-5.0, 5.0-10.0 μm (8 bins)							Water, BC, OC, sulfate, dust and sea salt	WRF-Chem codes [⊗]
WRF-Chem ^Δ	MADRID	0.0216-10 μm (8 bins)							Water, BC, OC, and sulfate, dust and sea salt	Zhang et al. (2016d)
WRF-Chem v4.3.3	GOCART	0.1-1.0, 1.0-1.8, 1.8-3.0, 3.0-6.0, 6.0-10.0 (5 bins for dust) 0.1-0.5, 0.5-1.5, 1.5-5.0, 5.0-10.0 (4 bins for sea salt)							Dust and sea salt	WRF-Chem codes [⊗]
GRAPES-CUACE	CUACE	0.005-0.01, 0.01-0.02, 0.02-0.04, 0.04-0.08, 0.08-0.16, 0.16-0.32, 0.32-0.64, 0.64-1.28, 1.28-2.56, 2.56-5.12, 5.12-10.24, 10.24-20.48 μm (12 bins)							Nitrate, dust, BC, OC, sea-salt, sulfate, ammonium	Zhou et al. (2012)
GATOR-GCMOM	GATOR2012	0.002-50 μm (14 bins)							42 species [‡]	Jacobson (2002, 2012b)

480 [⊗] Official released version of WRF-Chem.

481 ^Δ Specific version of WRF-Chem.

482 ^{*} https://github.com/USEPA/CMAQ/blob/5.1/models/CCTM/aero/aero6/AERO_DATA.F.

483 [†] https://github.com/USEPA/CMAQ/blob/5.2/CCTM/src/aero/aero6/AERO_DATA.F.

484 [‡] More detailed components were presented in the first column of Table 2.

485 ^{*} Initial size distribution is tri-modal log-normal distribution.

486

487 Not only the choice of methodologies for ARI and ACI calculations can impact simulation
488 results, but also the various aspects regarding the setup of modeling studies by applying two-way
489 coupled models. The extra/auxiliary information about model configuration, including horizontal
490 and vertical resolutions, aerosol and gas phase chemical mechanisms, PBL schemes, meteorological
491 and chemical ICs and BCs, anthropogenic and natural emissions, were extracted from the 160 papers
492 and presented in Table S4 of Supplement, which is organized in the same order as Table 1.

493 For two-way coupled model applications in Asia, horizontal resolutions were set from a few to
494 several hundred kilometers, sometimes with nests, and vertical resolutions were from 15 to about
495 50-70 levels, with only one study performed at 100 levels for studying a fog case (Wang et al.,
496 2019b). Wang et al. (2018b) evaluated the impacts of horizontal resolutions on simulation results
497 and found out surface meteorological variables were better modeled at finer resolution but no
498 significant improvements of ACI related meteorological variables and certain chemical species
499 between different grid resolutions. Through applying a single column model and then WRF-Chem
500 with ARI, Wang et al. (2019b) unraveled that better representation of PBL structure and relevant
501 variables with finer vertical resolution from the surface to PBL top could reduce model biases
502 noticeably, but balancing between vertical resolution and computational resource was important as
503 well. Among the 160 applications of two-way coupled models in Asia, the frequently used aerosol
504 module and gas-phase chemistry mechanism in WRF-CMAQ (WRF-Chem) were AERO6
505 (MOSAIC and MADE/SOGARM) and CB05 (CBMZ and RADM2), respectively. For PBL
506 schemes, most studies selected YSU in WRF-Chem and ACM2 in WRF-CMAQ. Regarding to

507 meteorological ICs and BCs, the FNL data were the first choice, and outputs from the Model for
508 Ozone and Related Chemical Tracer (MOZART) were used to generate chemical ICs and BCs by
509 most researchers. Georgiou et al. (2018) also unraveled that boundary conditions of dust and O₃
510 played an important role in WRF-Chem simulations. The modeling applications in Asia utilized
511 global (EDGAR), regional (e.g., MIX, INTEX-B, and REAS), and national (e.g., MEIC and JEI-
512 DB) anthropogenic emission inventories. Natural emission sources, such as mineral dust (Shao,
513 2004), biomass burning (FINN (Wiedinmyer et al., 2011) and GFED (Giglio et al., 2010)), biogenic
514 VOCs (MEGAN (Guenther et al., 2006)), and sea salt (Gong et al., 1997) were also considered. It
515 should be noted that only one paper by Gao et al. (2017c) reported that the WRF-Chem model with
516 the Gridpoint Statistical Interpolation (GSI) data assimilation could improve the simulation
517 accuracy during a wintertime pollution period.

518

519 **4 Overview of research focuses in Asia**

520 **4.1 Feedbacks of natural aerosols**

521 **4.1.1 Mineral dust aerosols**

522 Due to the fact that dust storm events frequently occurred over Asia during 2000-2010, the
523 research community has focused on dust transportation and associated climatic effects (Gong et al.,
524 2003b; Zhang et al., 2003a, b; Yasunari and Yamazaki, 2009; Lee et al., 2010; Choobari et al., 2014).
525 Also the detailed processes and physiochemical mechanisms of dust storms had been well
526 understood and reviewed in detail (Shao and Dong, 2006; Uno et al., 2006; Huang et al., 2014; Chen
527 et al., 2017b). To probe into the radiative feedbacks of dust aerosols in Asia, Wang et al. (2010, 2013)
528 initiated modeling studies by a two-way coupled model, i.e., the GRAPES-CUAUE model, to
529 simulate direct radiative forcing (DRF) of dust, and revealed that the feedback effects of dust
530 aerosols could lead to decreasing of surface wind speeds and then suppress dust emissions. Further
531 modeling simulations by the same model (Wang and Niu, 2013) indicated that considering dust
532 radiative effects did not substantially improve the model performance of the air temperature at 2
533 meters above the surface (T2), even with assimilating data from in-situ and satellite observations
534 into the model. Subsequently, several similar studies based on another two-way coupled model
535 (WRF-Chem with GOCART scheme) were conducted to investigate dust radiative forcing
536 (including shortwave radiative forcing (SWRF) and longwave radiative forcing (LWRF)) and ARI
537 effects of dust on meteorological variables (PBLH, T2 and WS10) in different regions of Asia
538 (Kumar et al., 2014; Chen et al., 2014; Jin et al., 2015, 2016b; Liu et al., 2016a; Bran et al., 2018;
539 Su and Fung, 2018a, b; Zhou et al., 2018). These studies demonstrated that dust aerosols could
540 induced negative radiative forcing (cooling effect) at top of atmosphere (TOA) as well as the surface
541 (including both Earth's and sea surfaces) and positive radiative forcing (warming effect) in the ATM
542 (Wang et al., 2013; Chen et al., 2014; Kumar et al., 2014; Li et al., 2017c; Bran et al., 2018; Li and
543 Sokolik, 2018; Su and Fung, 2018b). More thorough analyses of the radiative effects of dust in Asia
544 (Wang et al., 2013; Li and Sokolik, 2018) pointed out that dust aerosols played opposite roles in the
545 shortwave and longwave bands, so that the dust SWRF at TOA and the surface (cooling effects) as
546 well as in the ATM (warming effects) was offset partially by the dust LWRF (warming effects at
547 TOA and the surface but cooling effects in the ATM). It was noteworthy that adding more detailed
548 mineralogical composition into the dust emission for WRF-Chem could alter the dust SWRF at TOA
549 from cooling to warming and then lead to a positive net radiative forcing at TOA (Li and Sokolik,
550 2018). These different conclusions showed some degrees of uncertainties in the coupled model
551 simulations of dust aerosols' radiative forcing that need to be further investigated in the future.

552 Dust aerosols can act not only as water-insoluble cloud condensation nuclei (CCN) (Kumar et
553 al., 2009) but also as ice nuclei (IN) (Lohmann and Diehl, 2006) since they are referred to as ice
554 friendly (Thompson and Eidhammer, 2014). Therefore, activation and heterogeneous ice nucleation
555 parameterizations (INPs) with respect to dust aerosols were developed and incorporated into WRF-
556 Chem to explore ACI effects as well as both ARI and ACI effects of dust aerosols in Asia (Jin et al.,
557 2015, 2016b; Zhang et al., 2015c; Su and Fung, 2018a, b; Wang et al., 2018b). During dust storms,
558 including the adsorption activation of dust particles played vital roles in the simulations of ACI-
559 related cloud properties and a 45 % of increase of cloud droplet number concentration (CDNC),
560 comparing to a simpler aerosols activation scheme in WRF-Chem (Wang et al., 2018b). More
561 sophisticated INPs implemented in WRF-Chem that taking dust particles into account as IN resulted
562 in substantial modifications of cloud and ice properties as well as surface meteorological variables
563 and air pollutant concentrations in model simulations (Zhang et al., 2015c; Su and Fung, 2018b).

564 Zhang et al. (2015c) delineated that dust aerosols acting either as CCN or IN made model results
565 rather different regarding radiation, T2, precipitation, and number concentrations of cloud water and
566 ice. Su and Fu (2018b) described that the ACI effects of dust had less impacts on the radiative forcing
567 than its ARI effects and dust particles could promote (demote) ice (liquid) clouds in mid-upper (low-
568 mid) troposphere over EA. With turning on both ARI and ACI effects of dust, less low-level clouds
569 and more mid- and high-level clouds were detected that contributed to cooling at the Earth's surface
570 and in the lower atmosphere and warming in the mid-upper troposphere (Su and Fung, 2018b).
571 Mineral dust particles transported by the westerly and southwesterly winds from the Middle East
572 (ME) affected the radiative forcing at TOA and the Earth's surface and in the ATM by the dust-
573 induced ARI and ACI in the Arabian Sea and the India subcontinent, and subsequently changed the
574 circulation patterns, cloud properties, and characteristics related to the India summer monsoon (ISM;
575 Jin et al., 2015, 2016a). Moreover, the effects of dust on precipitation are not only complex but also
576 highly uncertain, evidencing from several modeling investigations targeting a variety of areas in
577 Asia (Jin et al., 2015, 2016a, b; Zhang et al., 2015c; Su and Fung, 2018b). Less precipitation from
578 model simulations including dust effects was found at EA and dust particles acting mainly as CCN
579 or IN influenced precipitation in a rather different way (Zhang et al., 2015c). A positive response of
580 ISM rainfall to dust particles from the ME was reported by Jin et al. (2015) and less affected by dust
581 storms from the local sources and NWC (Jin et al., 2016b). Jin et al. (2016a) further elucidated that
582 the impacts of ME dust on ISM rainfall were highly sensitive to the imaginary refractive index of
583 dust setting in the model, so that accurate simulations of the dust-rainfall interaction depended on
584 more precise representation of radiative absorptions of dust in two-way coupled models. About 20 %
585 of increase or decrease in rainfall due to the dust effects were detected in different areas over EA
586 from the WRF-Chem simulations (Su and Fung, 2018b). However, it should be mentioned that a
587 few studies that targeting DRF of dust in Asia based on WRF-Chem simulations but without
588 enabling aerosol-radiation feedbacks (Ashrafi et al., 2017; Chen et al., 2017c; Tang et al., 2018)
589 were not included in this paper.

590 Along with the modeling research on the effects of dust aerosols on meteorology, their impacts
591 on air quality in Asia were explored using two-way coupled models (Wang et al., 2013; Chen et al.,
592 2014; Kumar et al., 2014; Li et al., 2017c; Li and Sokolik, 2018). Many early modeling research
593 work involving two-way coupled models with dust only looked into the ARI or direct radiative
594 effects of dust particles, which are described as follows. Taking a spring-time dust storm from the
595 Thar Desert into consideration in WRF-Chem, the modeled aerosol optical depth (AOD) and
596 Angstrom exponent (as indicators of aerosol optical properties and unique proxies of the surface
597 particulate matter pollution) demonstrated that turning on the ARI effects of dust could reduce biases
598 in their simulations, but were underestimated in North India (Kumar et al., 2014). Wang et al. (2013)
599 pointed out that in EA, including the longwave radiative effects of dust in the GRAPES-
600 CUACE/dust model lowered relative errors of the modeled AOD by 15 %, as compared to
601 simulations that only considering shortwave effects of dust. Comparisons against both satellite and
602 in situ observations depicted that the WRF-Chem model was able to capture the general
603 spatiotemporal variations of the optical properties and size distribution of dust particles over the
604 main dust sources in EA, such as the Taklimakan Desert and Gobi Desert, but overestimated AOD
605 during summer and fall and also exhibited positive (negative) biases in the fine (coarse) mode of
606 dust particles (Chen et al., 2014). Besides the ARI effects of dust, the heterogeneous chemistry on
607 dust particles' surface added in WRF-Chem was accounted for 80 % of the net reductions of O₃,
608 NO₂, NO₃, N₂O₅, HNO₃, ·OH, HO₂· and H₂O₂ when a springtime dust storm striking the Nanjing
609 megacity of EC (Li et al., 2017c). In CA, AOD was overestimated by WRF-Chem model but its
610 simulation was improved when more detailed mineral components of dust particles were
611 incorporated in the model (Li and Sokolik, 2018). Later on, more investigations started to focus on
612 both ARI and ACI effects of dust aerosols. With consideration of ARI as well as both ARI and ACI
613 of dust particles from the ME, during the ISM period, the WRF-Chem model reproduced AOD's
614 spatial distributions but underpredicted (overpredicted) AOD over the Arabian Sea (the Arabian
615 Peninsula) comparing with satellite observations and AOD reanalysis data (Jin et al., 2015, 2016a,
616 b). In EA, Wang et al. (2018b) demonstrated that including both ARI and ACI effects of dust in
617 WRF-Chem caused lower O₃ concentrations and by incorporating INPs, the WRF-Chem model well
618 simulated the surface PM₁₀ concentrations (Su and Fung, 2018a) with reduced (elevated) surface
619 concentrations of OH, O₃, SO₄²⁻, and PM_{2.5} (CO, NO₂, and SO₂) (Zhang et al., 2015c). It is worth
620 noting that how to partition dust particles into fine mode and coarse mode or initialize their size

621 distribution in coupled models can affect simulations in many ways and requires more detailed
622 measurements at the source areas and further modeling studies.

623

624 **4.1.2 Wildfire, sea salt and volcanic ash**

625 In the Maritime SEA region, peat and forest fire triggered by El Niño induced drought
626 conditions released huge amount of smoke particles, which promoted dire air pollution problems in
627 the downstream areas, and their ARI effects simulated by WRF-Chem enhanced radiative forcing at
628 the TOA and the atmospheric stability (Ge et al., 2014). Ge et al. (2014) also pointed out the ARI
629 effects of these fires impaired (intensified) sea breeze at daytime (land breeze at nighttime) over this
630 region so that their impacts on cloud cover could be positive or negative in different areas and time
631 period (day or night). Sea salt and volcanic ash are also important natural aerosols for regions near
632 seashores and active volcanoes and surrounding areas but modeling studies of their ARI and ACI
633 effects are relatively scarce in Asia. Based on WRF-Chem simulations, Kedia et al. (2019b)
634 demonstrated that the feedbacks of sea salt aerosols impacted convective and nonconvective
635 precipitation rather variously in different areas of the India subcontinent. Jiang et al. (2019a, b) also
636 used WRF-Chem with/without sea-salt emissions to evaluate the effects of sea salt on rainfall in
637 Guangdong Province of China, but unfortunately, no feedbacks were considered in the simulations.
638 So far there is no investigation targeting aerosol effects of volcanic ash from volcano eruptions in
639 Asia using coupled models.

640

641 **4.2 Feedbacks of anthropogenic aerosols**

642 Atmospheric pollutants from anthropogenic sources are the leading causes of heavy pollution
643 events occurring in Asia due to the acceleration of urbanization, industrialization, and population
644 growth in recent decades, particularly in China and India, and their ARI or/and ACI effects on
645 meteorology and air quality had been quantitatively examined using two-way coupled models
646 (Kumar et al., 2012a, b; Li and Liao, 2014; Wang et al., 2014a; Zhang et al., 2015a; Gao et al., 2016a;
647 Yao et al., 2017; Wang et al., 2018d; Archer-Nicholls et al., 2019; Bharali et al., 2019). These
648 modeling research work had been primarily focused on the ARI or/and ACI effects of anthropogenic
649 aerosols, their specific chemical components (especially the light-absorbing aerosols, i.e., BC and
650 brown carbon (BrC)) and aerosols originated from different sources. The major findings are outlined
651 as follows, with respect to the effects of anthropogenic aerosol feedbacks on meteorology and air
652 quality.

653 Concerning the meteorological responses, most papers treated anthropogenic aerosols as a
654 whole to explore their effects on meteorological variables based on coupled model simulations with
655 enabling ARI or/and ACI in WRF-Chem, WRF-CMAQ, WRF-CMAQ, GRAPES-CUACE and
656 WRF-NAQPMS (Kumar et al., 2012a; Wang et al., 2014a, c, 2015a; Zhang et al., 2015a, 2018;
657 Zhao et al., 2017; Nguyen et al., 2019a, b; Bai et al., 2020). Generally, the main ARI effects of
658 anthropogenic aerosols resulted in decreases of SWRF, T2 and WS10, and PBLH, as well as
659 increases of surface relative humidity (RH2) and temperature in the ATM, which further suppressed
660 PBL development (Gao et al., 2015b; Xing et al., 2015a; Li et al., 2017b; Zhang et al., 2018; Nguyen
661 et al., 2019a, b). Wang et al. (2015a) utilized GRAPES-CUACE with ARI to study a summer haze
662 case in the NCP area and discovered that the ARI effects made the subtropical high less intense (-
663 14 hPa) to help pollutants in the area to dissipate. In Asia, ACI effects of anthropogenic aerosols on
664 cloud properties and precipitation are relatively complex. On the one hand, anthropogenic aerosols,
665 that being activated as CCN, enhanced CDNC and LWP and then slowed down the precipitation
666 onset, but their impacts on precipitation amounts varied in different seasons and areas in China
667 (Zhao et al., 2017). Targeting a summertime rainstorm in the middle reaches of the Yangtze River
668 (MRYR) in China, sensitivity studies using WRF-Chem unveiled that CDNC, cloud water contents,
669 and precipitation decreased (increased) with low (high) anthropogenic emission scenarios due to the
670 ACI effects and these variations tended to depend on atmospheric humidity (Bai et al., 2020). The
671 modeling investigations with WRF-Chem aiming at the ISM (Kedia et al., 2019b) and a disastrous
672 flood event in Southwest China (SWC) (Fan et al., 2015) pointed out that the simulated convective
673 process was suppressed and convective (nonconvective) precipitation was inhibited (enhanced) by
674 the ARI and ACI effects of accumulated anthropogenic aerosols, but these effects could invigorate
675 convection and rainfall in the downwind mountainous area at nighttime (Fan et al., 2015). On the
676 other hand, how anthropogenic aerosols act in the ice nucleation processes is still open to question

677 (Zhao et al., 2019) and these processes need to be represented accurately in two-way coupled models,
678 however until now no study had been performed to simulate the ACI effects of anthropogenic
679 aerosol serving as IN in Asia using two-way coupled models. Therefore, in Asia, further
680 investigations are needed that targeting cloud or/and ice processes involving anthropogenic aerosols
681 (including their size, composition, and mixing state) in two-way coupled models. Meanwhile,
682 several studies not only discussed aerosol feedbacks but also focused on the additional effects of
683 topography or urban heat island on meteorology (Zhong et al., 2015, 2017; Wang et al., 2019a).
684 Utilizing the GATOR-GCMOM model at global and local scales, Jacobson et al. (2015, 2019)
685 explored the impacts of landuse changes due to the unprecedented expansions of megacities, such
686 as Beijing and New Delhi in Asia, from 2000 to 2009 on meteorology and air quality.

687 Hitherto there were several attempts to ascertain the effects of different chemical components
688 of anthropogenic aerosols on meteorology in Asia (Huang et al., 2015; Ding et al., 2016, 2019; Gao
689 et al., 2018a; Wang et al., 2018d; Archer-Nicholls et al., 2019). First of all, Asia is the region in the
690 world with the highest BC emissions due to burning of large amount of fossil fuels and biomass and
691 this has increasingly attracted many researchers to probe into the ARI or/and ACI effects of BC
692 (IPCC, 2014). As the most important absorbing aerosol, BC induced the largest positive, positive
693 and negative mean DRF at the TOA, in the ATM, and at the surface, respectively, over China during
694 2006 (Huang et al., 2015). Ding et al. (2016) and Wang et al. (2018d) further applied WRF-Chem
695 with feedbacks to investigate how aerosol-PBL interactions involving BC suppressed the PBL
696 development, which deteriorated air quality in Chinese cities and was described as “dome effect”
697 (namely BC warms the atmosphere and cools the surface, suppresses the PBL development and
698 eventually results in more accumulation of pollutants). This “dome effect” of BC promoted the
699 advection-radiation fog and fog-haze formation in the YRD area through altering the land-sea
700 circulation pattern and increasing the moisture level (Ding et al., 2019). Gao et al. (2018a) also
701 pointed out BC in the ATM modified the vertical profiles of heating rate and equivalent potential
702 temperature in Nanjing, China. In India, the ARI effects of BC enhanced convective activities,
703 meridional flows, and rainfall in North-East India during the pre-monsoon season but could either
704 enhance or suppress precipitation during the monsoon season in different parts of the India
705 subcontinent (Soni et al., 2018). Moreover, the ARI effects of BC on surface meteorological
706 variables were larger than its ACI effects in EC (Archer-Nicholls et al., 2019; Ding et al., 2019).
707 Besides BC, the BrC portion of organic aerosols (OA) emitted from agriculture residue burning
708 (ARB) were included in WRF-Chem with the parameterization scheme suggested by Saleh et al.
709 (2014) and the model simulations in EC revealed that at the TOA, the net DRF of OA was -0.22
710 $\text{W}\cdot\text{m}^{-2}$ (absorption and scattering DRF were $+0.21$ $\text{W}\cdot\text{m}^{-2}$ and -0.43 $\text{W}\cdot\text{m}^{-2}$ respectively), but the
711 BC’s DRF was still the highest ($+0.79$ $\text{W}\cdot\text{m}^{-2}$) (Yao et al., 2017). As mentioned above, it is obvious
712 that ARI and ACI effects of different aerosol components are substantially distinctive, and many
713 other aerosol compositions (e.g., sulfate, nitrate and ammonium) besides BC and BrC should be
714 taken into considerations in future modeling studies in Asia.

715 ARB is a common practice in many Asian countries after harvesting and before planting and
716 can deteriorate air quality quickly as one of the most important sources of anthropogenic aerosols,
717 so that it has been attracting much attention among the public and scientists worldwide (Reid et al.,
718 2005; Koch and Del Genio, 2010; Chen et al., 2017a; Yan et al., 2018; Hodshire et al., 2019).
719 Recently, the effects of ARB aerosols on meteorology had widely been explored using the two-way
720 coupled model (WRF-Chem) in many Asian countries and regions, such as EC (Huang et al., 2016;
721 Wu et al., 2017; Yao et al., 2017; Li et al., 2018b), South China (SC) (Huang et al., 2019), and South
722 Asia (SA) (Singh et al., 2020). In general, when ARB occurred, the WRF-Chem simulations from
723 all the studies showed that the changes in radiative forcing induced by ARB aerosols were greater
724 than by those from other anthropogenic sources, especially in the ATM. Also all the modeling studies
725 indicated that ARB aerosols reduced (increased) radiative forcing at the surface (in the ATM), cooled
726 (warmed) the surface (the atmosphere), and increased (decreased) atmospheric stability (PBLH).
727 Furthermore, the WRF-Chem simulations with ARI demonstrated that light-absorbing carbonaceous
728 aerosols (CAs) from ARB caused daytime (nighttime) precipitation decreased (increased) over
729 Nanjing in EC during a post-harvest ARB event (Huang et al., 2016). Yao et al. (2017) pointed out
730 their WRF-Chem simulations in EC exhibited larger DRE induced by BC from ARB at the TOA
731 than previous studies. Lately, several modeling studies using WRF-Chem had targeted the effects of
732 ARI and both ARI and ACI due to ARB aerosols from countries in the Indochina, SEA, and SA
733 regions during the planting and harvesting time (Zhou et al., 2018; Dong et al., 2019; Huang et al.,

734 2019; Singh et al., 2020). Zhou et al. (2018) investigated how ARB aerosols from SEA mixed with
735 mineral dust and other anthropogenic aerosols while being lifted to the mid-low troposphere over
736 the source region and transported to the YRD area and then affected meteorology and air quality
737 there. The influences of ARI and ACI caused by ARB aerosols from Indochina were contrary,
738 namely, the ARI (ACI) effects made the atmosphere over SC warmer (cooler) and drier (wetter),
739 and the ARI effects hindered cloud formation and suppressed precipitation there (Huang et al., 2019).
740 Dong et al. (2019) found the warming ARI effects of ARB aerosols were smaller over the source
741 region (i.e., SEA) than the downwind region (i.e., SC) with cloudier conditions. Annual simulations
742 regarding the ARI effects of ARB aerosols from SA (especially Myanmar and Punjab) indicated that
743 CAs released by ARB reduced the radiative forcing at the TOA but did not change the precipitation
744 processes much when only the ARI effects were considered in WRF-Chem (Singh et al., 2020).

745 Besides ARB, to our best knowledge, there were only a few research work quantitatively
746 assessing the effects of anthropogenic aerosols from different emission sources on meteorology
747 using WRF-Chem. Gao et al. (2018c) evaluated the responses of radiative forcing in China and India
748 to aerosols from five emission sectors (power, industry, residential, BB, and transportation), and
749 found that the power (residential) sector was the dominate contributor to the negative (positive)
750 DRF at the TOA over both countries due to high emissions of sulfate and nitrate precursors (BC
751 and the total sectoral contributions were in the order of power > residential > industry > BB >
752 transportation (power > residential > transportation > industry > BB) for China (India) during 2013.
753 To pinpoint the ARI and ACI effects, Archer-Nicholls et al. (2019) reported that during January
754 2014, the aerosols from the residential emission sector induced larger SWRF (+1.04 W·m⁻²) than
755 LWRF (+0.18 W·m⁻²) at the TOA and their DRF (+0.79 W·m⁻²) was the largest, followed by their
756 semidirect effects (+0.54 W·m⁻²) and indirect effects (-0.29 W·m⁻²) over EC. This study further
757 emphasized a realistic ratio of BC to total carbon from the residential emission was critical for
758 accurate simulations of the ARI and ACI effects with two-way coupled models.

759 In terms of anthropogenic aerosol effects on air quality, the responses of PM_{2.5} had been widely
760 investigated (Wang et al., 2014a, c, 2015a; Gao et al., 2015b, 2016a, 2018a; Zhang et al., 2015a,
761 2018; Zhao et al., 2017; Chen et al., 2019a; Nguyen et al., 2019a, b; Wu et al., 2019a) but less studies
762 explored the responses of O₃ and other species (Kumar et al., 2012a; Zhang et al., 2015a; Xing et
763 al., 2017; Li et al., 2018a; Nguyen et al., 2019a, b). As summarized by Wu et al. (2019a) in their
764 Table 1, observations and model simulations with WRF-Chem, WRF-CMAQ, WRF-CMAQ,
765 GRAPES-CUACE, and WRF-NAQPMS all pointed out that the ARI effects promoted higher PM_{2.5}
766 concentrations in China (Wang et al., 2014a, c, 2015a; Gao et al., 2015b, 2016a; Zhang et al., 2015a,
767 2018; Chen et al., 2019a) and this was also true in other areas of Asia (e.g., India, EA, Continental
768 SEA) (Gao et al., 2018c; Nguyen et al., 2019a, b) during different seasons. At the same time, all the
769 modeling investigations revealed that the positive aerosol-meteorology feedbacks could further
770 exacerbate pollution problems during heavy haze episodes. Based on WRF-Chem simulations, the
771 ACI effects on PM_{2.5} was negligible comparing to the ARI effects over EC (Zhang et al., 2015a) but
772 was subject to a certain degree of uncertainty if no consideration of the ACI effects induced by
773 cumulus clouds in the model (Gao et al., 2015b). Annual WRF-Chem simulations for 2014 by Zhang
774 et al. (2018) indicated that even though the ARI effects had bigger impacts on PM_{2.5} during
775 wintertime than the ACI effects, the ARI and ACI impacts on PM_{2.5} were similar during other
776 seasons and the increase of PM_{2.5} due to the ACI effects was more noticeable in wet season than dry
777 season. Using the process analysis method to distinguish the contributions of different physical and
778 chemical processes to PM_{2.5} over the NCP area, Chen et al. (2019a) applied WRF-Chem with ARI
779 and ACI and found that besides local emissions and regional transport processes, vertical mixing
780 contributed the most to the accumulation and dispersion of PM_{2.5}, comparing to chemistry and
781 advection, and the ARI effects changed the vertical mixing contribution to daily PM_{2.5} variation
782 from negative to positive. Regarding surface O₃ concentrations, all the two-way coupled models
783 with ARI, ACI, and both ARI and ACI predicted reduced photolysis rate and O₃ concentrations
784 under heavy pollution conditions, through the radiation attenuation induced by aerosols and clouds.
785 Further analyses indicated that the ARI effects impacted O₃ positively through reducing vertical
786 dispersions (WRF-CMAQ, Xing et al., 2017), reduced O₃ more during wintertime than summertime
787 in EC (WRF-NAQPMS, Li et al., 2018a), and suppressed (enhanced) O₃ in dry (wet) season in
788 continental SEA (WRF-CMAQ, Nguyen et al., 2019b). Xing et al. (2017) applied the process
789 analysis method in WRF-CMAQ with ARI and revealed that the impacts of ARI on the contributions
790 of atmospheric dynamics and photochemistry processes to O₃ over China varied in winter and

791 summer months and ARI induced largest changes in photochemistry (dry deposition) of surface O₃
792 at noon time in January (July). The process analysis in WRF-Chem with ARI and ACI identified
793 that the vertical mixing process played the most important role among the other physical and
794 chemical processes (advection and photochemistry) in surface O₃ growth during 10-14 local time in
795 Nanjing, China (Gao et al., 2018a). ARI and ACI not only affected PM_{2.5} and O₃, but also other
796 chemical species. For instance, CO and SO₂ increased due to ARI and ACI over EC (Zhang et al.,
797 2015a), ARI caused midday (daily average) OH increased (decreased) in July (January) over China
798 (Xing et al., 2017), SO₂, NO₂, BC, SO₄²⁻, NO₃⁻ were enhanced but OH was reduced over China by
799 ACI (Zhao et al., 2017), and ARI impacted SO₂ and NO₂ positively over EA (Nguyen et al., 2019a).
800 Wu et al. (2019b) further analyzed how the aerosol liquid water involved in ARI and chemical
801 processes (i.e., photochemistry and heterogeneous reactions) and influenced radiation and PM_{2.5}
802 (esp. secondary aerosols) over NCP during an intense haze event. Moreover, evaluations and
803 sensitivity studies indicated that turning on aerosol feedbacks could improve the model performance
804 for surface PM_{2.5}, particularly during severe haze episodes (Zhang et al., 2015a, 2018; Li et al.,
805 2018a; Wang et al., 2018a).

806 With reference to the feedback effects of anthropogenic aerosol compositions on air quality,
807 most modeling research work with WRF-Chem had focused on the ARI and ACI effects of BC and
808 BrC, especially the “dome effect” that prompted the accumulation of pollutants (aerosols and O₃)
809 near surface and in PBL (Li and Liao, 2014; Ding et al., 2016, 2019; Gao et al., 2018a; Wang et al.,
810 2018d). At the same time, the ARI effects of BC undermined the low-level wind convergence and
811 then led to decrease of aerosols (sulfate and nitrate) and O₃ (Li and Liao, 2014). With the process
812 analysis methodology in WRF-Chem, Gao et al. (2018a) indicated that comparing to simulations
813 without BC, the BC and PBL interaction slowed the O₃ growth from late morning to early afternoon
814 somewhat before O₃ reaching its maximum value at noon due to less vertical mixing in PBL.

815 Studies on the feedback effects of aerosols from different emission sectors on air quality were
816 relatively limited and mainly involved with ARB emissions and assessments of emission controls
817 during certain major air pollution events. Jena et al. (2015) applied WRF-Chem with aerosol
818 feedbacks and investigated O₃ and its precursors in SA due to regional ARB. Based on WRF-Chem
819 simulations with enabling ARI and ACI, Wu et al. (2017) denoted that aerosols emitted from ARB
820 could be mixed or/and coated with urban aerosols while being transported to cities and contributed
821 to heavy air pollution events there, such as in Nanjing, China. The ARI effects induced by ARB
822 aerosols on O₃ and NO₂ concentrations (-1 % and 2 %, respectively) were small compared to the
823 contribution of precursors emitted from ARB to O₃ chemistry (40 %) in the ARB zone (Li et al.,
824 2018b). Pollutants emitted from natural and anthropogenic BB over Indochina affected pollution
825 levels over SC and their ACI effects removed aerosols more efficiently than the ARI effects that
826 could make BB aerosols last longer in the ATM (Huang et al., 2019). Gao et al. (2017b) and Zhou
827 et al. (2019) both utilized WRF-Chem to evaluate what role the ARI effects played when dramatic
828 emission reductions implemented during the week of Asia Pacific Economic Cooperation Summit
829 and concluded that the ARI reduction induced by decreased emission led to 6.7-10.9 % decline in
830 PM_{2.5} concentrations in Beijing.

831

832 4.3 Human health effects

833 Poor air quality posts risks to human health (Brunekreef and Holgate, 2002; Manisalidis et al.,
834 2020), therefore, in the past several decades, air quality models had been used in epidemiology
835 related research to establish quantitative relationships between concentrations of various pollutants
836 and burden of disease (including mortality or/and morbidity) as well as associated economic loss
837 (Conti et al., 2017). In Asia, there were several studies that applied coupled air quality models with
838 feedbacks to assess human health effects of air pollutants under historical and future scenarios (Gao
839 et al., 2015a, 2017c; Ghude et al., 2016; Xing et al., 2016; Wang et al., 2017; Conibear et al., 2018a,
840 b; Hong et al., 2019; Zhong et al., 2019). By applying WRF-Chem with ARI and ACI, Gao et al.
841 (2015a) estimated the health and financial impacts induced by an intense air pollution event
842 happened in the NCP area during January, 2013 and concluded that the mortality, morbidity, and
843 financial loss over Beijing area were 690, 69070, and 253.8 million US\$, respectively. Targeting
844 the same case, Gao et al. (2017c) pointed out that turning on the data assimilation of surface PM_{2.5}
845 observations in WRF-Chem not only improved model simulations but also made the premature
846 death numbers increased by 2 % in the NCP area, comparing to simulations without the PM_{2.5} data
847 assimilation. In India, WRF-Chem simulations with aerosol feedbacks and updated population data

848 revealed that the premature (COPD related) deaths caused by PM_{2.5} (O₃) were 570,000 (12,000),
849 resulting in shortened life expectancy (3.4±1.1 years) and financial expenses (640 million US\$)
850 during 2011 (Ghude et al., 2016). Based on WRF-CMAQ simulations with ARI for 21 years (1990-
851 2010), Xing et al. (2016) pointed out that in EA the population-weighted PM_{2.5} induced mortality
852 had an upward trend from 1990 (+3187) to 2010 (+3548) and the mean mortality caused by ARI-
853 enhanced PM_{2.5} was 3.68 times more than that decreased by ARI-reduced temperature. The same
854 21 year simulations also showed that from 1990 to 2010, the PM_{2.5} related mortalities in EA and
855 SA rose by 21 % and 85 %, respectively, while they declined in Europe and high-income North
856 America by 67 % and 58 %, respectively (Wang et al., 2017). Conibear et al. (2018a) applied WRF-
857 Chem with ARI to study how different emission sectors affected human health in India and
858 demonstrated that the residential energy use sector played the most critical role among other sectors
859 and could cause 511,000 premature deaths in 2014. Furthermore, Conibear et al. (2018b)
860 investigated future PM_{2.5} pollution levels as well as health impacts in India under different emission
861 scenarios (business as usual and two emission control pathways) and deduced that the burden of
862 disease driven by PM_{2.5} and population factors (growth and aging) in 2050 increased by 75 % under
863 the business as usual scenario but decreased by 9 % and 91 % under the International Energy
864 Agencies New Policy Scenario and Clean Air Scenario, respectively, comparing with that in 2015.
865 The sensitivity study using WRF-Chem with ARI under a variety of emission scenarios, population
866 projections, and concentration-response functions (CRFs) for the years of 2008 and 2050
867 demonstrated that CRFs (future emission projections) were the main sources of uncertainty in the
868 total mortality estimations related to PM_{2.5} (O₃) in China (Zhong et al., 2019). Applying a suite of
869 models, including WRF-CMAQ with ARI, climate and epidemiology, Hong et al. (2019) inferred
870 that under Representative Concentration Pathway 4.5, the future mortalities could be 12100 and
871 8900 per year in China led by PM_{2.5} and O₃, respectively, and the climate-driven weather extremes
872 could add 39 % and 6 % to future mortalities due to stable atmosphere and heat waves, respectively.
873 Ten Hoeve and Jacobson (2012) applied GATOR-GCMOM and a human exposure model to
874 estimate the local and worldwide health effects induced by the 2011 Fukushima nuclear accident
875 and a hypothetical one in California of US.

876

877 **5 Effects of aerosol feedbacks on model performance**

878 Even though there are a certain number of research papers using two-way coupled models to
879 quantify the effects of aerosol feedbacks on regional meteorology and air quality in Asia, model
880 performances impacted by considering aerosol effects varied to some extent. This section provides
881 a summary of model performance by presenting the SI of meteorology and air quality variables as
882 shown in Table S2. These SI were collected from the selected papers that supplying these indices
883 and being defined as papers with SI (PSI) (listed in Tables B2-B3 of Appendix B). As
884 aforementioned in Section 3, investigations of ACI effects were very limited and no former studies
885 simultaneously exploring aerosol feedbacks with and without both ARI and ACI turned on. Here,
886 we only compared the SI for simulations with and without ARI in the same study, as summarized in
887 Appendix Tables B4-B5. It should be pointed out that all the reported evaluation results either from
888 individual model or inter-model comparison studies were extracted and put into the Table S2.

889

890 **5.1 Model performance for meteorology variables**

891 With certain emissions, accurate simulations of meteorological elements are critical to air
892 quality modeling and prediction (Seaman, 2000; Bauer et al., 2015; Appel et al., 2017; Saylor et al.,
893 2019). Targeting meteorological variables, we summarized their SI and further analyzed the
894 variations of SI on different simulated time scales and among multiple models.

895

896 **5.1.1 Overall performance**

897 Figure 3 shows the compiled statistical indicators (correlation coefficient (R) is in black, and
898 mean bias (MB) and root mean square error (RMSE) are in blue) of T2 (°C), RH2(%) and specific
899 humidity (SH2, g·kg⁻¹) at 2 meters, and WS10 (m·s⁻¹) from PSI (a-d), and simulations with and
900 without ARI (marked as ARI and NO-ARI in e-h). In this figure and following figures, NP and NS
901 are number of publications and samples with SI, respectively and summed up in Appendix Table
902 B2. In these two tables, we also listed the NS of positive (red upward arrow) and negative (blue
903 downward arrow) biases for the meteorological and air quality variables in parentheses in the MB

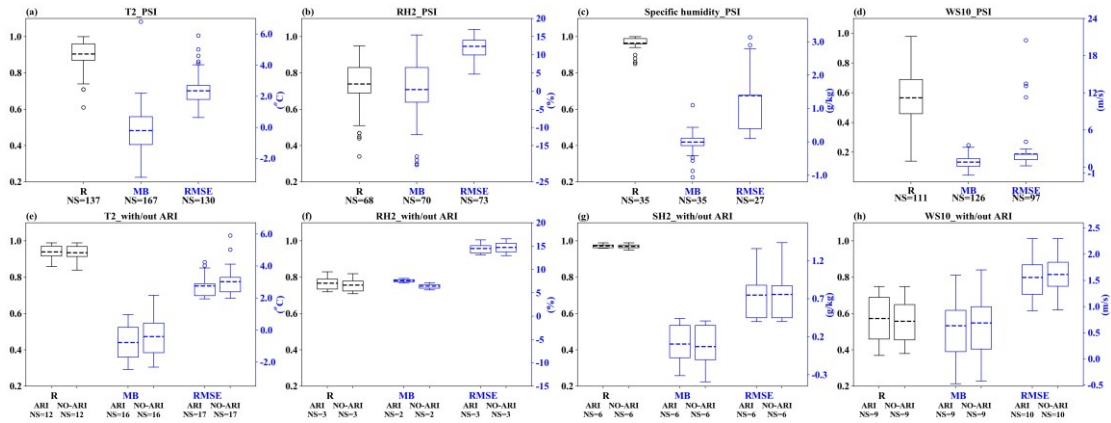
904 column. Note that NS in Fig. 3e-h and Appendix Table B4 counted the samples of SI provided by
905 the simulations simultaneously with and without ARI. Also, the 5th, 25th, 75th and 95th percentiles
906 of SI are illustrated in box-and-whisker plots, and the dashed line in the box is the mean value (not
907 median) and the circles are outliers.

908 The evaluations for T2 (Fig. 3a) from PSI revealed that in Asia coupled models performed
909 rather well for temperature (mean $R = 0.90$) with RMSE ranging from 0.64 to 5.90 °C, but 60 % of
910 samples showed the tendency towards temperature underestimations (mean value of MB = -0.20 °C)
911 with the largest average MB (-0.31 °C) occurring during winter months (70 samples). The
912 underestimations of temperature had been reported not only from modeling studies by using WRF
913 or coupled models, but also in Asia, Europe and North America (García-Díez et al., 2013; Brunner
914 et al., 2015; Makar et al., 2015a; Yahya et al., 2015; Gao et al., 2019). The WRF simulations in
915 China (Gao et al., 2019) and US (EPA, 2018) also showed wintertime cold biases of T2 but in Europe
916 warm biases were reported (García-Díez et al., 2013). This temperature bias was probably related
917 to the impacts of model resolutions (Kuik et al., 2016), urban canopies (Liao et al., 2014) and PBL
918 schemes (Hu et al., 2013). With the ARI turned on in the coupled models, modeled temperatures
919 (limited papers with 12 samples) were improved somewhat and the mean correlation coefficient
920 increased from 0.93 to 0.95 and RMSE decreased slightly (Fig. 3e), but average MB of temperature
921 was decreased from -0.98 to -1.24 °C. In short, temperatures from PSI or simulations with/without
922 ARI turned on agreed well with observations but were mostly underestimated, and the negative bias
923 of T2 simulated by models with ARI turned on got worse and reasons behind it will be explained in
924 Section 6.

925 Figures 3b-c illustrate that RH2 was simulated reasonably well (mean $R = 0.73$) and the
926 modeled SH2 was also well correlated with observations (R varied between 0.85 and 1.00). RH2
927 and SH2 from more than half of samples had slightly positive and negative mean biases with average
928 MB values of 0.4 % and -0.01 $\text{g}\cdot\text{kg}^{-1}$, respectively. The overestimations of RH2 could be caused by
929 the negative bias of T2 (Cuchiara et al., 2014). Compared with results without ARI effects, statistics
930 of RH2 and SH2 from simulations with ARI showed better R and RMSE. However, the increased
931 positive mean biases (average MBs of RH2 and SH2 were from 6.4 % to 7.6 % and from 0.07 $\text{g}\cdot\text{kg}^{-1}$
932 to 0.11 $\text{g}\cdot\text{kg}^{-1}$, respectively) indicated that turning on ARI could cause further overprediction of
933 humidity variables. Overall, the modeled RH2 and SH2 were in good agreement with observations
934 with slight over- and under-estimations, respectively, and the limited studies showed that RH2 and
935 SH2 simulated by models with ARI turned on had marginally larger positive biases relative to the
936 results without ARI.

937 Compared with the correlation coefficients of T2, RH2 and SH2, mean R (0.59) of WS10 was
938 smallest with a large fluctuation ranging from 0.14 to 0.98 (Fig. 3d). The meta-analysis also
939 indicated that most modeled WS10 tended to be overestimated (81 % of the samples) with the
940 average MB value of 0.79 $\text{m}\cdot\text{s}^{-1}$, and the mean RMSE value was 2.76 $\text{m}\cdot\text{s}^{-1}$. The general
941 overpredictions of WS10 by WRF (Mass and Ovens, 2011) and coupled models (Gao et al., 2015b,
942 2015bs) had been explained with possible reasons such as out-of-date geographical data, coarse
943 model resolutions and lacking of better representations of urban canopy physics. The PSI with ARI
944 effects suggested that the correlation of wind speed was slightly improved (mean R from 0.56 to
945 0.57) and the average RMSE and positive MB decreased by 0.003 $\text{m}\cdot\text{s}^{-1}$ and 0.051 $\text{m}\cdot\text{s}^{-1}$,
946 respectively (Fig. 3h). The collected SI indicated relatively poor performance of modeled WS10
947 (most wind speeds were overestimated) compared to T2 and humidity, but turning on ARI in coupled
948 models could improve WS10 simulations somewhat.

949 Besides the SI discussed above, very limited papers reported the normalized mean error (NME)
950 (%) of surface meteorological variables (T2, SH2, RH2 and WS10) simulated by two-way coupled
951 models (WRF-Chem and WRF-CMAQ) in Asia, which is summarized in Appendix Table B7. The
952 evaluations with two-way coupled models in Asia showed that the overall mean percent errors of
953 T2, SH2, RH2 and WS10 were 22.71%, 10.32%, 13.94%, and 51.28%, respectively. The ranges of
954 NME (%) values were quite wide for T2 (from -0.48 to 270.20 %) and WS10 (from 0.33 to 112.28%)
955 reported by the limited studies. Note that no NME of surface meteorological variables simulated by
956 two-way coupled models simultaneously with and without enabling the ARI effects was mentioned
957 in these studies.



958

959

960

961

962

963

Figure 3. Quantile distributions of R, MB and RMSE for simulated surface meteorological variables by the five coupled models (WRF-Chem, WRF-CMAQ, GRAPES-CUACE, WRF-NAQPMS and GATOR-GCMOM) (a-d) and comparisons of statistical indices with/out ARI (e-h) in Asia.

5.1.2 Comparisons of SI for meteorology using different coupled models

964

965

966

967

968

969

970

971

Also, to examine how different coupled models (i.e., WRF-Chem, WRF-CMAQ, WRF-NAQPMS, GRAPES-CUACE and GATOR-GCMOM) performed in Asia with respect to meteorological variables, the SI were extracted from PSI in term of these five coupled models and displayed in Fig. 4. The SI for T2, RH2, SH2, and WS10 from WRF-NAQPMS, GRAPES-CUACE and GATOR-GCMOM simulations were missing or with rather limited samples so that the discussions here only focused on the WRF-Chem and WRF-CMAQ simulations. Moreover, the SI sample size from studies involving WRF-Chem was generally larger than that involving WRF-CMAQ, except for SH2.

972

973

974

975

976

977

As seen in Fig. 4a, the modeled T2 by both WRF-CMAQ and WRF-Chem was well correlated with observations but WRF-CMAQ (mean R = 0.95) outperformed WRF-Chem (mean R = 0.90) to some extent. On the other hand, WRF-CMAQ underestimated T2 (mean MB = -1.39 °C) but WRF-Chem slightly overestimated it (mean MB = 0.09 °C) (Fig. 4e). The RMSE of modeled T2 by both models was at the similar level with mean RMSE values of 2.51 °C and 2.31 °C by WRF-CMAQ and WRF-Chem simulations, respectively (Fig. 4i).

978

979

980

981

982

983

984

985

986

987

988

Both WRF-Chem and WRF-CMAQ performed better for SH2 (mean R = 0.96 and 0.97, respectively) than RH2 (mean R = 0.75 and 0.73, respectively) (Figures 4b and 4c), which might be due to the influence of temperature on RH2 (Bei et al., 2017). Also the modeled RH2 (SH2) by WRF-Chem correlated better (worsen) with observations than those by WRF-CMAQ. The mean RMSE of modeled RH2 (Fig. 4j) by WRF-Chem (11.1 %) was lower than that by WRF-CMAQ (14.3%) but the mean RMSE of modeled SH2 (Fig. 4k) by WRF-Chem (2.25 g·kg⁻¹) higher than that by WRF-CMAQ (0.71 g·kg⁻¹). It was seen in Figures 4f and 4d that WRF-CMAQ overestimated RH2 and SH2 (average MB were 5.30 % and 0.07 g·kg⁻¹, respectively), and WRF-Chem underpredicted RH2 (average MB = -0.32 %) and SH2 (average MB = -0.06 g·kg⁻¹). Generally, the modeled RH2 and SH2 were reproduced more reasonably by WRF-Chem than those by WRF-CMAQ.

989

990

991

992

993

994

The modeled WS10 by both WRF-Chem and WRF-CMAQ (Fig. 4d) correlated with observations on the same level with the mean R of 0.56. The mean RMSE of modeled WS10 by WRF-Chem and WRF-CMAQ were 1.54 m·s⁻¹ and 2.28 m·s⁻¹, respectively, as depicted in Fig. 4l. Both models overpredicted WS10 to some extent with average MBs of 0.55 m·s⁻¹ (WRF-CAMQ) and 0.84 m·s⁻¹ (WRF-Chem), respectively. These results demonstrated that overall WRF-CMAQ and WRF-Chem had similar model performance of WS10.

995

996

997

998

999

1000

1001

1002

In general, WRF-CMAQ performed better than WRF-Chem for T2 but worse for humidity (RH2 and SH2), and both models' performance for WS10 was very similar. WRF-Chem overestimated T2, RH2 and WS10 and underestimated SH2 slightly, while WRF-CMAQ overpredicted humidity and WS10 but underpredicted T2. Compared to WRF-Chem and WRF-CMAQ, the very few SI samples indicated that for the meteorological variables excluding SH2, WRF-NAQPMS simulations matched with observations better than GRAPES-CUACE simulations but more applications and statistical analysis of these two models are needed to make this kind of comparison conclusive.

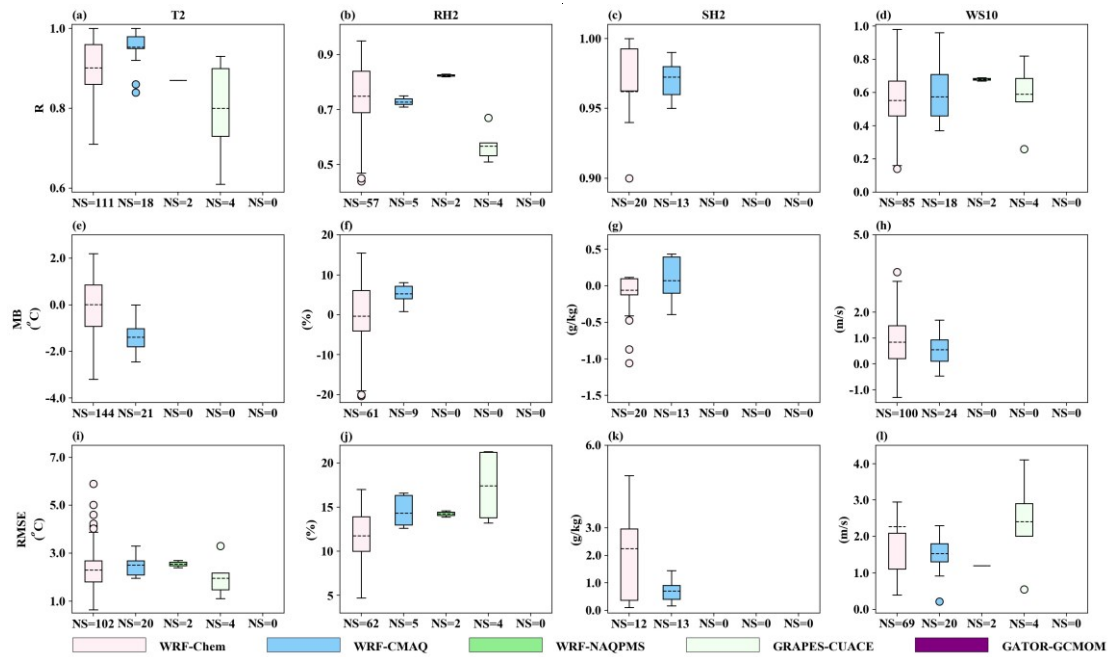


Figure 4. Quantile distributions of the statistical indices for simulated surface meteorological variables by WRF-Chem, WRF-CMAQ, GRAPES-CUACE, WRF-NAQPMS and GATOR-GCMOM in Asia.

1005
1006
1007
1008
1009
1010

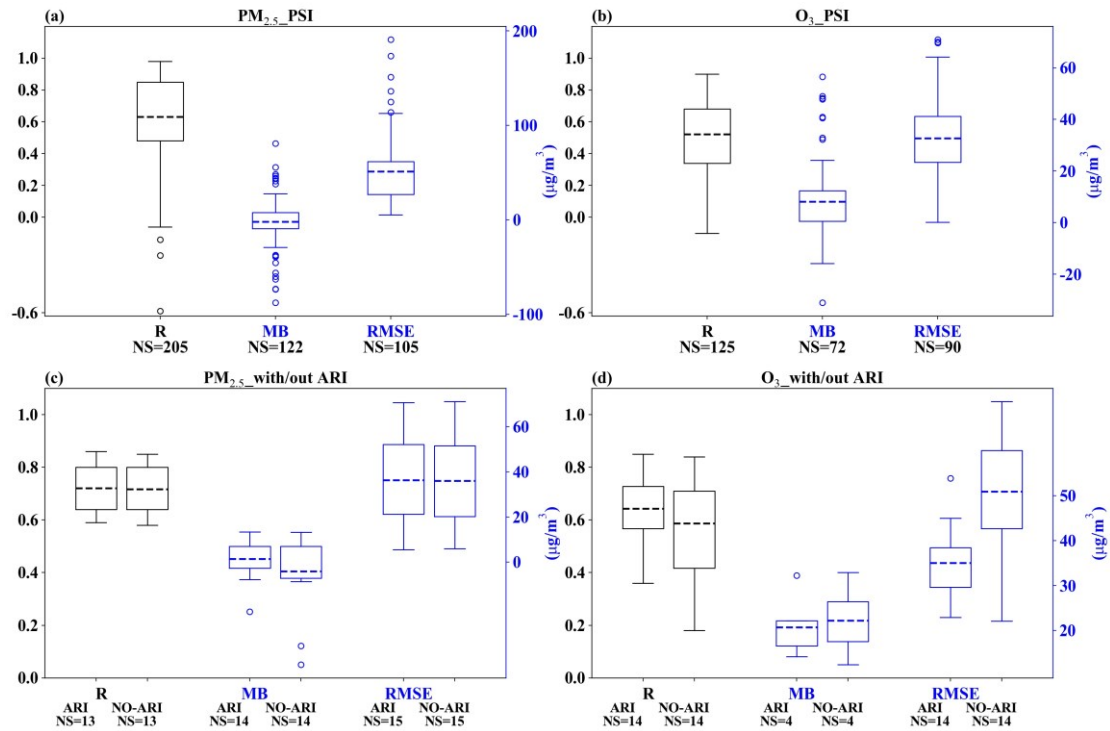
5.2 Model performance for air quality variables

5.2.1 Overall performance

1011 The results of the overall statistical evaluation for the online air quality simulations are
1012 presented in Figure 5, and all labels and colors indicating SI were the same as those for
1013 meteorological variables. In this figure and following figures, NP and NS are number of publications
1014 and samples with SI, respectively and summed up in Appendix Table B3. In Fig. 5a, the correlation
1015 between the simulated and observed $PM_{2.5}$ concentrations from PSI showed that in Asia coupled
1016 models performed relatively well for $PM_{2.5}$ (mean $R = 0.63$), but RMSE was between -87.60 and
1017 80.90 and more than half of samples of simulated $PM_{2.5}$ were underestimated (mean $MB = -2.08$
1018 $\mu\text{g}\cdot\text{m}^{-3}$). Note that NS in Fig. 5c-d and Appendix Table B5 counted the samples of SI provided by
1019 the simulations simultaneously with and without ARI. With the ARI turned on in the coupled models,
1020 modeled $PM_{2.5}$ concentrations (limited papers with 15 samples) were improved somewhat and the
1021 mean R slightly increased from 0.71 to 0.72 and mean absolute MB decreased from 4.10 to 1.33
1022 $\mu\text{g}\cdot\text{m}^{-3}$ (Fig. 5c), but RMSE of $PM_{2.5}$ concentrations slightly increased from 35.40 to 36.20
1023 $\mu\text{g}\cdot\text{m}^{-3}$. In short, $PM_{2.5}$ with/without ARI agreed well with observations but were mostly underestimated,
1024 and $PM_{2.5}$ bias simulated by models became overpredicted.

1025 Compared with $PM_{2.5}$, mean R (0.59) of O_3 was relatively smaller (Fig. 5b). The statistical
1026 analysis also showed the most modeled O_3 concentrations tended to be overestimated (76 % of the
1027 samples) with the average MB value of 8.05 $\mu\text{g}\cdot\text{m}^{-3}$, and the mean RMSE value was 32.65
1028 $\mu\text{g}\cdot\text{m}^{-3}$. The 14 PSI with ARI effects suggested that the correlation of O_3 was slightly improved (mean R
1029 from 0.58 to 0.64) and the average RMSE and MB were decreased by 15.93 $\mu\text{g}\cdot\text{m}^{-3}$ and 1.55 $\mu\text{g}\cdot\text{m}^{-3}$,
1030 respectively (Fig. 5d). The collected studies indicated relatively poor performance of modeled O_3
1031 compared to $PM_{2.5}$, but turning on ARI in coupled models improved O_3 simulations somewhat.

1032 In addition to the SI analyzed above and similar to the surface meteorological variables, the
1033 NME (%) of $PM_{2.5}$ and O_3 is listed in Table B7. The limited studies with WRF-Chem and WRF-
1034 CMAQ indicated that the overall mean percent errors of $PM_{2.5}$ and O_3 were 47.63% (from 29.55 to
1035 104.70 %) and 43.03% (from 21.10 to 127.00 %), respectively. With the ARI effects enabled in
1036 WRF-Chem in different seasons over the China domain, the NME (%) of $PM_{2.5}$ increased slightly
1037 during most seasons, except during a spring month with little change (Zhang et al., 2018). Another
1038 study by Nguyen et al. (2019b) revealed that the NME (%) of $PM_{2.5}$ and O_3 simulated by WRF-
1039 CMAQ became a little worse in SEA comparing to the simulations without ARI.



1040

1041 Figure 5. Quantile distributions of statistical indices for simulated PM_{2.5} and O₃ (a-b) by the five two-way coupled
 1042 models (WRF-Chem, WRF-CMAQ, GRAPES-CUACE, WRF-NAQPMS and GATOR-GCMOM) and comparisons
 1043 of statistical indices with/out ARI (c-d) in Asia.
 1044

1044

1045

5.2.2 Comparisons of SI for air quality using different coupled models

1046

1047

1048

1049

1050

1051

1052

1053

1054

1055

1056

1057

1058

1059

Figure 6 showed the SI for PM_{2.5} and O₃ from different coupled models, and only WRF-Chem and WRF-CMAQ simulations were discussed for the same reason as in Section 5.1.2. The modeled PM_{2.5} by WRF-CMAQ (mean R = 0.69) outperformed WRF-Chem (mean R = 0.62) to some extent (Fig. 6a) and the RMSE of modeled PM_{2.5} by WRF-CMAQ (33.24 μg·m⁻³) was smaller than that by WRF-Chem (56.16 μg·m⁻³). With respect to MB, WRF-CMAQ overestimated PM_{2.5} (mean MB = +1.60 μg·m⁻³) but WRF-Chem slightly underestimated it (mean R = -3.12 μg·m⁻³) (Fig. 6c). Figure 6b showed that the modeled O₃ by WRF-CMAQ (0.60) correlated better with observations than those by WRF-Chem (0.47), but the mean RMSE of modeled O₃ (Fig. 6f) by WRF-Chem (27.13 μg·m⁻³) was lower than that by WRF-CMAQ (35.19 μg·m⁻³). It was seen in Figures 6d that both WRF-CMAQ and WRF-Chem overestimated O₃, with mean MBs as 11.98 and 7.21 μg·m⁻³, respectively. Generally, the modeled PM_{2.5} and O₃ were reproduced more reasonably by WRF-CMAQ than by WRF-Chem, even though there were much more samples available from WRF-Chem simulations than WRF-CMAQ simulations.

1060

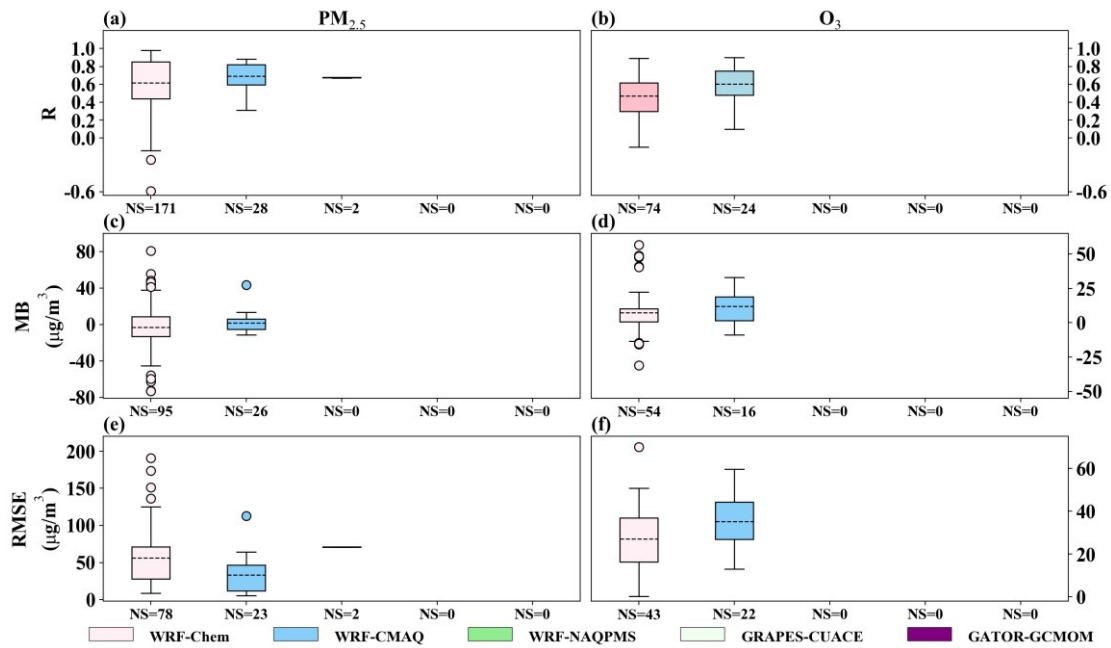


Figure 6. Quantile distributions of R, MB and RMSE of PM_{2.5} and O₃ simulated by WRF-Chem, WRF-CMAQ, GRAPES-CUACE, WRF-NAQPMS and GATOR-GCMOM in Asia.

6 Impacts of aerosol feedbacks in Asia

Aerosol feedbacks not only impact the performances of two-way coupled models but also the simulated meteorological and air quality variables to a certain extent. In this section, we collected and quantified the variations (Table S3) of these variables induced by ARI or/and ACI from the modeling studies in Asia. Due to limited sample sizes in the collected papers, the target variables only include radiative forcing, surface meteorological parameters (T2, RH2, SH2 and WS10), PBLH, cloud, precipitation, and PM_{2.5} and gaseous pollutants.

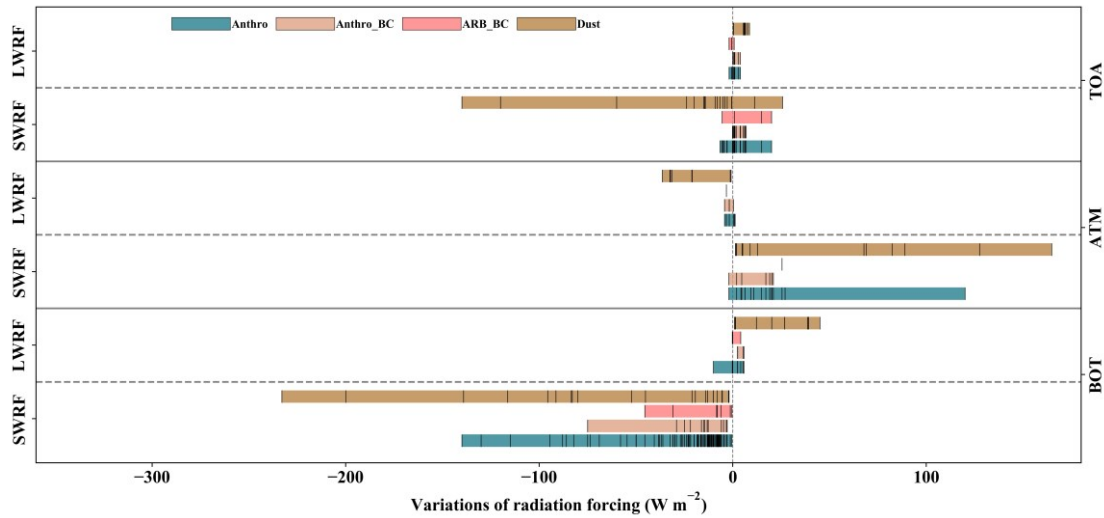
6.1 Impacts of aerosol feedbacks on meteorology

6.1.1 Radiative forcing

With regard to radiative forcing, most studies with two-way coupled models in Asia had focused on the effects of dust aerosols (Dust), BC emitted from ARB (ARB_BC) and anthropogenic sources (Anthro_BC), and total anthropogenic aerosols (Anthro). Figure 7 presents the variations of simulated SWRF and LWRF at the bottom (BOT) and TOA and in the ATM due to aerosol feedbacks, and detailed information of these variations are compiled in Table S5. In this figure, the color bars show the range of radiative forcing variations and the black tick marks inside the color bars represent these variations extracted from all the collected papers. It should be noted that in this figure all the radiative forcing variations were plotted regardless of temporal resolutions of data reporting and simulation durations. Apparently in Asia, most studies targeted the SWRF variations induced by anthropogenic aerosols at the BOT that exhibited the largest differences ranging from -140.00 to -0.45 W·m⁻², with the most variations (88 % of samples) concentrated in the range of -50.00 to -0.45 W·m⁻². The SWRF variations due to anthropogenic aerosols in the ATM and at the TOA were -2.00 to +120.00 W·m⁻² and -6.50 to 20.00 W·m⁻², respectively. There were much less studies reported LWRF variations caused by anthropogenic aerosols, which ranged from -10.00 to +5.78 W·m⁻², -1.91 to +3.94 W·m⁻², and -4.26 to +1.21 W·m⁻² at the BOT and TOA, and in the ATM, respectively.

Considering BC from anthropogenic sources and ARB, they both led to positive SWRF at the TOA (with mean values of 2.69 and 7.55 W·m⁻², respectively) and in the ATM (with mean values of 11.70 and 25.45 W·m⁻², respectively) but negative SWRF at the BOT (with mean values of -18.43 and -14.39 W·m⁻², respectively). The responses of LWRF to Anthro_BC and ARB_BC at the BOT (in the ATM) on average were 4.01 and 0.72 W·m⁻² (-1.89 and -3.24 W·m⁻²), respectively, and weak at the TOA (+0.92 and -0.53 W·m⁻², respectively). The SWRF variations induced by dust were in the range of -233.00 to -1.94 W·m⁻² and -140.00 to +25.70 W·m⁻², and +1.44 to +164.80 W·m⁻² at the BOT and TOA, and in the ATM, respectively. The LWRF variations caused by dust were the

1099 largest (with mean values of $22.83 \text{ W}\cdot\text{m}^{-2}$ and $+5.20 \text{ W}\cdot\text{m}^{-2}$, and $-22.12 \text{ W}\cdot\text{m}^{-2}$ at the BOT and TOA,
 1100 and in the ATM, respectively), comparing to the ones caused by anthropogenic aerosols and BC
 1101 aerosols from anthropogenic sources and ARB.
 1102



1103 Figure 7. Variations of shortwave and longwave radiative forcing (SWRF and LWRF) simulated by two-way
 1104 coupled models (WRF-Chem, WRF-CMAQ, GRAPES-CUACE, WRF-NAQPMS and GATOR-GCMOM) with
 1105 aerosol feedbacks at the bottom and top of atmosphere (BOT and TOA), and in the atmosphere (ATM) in Asia.
 1106
 1107

1108 As shown in Fig. 7, SWRF variations at the BOT caused by total aerosols (sum of Anthro,
 1109 Anthro_BC, ARB_BC and Dust) had been widely assessed in Asia. Therefore, we further analyzed
 1110 their spatiotemporal distributions and inter-regional differences, which are displayed in Fig. 8.
 1111 Figure 8a presents the SWRF variations over different areas of Asia (the acronyms used in Fig. 8
 1112 are listed in Appendix Table B1) at different time scales. In Asia, almost 41 % of the selected papers
 1113 investigated SWRF towards its monthly variations, 36 % towards its hourly and daily variations,
 1114 and 23 % towards its seasonal and yearly variations. Most studies reported aerosol-induced SWRF
 1115 variations were primarily conducted in NCP, EA, China, and India. At the hourly scale, the range of
 1116 SWRF decreases was from -350.00 to $-5.90 \text{ W}\cdot\text{m}^{-2}$ (mean value of $-106.92 \text{ W}\cdot\text{m}^{-2}$) during typical
 1117 pollution episodes, and significant variations occurred in EA. The daily and monthly mean SWRF
 1118 reductions varied from -73.71 to $-5.58 \text{ W}\cdot\text{m}^{-2}$ and -82.20 to $-0.45 \text{ W}\cdot\text{m}^{-2}$, respectively, with relative
 1119 large perturbations in NCP. At the seasonal and yearly scales, the SWRF changes ranged from $-$
 1120 22.54 to $-3.30 \text{ W}\cdot\text{m}^{-2}$ and -30.00 to $-2.90 \text{ W}\cdot\text{m}^{-2}$ with mean value of -11.28 and $-11.82 \text{ W}\cdot\text{m}^{-2}$,
 1121 respectively, with EA as the most researched area.

1122 To identify the differences of aerosol-induced SWRF variations between high- (Asia) and low-
 1123 polluted regions (Europe and North America), their inter-regional comparisons are depicted in Fig.
 1124 8b. This figure does not include information about temporal resolutions of data reporting and
 1125 durations of model simulations with ARI or/and ACI, but intends to delineate the range of SWRF
 1126 changes due to aerosol feedbacks. The SWRF variations fluctuated from -233.00 to $-0.45 \text{ W}\cdot\text{m}^{-2}$, $-$
 1127 100.00 to $-1.00 \text{ W}\cdot\text{m}^{-2}$, and -600.00 to $-1.00 \text{ W}\cdot\text{m}^{-2}$ in Asia, Europe, and North America, respectively.
 1128 It should be pointed out that the two extreme values were caused by dust ($-233.00 \text{ W}\cdot\text{m}^{-2}$) in Asia
 1129 and wildfire ($-600.00 \text{ W}\cdot\text{m}^{-2}$) in North America. Overall, the median value of SWRF reductions due
 1130 to ARI or/and ACI in Asia ($-15.92 \text{ W}\cdot\text{m}^{-2}$) was larger than those in North America ($-10.50 \text{ W}\cdot\text{m}^{-2}$)
 1131 and Europe ($-7.00 \text{ W}\cdot\text{m}^{-2}$).

1132
 1133

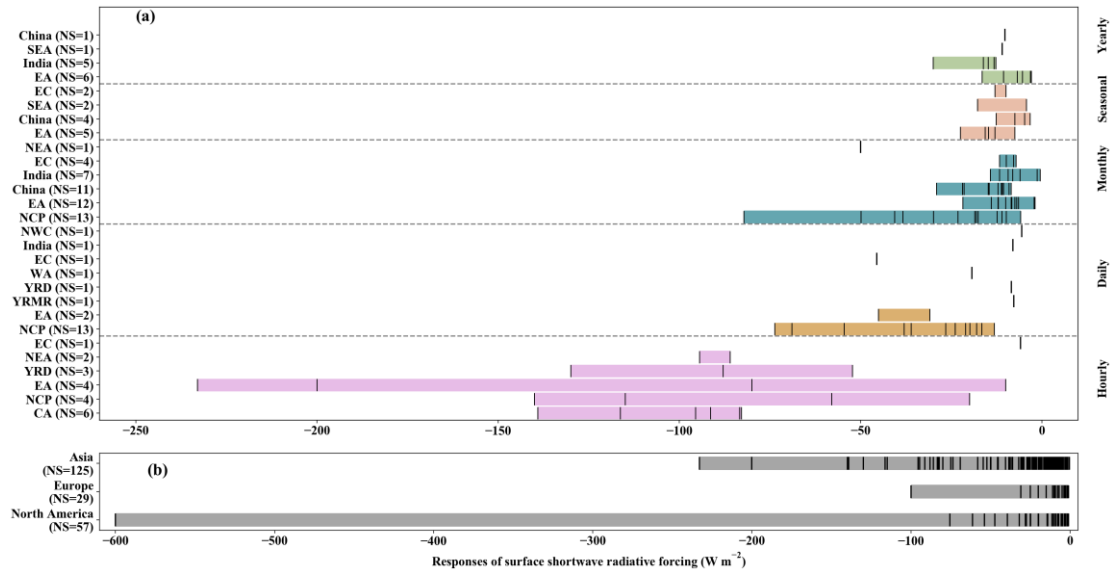


Figure 8. Responses of shortwave radiation forcing to aerosol feedbacks in different areas/periods in Asia (a) and the inter-regional comparisons of its variations in Asia, Europe and North America (b).

6.1.2 Temperature, wind speed, humidity and PBLH

The impact of aerosols on radiation can influence energy balance, which eventually alter other meteorological variables. The summary of aerosol-induced variations of T2, WS10, RH2, SH2 and PBLH in different regions of Asia as well as at different temporal scales are provided in Table 6. In this table, the minimum and maximum values were collected from the corresponding papers and the mean values were calculated with adding all the variations from these papers and then divided by the number of samples.

Overall, aerosol effects led to decreases of T2, WS10 and PBLH with average changes of -0.65 °C, -0.13 m·s⁻¹ and -60.70 m, respectively, and increases of humidity (mean Δ RH2 = 2.56 %) in most regions of Asia. On average, the hourly aerosol-induced changes of surface meteorological variables (T2, WS10 and RH2) and PBLH were the largest among the different time scales. At the hourly time scale, the mean variations of T2, WS10, RH2 and PBLH due to ARI or/and ACI were -1.85 °C, -0.32 m·s⁻¹, 4.60 % and -165.84 m, respectively, and their absolute maximum values in EC, YRD, NCP and NCP, respectively. Compared to variations at the hourly time scale, smaller daily variations of T2, WS10, RH2 and PBLH were caused by aerosol effects, and their mean values were -0.63 °C, -0.15 m·s⁻¹, +2.89 % and -34.61 m, respectively. The largest daily variations of T2, WS10, RH2 and PBLH occurred in NCP, EC, EC and SEC, respectively. For other time scales (monthly, seasonal and yearly), the respective mean variations of T2, RH2 and PBLH induced by aerosol effects were comparable. However, the WS10 perturbations at the monthly time scale were about two to three times higher than those at the seasonal and yearly time scales. High variations at the monthly, seasonal and yearly time scales were reported in NCP (T2, RH2 and PBLH), EA (T2, WS10 and PBLH) and PRD (T2 and PBLH), respectively. In addition, comparing to T2 and PBLH, the aerosol-induced variations of WS10 and humidity were less revealed.

Table 6. Summary of variations of surface meteorological variables and planetary boundary layer height (PBLH) caused by aerosol feedbacks simulated by two-way coupled models (WRF-Chem, WRF-CMAQ, GRAPES-CUACE, WRF-NAQPMS and GATOR-GCMOM) in different regions of Asia and at different temporal scales.

Region	Time scale	Δ T2 [mean] (°C)	Δ WS10 [mean] (m·s ⁻¹)	Δ RH2/SH2 [mean]	Δ PBLH [mean] (m)
EC	hours	-8.00 to -0.20 [-2.68]			-300.00 to -50.00 [-175.00]
EA	hours	-3.00 to -2.00 [-2.50]			
YRD	hours	-1.40 to -1.00 [-1.15]	-0.80 to -0.10 [-0.41]		-276.00 to -29.90 [-105.42]
NCP	hours	-2.80 to -0.20 [-1.05]	-0.30 to -0.10 [-0.23]	1.00 % to 12.00 % [4.60 %]	-287.20 to -147.00 [-217.10]
Hourly mean		-1.85	-0.32	4.60%	-165.84
NCP	days	-2.00 to -0.10 [-0.88]	-0.4 to -0.01 [-0.17]	0.51 % to 4.10 % [2.52 %]	-111.40 to -10.00 [-49.07]

EC	days	-0.94 to -0.65 [-0.79]	-0.52 to -0.37 [-0.45]	1.92 % to 9.75 % [5.84 %]	
India	days	-1.60 to 0.10 [-0.75]			
SEC	days	-1.38 to -0.18 [-0.70]	-0.07 to 0.05 [-0.023]	-0.37 % to 6.57 % [2.63 %]	-84.1 to -27.55 [-53.62]
NEA	days	-0.52	-0.08		-46.39
MRYR	days	-0.16	-0.01	0.56 %	-16.46
India	days				-6.90
Daily mean		-0.63	-0.15	2.89 %	-34.61
India	months	-0.45			
NCP	months	-1.30 to -0.06 [-0.43]		1.30 % to 4.70 % [2.53 %]	-109.00 to -5.48 [-36.01]
NEA	months	-0.30	-0.10		-50.00
PRD	months	-0.60 to 0.13 [-0.16]			
EA	months	-0.45 to -0.03 [-0.13]			-35.70 to -13.00 [-24.35]
China	months	-0.89 to 0.60 [-0.12]			-66.60 to -2.30 [-25.67]
EC	months	-0.30 to -0.05 [-0.11]			-13.10 to -6.20 [-9.65]
Monthly mean		-0.24	-0.10	2.53 %	-29.13
EA	seasons	-0.58 to -0.30 [-0.40]	-0.05 to -0.02 [-0.035]		-64.62 to -30.70 [-43.27]
SEA	seasons	-0.39 to -0.03 [-0.21]	-0.06 to -0.01 [-0.035]		-48.33 to -6.71 [-27.52]
Seasonal mean		-0.31	-0.035		-34.61
PRD	years	-0.27			-45.00
TP	years	-0.24			
SEA	years	-0.21	-0.03		-27.25
EA	years		-0.03	0.13 g·kg ⁻¹	-46.47 to -45.00 [-45.74]
EC	years		-0.014	0.21 %	
Yearly mean		-0.24	-0.025	0.21 %	-39.33

1165

1166 6.1.3 Cloud and precipitation

1167 In the included publications, only a few papers focusing on the effects of aerosol feedbacks on
1168 cloud properties (cloud fraction, LWP, ice water path (IWP), CDNC and cloud effective radius) and
1169 precipitation characteristics (amount, spatial distribution, peak occurrence and onset time) using
1170 two-way coupled models in Asia, as shown in Table 7. In this table, the abbreviations representing
1171 aerosol emission sources (Dust, ARB_BC, Anthro_BC, and Anthro) and regions in Asia are defined
1172 in Appendix Table B1. The plus and minus signs indicate increase and decrease, respectively.

1173 The variations of cloud properties and precipitation characteristics induced by ARI or/and ACI
1174 are rather complex and not uniform in different parts of Asia and time periods. BC from both ARB
1175 and anthropogenic sources reduced cloud fraction through ARI and both ARI and ACI in several
1176 areas in China. ARI or/and ACI induced by anthropogenic aerosols could increase or decrease cloud
1177 fraction and affect cloud fraction differently in various atmospheric layers and time periods.
1178 Considering EA and subareas in China, anthropogenic aerosols tended to increase LWP through ARI
1179 and ACI as well as ACI alone but decrease LWP in some areas of SC (ARI and ACI) at noon and in
1180 afternoon during summertime and NC (ACI) in winter. ARI and ACI induced by anthropogenic BC
1181 aerosols had negative effects on LWP except at daytime in CC. Dust aerosols increased both LWP
1182 and IWP through ACI in EA, which was reported only by one study. The increase (decrease) of
1183 CDNC caused by the ARI and ACI effects of anthropogenic (anthropogenic BC) aerosols in EC
1184 during summertime was reported. Through ACI, anthropogenic aerosols affected CDNC positively
1185 in EA and China. Compared to anthropogenic aerosols, dust aerosols could have much larger
1186 positive impacts on CDNC via ACI in springtime over EA. The ACI effects of anthropogenic
1187 aerosols reduced cloud effective radius over China (January) and EA (July).

1188 Among all the variables describing cloud properties and precipitation characteristics, the
1189 variations of precipitation amount were studied the most using two-way coupled models in Asia.
1190 How turning on ARI or/and ACI in coupled models can change precipitation amount is not
1191 unidirectional and depends on many factors, including different aerosol sources, areas, emission
1192 levels, atmospheric humidity, precipitation types, seasons, and time of a day. Under the high

1193 emission levels as well as at slightly different humidity levels of $RH > 85\%$ with increasing
1194 emissions, the ACI effects of anthropogenic aerosols induced precipitation increase in the MRYSR
1195 area of China. Over the same area, precipitation decreased due to the ACI effects of anthropogenic
1196 aerosols with the low emission levels and $RH < 80\%$. In PRD, wintertime precipitation was
1197 enhanced by the ACI effects of anthropogenic aerosols but inhibited by ARI. In SK, summertime
1198 precipitation was both enhanced and inhibited by the ACI and ARI effects of anthropogenic aerosols.
1199 In locations upwind (downwind) of Beijing, rainfall amount was raised (lowered) by the ARI effects
1200 of anthropogenic aerosols but lowered (raised) by ACI. Both ARI and ACI induced by anthropogenic
1201 aerosols had positive impacts on total, convective, and stratiform rain in India during the summer
1202 season and the increase of convective rain was larger than those of stratiform. Summertime
1203 precipitation amounts could be enhanced or inhibited at various subareas inside simulation domains
1204 over India, China, and Korea and during day- or night-time due to ARI and ACI of anthropogenic
1205 aerosols. Over China, dust-induced ACI decreased (increased) springtime precipitation in CC
1206 (western part of NC), and over India, dust aerosols from local sources and ME had positive impacts
1207 on total, convective, and stratiform rain through ARI and ACI. Simulations in India also revealed
1208 that precipitation could be increased in some subareas but decreased in another and absorptive (non-
1209 absorptive) dust enhanced (inhibited) summertime precipitation via ARI and ACI. The ARI (ACI)
1210 effects of BC from ARB caused precipitation reduction (increase) in SEC but CAs emitted from
1211 ARB (ARB_CAs) caused rainfall enhancement in Myanmar. During pre-monsoon (monsoon)
1212 season, ARI induced by anthropogenic BC could lead to $+42\%$ (-5% to -8%) variations of
1213 precipitation in NEI (SI). Considering both ARI and ACI effects, BC from ARB and sea salt aerosols
1214 enhanced or inhibited precipitation in different parts of India and BC from anthropogenic sources
1215 enhanced (inhibited) nighttime (daytime) rainfall in CC (NC and SC) at the rate of $+1$ to $+4\text{ mm}\cdot\text{day}^{-1}$
1216 (-2 to $-6\text{ mm}\cdot\text{day}^{-1}$) during summer season. With respect to spatial variations, 6.5% larger rainfall
1217 area in PRD was caused by ARI and ACI effects under 50% reduced anthropogenic emissions. ACI
1218 induced by anthropogenic aerosols tended to delay the peak occurrence time and onset time of
1219 precipitation by one to nine hours in China and South Korea.

1220
1221
1222
1223

Table 7. Summary of changes of cloud properties and precipitation characteristics due to aerosol feedbacks simulated by two-way coupled models (WRF-Chem, WRF-CMAQ, GRAPES-CUACE, WRF-NAQPMS and GATOR-GCMOM) in Asia.

Variables	Variations (aerosol effects)	Simulation time period	Regions	References	
Cloud fraction	-7 % low-level cloud (ARB_BC ARI)	Apr., 2013	SEC	Huang et al., 2019	
	+0.03 to +0.08 below 850 hPa and at 750 hPa (Anthro ARI & ACI), esp. at early morning and nighttime	Aug., 2008	EC	Gao and Zhang, 2018	
	Max -0.06 between 750 hPa and 850 hPa (Anthro ARI & ACI), esp. in afternoon and evening	Aug., 2008	CC	Gao and Zhang, 2018	
	-0.02 to -0.06 below 750 hPa (Anthro_BC ARI & ACI), esp. in afternoon	Aug., 2008	SC & NC	Gao and Zhang, 2018	
	-0.04 to -0.06 between 750 hPa and 850 hPa (Anthro_BC ARI & ACI), esp. in afternoon	Aug., 2008	CC	Gao and Zhang, 2018	
	-6.7 % to +3.8 % (Anthro ARI)	Jun. 6-9 & Jun. 11-14, 2015	SK	Park et al., 2018	
	+22.7 % (Anthro ACI)	Jun. 6-9 & Jun. 11-14, 2015	SK	Park et al., 2018	
	-0.03 % low-, -0.54 % middle- and -0.58 % high-level cloud (Anthro ACI)	2008 to 2012	PRD	Liu et al., 2018c	
	Cloud properties	+5 to +50 $\text{g}\cdot\text{m}^{-2}$ (Anthro ARI & ACI)	Aug., 2008	EC	Gao and Zhang, 2018
		+10 to +20 $\text{g}\cdot\text{m}^{-2}$ (Anthro_BC ARI & ACI) at daytime	Aug., 2008	CC	Gao and Zhang, 2018
-5 to -40 $\text{g}\cdot\text{m}^{-2}$ (Anthro ARI & ACI) at noon and in afternoon		Aug., 2008	Part of SC	Gao and Zhang, 2018	
-2 to -20 $\text{g}\cdot\text{m}^{-2}$ (Anthro_BC ARI & ACI)		Aug., 2008	SC	Gao and Zhang, 2018	
-2 to -30 $\text{g}\cdot\text{m}^{-2}$ (Anthro_BC ARI & ACI)		Aug., 2008	NC	Gao and Zhang, 2018	
LWP		Max+18 $\text{g}\cdot\text{m}^{-2}$ (Dust ACI)	Mar.-May., 2010	EA	Wang et al., 2018b
		+40 to +60 $\text{g}\cdot\text{m}^{-2}$ (Anthro ACI)	Jan., 2008	SC	Gao et al., 2012
		+40 $\text{g}\cdot\text{m}^{-2}$ (Anthro ACI)	Jan., 2008	CC	Gao et al., 2012
		Less than +5 $\text{g}\cdot\text{m}^{-2}$ or -5 $\text{g}\cdot\text{m}^{-2}$ (Anthro ACI)	Jan., 2008	NC	Gao et al., 2012
IWP		+30 to +50 $\text{g}\cdot\text{m}^{-2}$ (Anthro ACI)	Jul., 2008	EA	Gao et al., 2012
	+5 to +10 $\text{g}\cdot\text{m}^{-2}$ (Dust ACI)	Mar. 17-Apr. 30, 2012	EA	Su and Fung, 2018b	
CDNC	+20 to +160 cm^{-3} (Anthro ARI & ACI)	Aug., 2008	EC	Gao and Zhang, 2018	

		-5 to -60 cm ⁻³ (Anthro_BC ARI & ACI)	Aug., 2008	EC	Gao and Zhang, 2018		
		Max +10500 cm ⁻³ (Dust ACI)	Mar.-May., 2010	EA	Wang et al., 2018b		
		+650 cm ⁻³ (Anthro ACI)	Jan., 2008	EC	Gao et al., 2012		
		+400 cm ⁻³ (Anthro ACI)	Jan., 2008	CC & SWC	Gao et al., 2012		
		Less than +200 cm ⁻³ (Anthro ACI)	Jan., 2008	NC	Gao et al., 2012		
		+250 to +400 cm ⁻³ (Anthro ACI)	Jul., 2008	EA	Gao et al., 2012		
Cloud effective radius		More than -4 μm (Anthro ACI)	Jan., 2008	SWC, CC & SEC	Gao et al., 2012		
		More than -2 μm (Anthro ACI)	Jan., 2008	NC	Gao et al., 2012		
		-3 μm (Anthro ACI)	Jul., 2008	EA	Gao et al., 2012		
		Enhancement/inhibition of precip. due to high/low Anthro emissions, ACI inhibited (enhanced) precip. at RH < 80 % (> 85 %) with increasing Anthro emissions	Jun. 18-19, 2018	MRYR	Bai et al., 2020		
		-4.72 mm (Anthro ARI) and +33.7 mm (Anthro ACI)	Dec. 14-16, 2013	PRD	Liu Z. et al., 2020		
		+2 to +5 % (ARB CAs ARI)	Mar.-Apr., 2013	Myanmar SEC	Singh et al., 2020		
		-1.09 mm·day ⁻¹ (ARB_BC ARI)	Apr., 2013	SEC	Huang et al., 2019		
		+0.49 mm·day ⁻¹ (ARB_BC ACI)	Apr., 2013	SEC	Huang et al., 2019		
		-0 to -4 mm·day ⁻¹ (Anthro ARI & ACI)	Jun.-Sep., 2010	Indus basin & eastern IGP	Kedia et al., 2019b		
		+1 to +3 mm·day ⁻¹ non-convective rain (Anthro ARI & ACI)	Jun.-Sep., 2010	WG of India	Kedia et al., 2019b		
		+5 mm·day ⁻¹ non-convective rain (Anthro ARI & ACI)	Jun.-Sep., 2010	NEI	Kedia et al., 2019b		
		Increase of total rain (Dust ARI & ACI)	Jun.-Sep., 2010	NI, CI, WG, NEI & central IGP	Kedia et al., 2019b		
		Decrease of total rain (Dust ARI & ACI)	Jun.-Sep., 2010	NWI & SPI	Kedia et al., 2019b		
		Decrease of total rain (ARB_BC ARI & ACI)	Jun.-Sep., 2010	WG, SPI, NWI, EI & NEI	Kedia et al., 2019b		
		Increase of total rain (ARB_BC ARI & ACI)	Jun.-Sep., 2010	CI, Central IGP & EPI	Kedia et al., 2019b		
		Decrease of total rain (Sea salt ARI & ACI)	Jun.-Sep., 2010	EPI, WPI, CPI & SPI	Kedia et al., 2019b		
		Increase of total rain (Sea salt ARI & ACI)	Jun.-Sep., 2010	NCI & central IGP	Kedia et al., 2019b		
		-20 to -200mm (Anthro ARI & ACI)	Aug., 2008	SC & NC	Gao and Zhang, 2018		
Precipitation (precip.)	Amount	+20 to +100 mm (Anthro_BC ARI & ACI)	Aug., 2008	CC	Gao and Zhang, 2018		
		+1 to +4 mm·day ⁻¹ nighttime precip. (ARI & ACI of Anthro or Anthro_BC)	Aug., 2008	CC	Gao and Zhang, 2018		
		-2 to -6 mm·day ⁻¹ daytime precip. (ARI & ACI of Anthro or Anthro_BC)	Aug., 2008	NC	Gao and Zhang, 2018		
		-2 to -4 mm·day ⁻¹ daytime precip. (Anthro ARI & ACI)	Aug., 2008	SC	Gao and Zhang, 2018		
		-2 to -6 mm·day ⁻¹ daytime precip. (Anthro_BC ARI & ACI)	Aug., 2008	SC	Gao and Zhang, 2018		
				-54.6 to +24.1 mm (Anthro ARI)	Jun. 6-9, 2015	SK	Park et al., 2018
				-23.8 to +24.0 mm (Anthro ACI)	Jun. 6-9, 2015	SK	Park et al., 2018
				-63.2 to +27.1 mm (Anthro ARI & ACI)	Jun. 6-9, 2015	SK	Park et al., 2018
				Min -7.0 mm (Anthro ARI)	Jun. 11-14, 2015	SK	Park et al., 2018
				Min -36.6 mm (Anthro ACI)	Jun. 11-14, 2015	SK	Park et al., 2018
				+42 % (Anthro_BC ARI) during pre-monsoon season	Mar.-May., 2010	NEI	Soni et al., 2018
				-5 to -8 % (Anthro_BC ARI) during monsoon season	Jun.-Sep., 2010	SI	Soni et al., 2018
				+1 mm·day ⁻¹ precip. (Dust ACI)	Mar. 17-Apr. 30, 2012	Western part of NC	Su and Fung, 2018b
				-1 mm·day ⁻¹ precip. (Dust ACI)	Mar. 17-Apr. 30, 2012	CC	Su and Fung, 2018b
				+0.95 mm·day ⁻¹ precip. (absorptive Dust ARI & ACI)	Jun.-Aug., 2008	India	Jin et al., 2016a
				-0.4 mm·day ⁻¹ precip. (non-absorptive Dust ARI & ACI)	Jun.-Aug., 2008	India	Jin et al., 2016a
				+0.44 mm·day ⁻¹ total precip. (Dust ARI & ACI over whole study domain)	Jun.-Aug., 2008	India	Jin et al., 2016b

	+0.34 mm·day ⁻¹ total precip. (Dust ARI & ACI from ME)	Jun.-Aug., 2008	India	Jin et al., 2016b
	+0.31 mm·day ⁻¹ total precip. (Anthro ARI & ACI over whole study domain)	Jun.-Aug., 2008	India	Jin et al., 2016b
	+0.32 mm·day ⁻¹ convective precip. (Dust ARI & ACI over whole study domain)	Jun.-Aug., 2008	India	Jin et al., 2016b
	+0.24 mm·day ⁻¹ convective precip. (ARI & ACI of Dust from ME)	Jun.-Aug., 2008	India	Jin et al., 2016b
	+0.20 mm·day ⁻¹ convective precip. (Anthro ARI & ACI over whole study domain)	Jun.-Aug., 2008	India	Jin et al., 2016b
	+0.12 mm·day ⁻¹ stratiform precip. (Dust ARI & ACI over whole study domain)	Jun.-Aug., 2008	India	Jin et al., 2016b
	+0.10 mm·day ⁻¹ stratiform precip. (ARI & ACI of Dust from ME)	Jun.-Aug., 2008	India	Jin et al., 2016b
	+0.11 mm·day ⁻¹ stratiform precip. (Anthro ARI & ACI over whole study domain)	Jun.-Aug., 2008	India	Jin et al., 2016b
	-48.29 %/+24.87 % precip. in downwind/upwind regions (Anthro ARI)	Jun. 27-28, 2008	Beijing	Zhong et al. 2015
	+33.26 %/-4.64 % precip. in downwind/upwind regions (Anthro ACI)	Jun. 27-28, 2008	Beijing	Zhong et al. 2015
	+0.44 mm·day ⁻¹ precip. (Dust ARI & ACI)	Jun. 1-Aug. 31, 2008	India	Jin et al., 2015
Spatial variation	+6.5 % precip. area (ARI & ACI) with 50% Anthro emissions	Jun. 9-12, 2017	YRD	Liu C. et al., 2019
	1 to 2h delay (Anthro ACI)	Jun. 18-19, 2018	MRYS	Bai et al., 2020
Peak occurrence time	1h delay (ARI & ACI) with 50% Anthro emissions	Jun. 9-12, 2017	YRD	Liu et al., 2019
	9h delay (Anthro ACI)	Jun. 7, 2015	Gosan, SK	Park et al., 2018
	4h delay (Anthro ACI)	Jun. 7, 2015	Jinju, SK	Park et al., 2018
Onset time	9h delay (Anthro ACI)	Jun. 7, 2015	Gosan, SK	Park et al., 2018
	2h delay (Anthro ACI)	Jun. 7, 2015	Jinju, SK	Park et al., 2018

1224

1225

6.2 Impacts of aerosol feedbacks on air quality

1226

1227

1228

1229

1230

1231

1232

1233

1234

1235

1236

1237

1238

1239

1240

1241

1242

1243

1244

1245

1246

1247

1248

1249

1250

1251

1252

1253

1254

1255

Aerosol effects not only gave rise to changes in meteorological variables but also air quality. Table 8 (the minimum, maximum and mean values were defined in the same way as in Table 6) summarizes the variations of atmospheric pollutant concentrations induced by aerosol effects in different regions of Asia and at different time scales. In Asia, most modeling studies with coupled models targeted the impacts of aerosol feedbacks on surface PM_{2.5} and O₃ concentrations, with only few focusing on other gaseous pollutants.

Simulation results showed that turning on aerosol feedbacks in coupled models generally made PM_{2.5} concentrations increased in different regions of Asia at various time scales, which stemmed from decrease of shortwave radiation, T2, WS10 and PBLH and increase of RH2. Some studies did show negative impacts of aerosol effects on hourly, daily, and seasonal PM_{2.5} at some areas that could be attributed to ACI effects, changes in transport and dispersion patterns, reductions in humidity levels and secondary aerosol formations (Zhang et al., 2015a; Yang et al., 2017; Zhan et al., 2017; Wang et al., 2018b). Similar to the perturbations of surface meteorological variables due to aerosol effects, the hourly PM_{2.5} variations and the range were the largest compared to those at other time scales. The largest PM_{2.5} increases were reported in NCP, SEC, EA, SEA and PRD at the hourly, daily, monthly, seasonal and yearly time scales with average values of 23.48 μg·m⁻³, 14.73 μg·m⁻³, 16.50 μg·m⁻³, 1.12 μg·m⁻³ and 2.90 μg·m⁻³, respectively.

In addition to PM_{2.5}, gaseous pollutants (O₃, NO₂, SO₂, CO and NH₃) are impacted by ARI or/and ACI effects as well. As shown in Table 8, general reductions of ozone concentrations were reported in Asia across all the modeling domains and time scales based on coupled models' simulations. However, the influences of aerosol feedbacks on atmospheric dynamics and stability, and photochemistry (photolysis rate and ozone formation regimes) could make ozone concentrations increase somewhat in summer months or during wet season (Xing et al., 2017; Jung et al., 2019; Nguyen et al., 2019b). The largest hourly, daily, monthly, seasonal, and annual variations of O₃ occurred in YRD (-32.80 μg·m⁻³), EC (-5.97 μg·m⁻³), China (-23.90 μg·m⁻³), EA (-4.48 μg·m⁻³) and EA (-2.76 μg·m⁻³), respectively. Along with reduced O₃ due to ARI or/and ACI, NO₂ concentrations were enhanced with average changes of +12.30 μg·m⁻³ (YRD) at the hourly scale and +0.66 μg·m⁻³ (EA) at both the seasonal and yearly scales, which could be attributed to slower photochemical reactions, strengthened atmospheric stability and O₃ titration (Nguyen et al., 2019b). Regarding other gaseous pollutants, limited studies pointed out daily and annual SO₂ concentrations increased

1256 in NEA and EA due to lower PBLH induced by the ARI effects of anthropogenic aerosols (Jung et
 1257 al.,2019; Nguyen et al., 2019b). The seasonal SO₂ reduction was rather large, which related to higher
 1258 PBLH induced by the ACI effects of dust aerosols in the NCP area of EA (Wang et al., 2018b). The
 1259 slight increase of seasonal SO₂ was reported in the whole domain of EA due to lower PBLH caused
 1260 by ARI effects of anthropogenic aerosols (Nguyen et al., 2019b). There was only one study depicted
 1261 increased CO (NH₃) concentration in EC (NEA) due to both the ARI and ACI (ARI) effects of
 1262 anthropogenic aerosols but these results may not be conclusive.

1263

1264 Table 8. Compilation of aerosol-induced variations of PM_{2.5} and gaseous pollutants simulated by two-way
 1265 coupled models (WRF-Chem, WRF-CMAQ, GRAPES-CUACE, WRF-NAQPMS and GATOR-GCMOM) in
 1266 different regions of Asia and at different temporal scales.

Region	Time scale	$\Delta PM_{2.5}$ [mean] ($\mu\text{g}\cdot\text{m}^{-3}$)	ΔO_3 [mean] ($\mu\text{g}\cdot\text{m}^{-3}$)	ΔNO_2 [mean] ($\mu\text{g}\cdot\text{m}^{-3}$)	ΔSO_2 [mean] ($\mu\text{g}\cdot\text{m}^{-3}$)	ΔCO [mean] ($\mu\text{g}\cdot\text{m}^{-3}$)	ΔNH_3 [mean] ($\mu\text{g}\cdot\text{m}^{-3}$)
NCP	hours	-3.50 to 90.00 [23.48]					
YRD	hours	7.00 to 30.50 [15.17]	-32.80 to -0.20 [-11.25]	12.30			
Hourly mean		19.32	-11.25	12.30			
SEC	days	-1.91 to 32.49 [14.73]					
NCP	days	-5.00 to 56.00 [14.51]					
EC	days	2.87 to 18.60 [10.74]	-5.97 to -1.45 [-3.71]				
NEA	days	1.75			0.97		0.11
Daily mean		10.43	-3.71		0.97		0.11
India	months	3.00 to 30.00 [16.50]					
EC	months	1.00 to 40.00 [16.33]	-2.40 to -1.00 [-1.70]			4.00 to 6.00 [5.00]	
China	months	1.60 to 33.20 [14.38]	-23.90 to 4.92 [-3.42]				
EA	months	3.60 to 10.20 [5.79]					
Monthly mean		13.25	-2.56			5.00	
SEA	seasons	0.15 to 2.09 [1.12]	-1.92 to 0.26 [-0.83]				
EA	seasons	-8.00 to 2.70 [-0.14]	-4.48 to -1.00 [-2.99]	0.43 to 0.88 [0.66]	-4.29 to 0.72 [-0.42]		
Seasonal mean		0.49	-1.91	0.66	-0.42		
PRD	years	2.90					
EA	years	1.82	-2.76	0.66	0.54		
NCP	years	0.10 to 5.10 [1.70]					
SEA	years	1.21	-0.80				
Yearly mean		1.91	-1.78	0.66	0.54		

1267

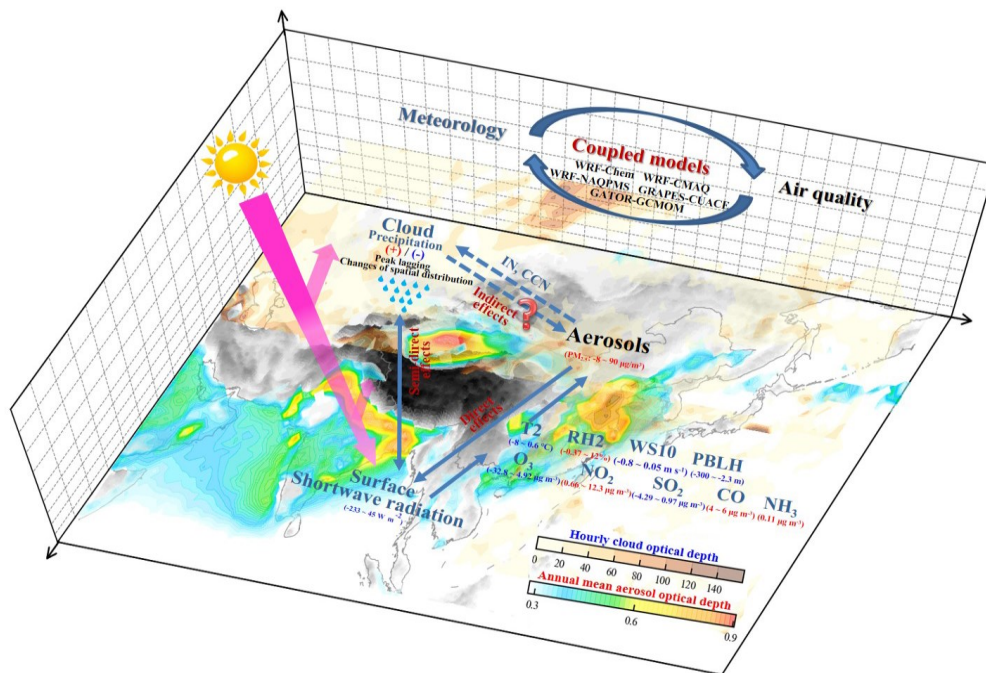


Figure 9. A schematic diagram depicting aerosol-radiation-cloud interactions and quantitative effects of aerosol feedbacks on meteorological and air quality variables simulated by two-way coupled models in Asia.

1269
 1270
 1271
 1272
 1273
 1274
 1275
 1276
 1277
 1278
 1279
 1280
 1281
 1282
 1283
 1284
 1285
 1286
 1287
 1288
 1289
 1290
 1291
 1292
 1293
 1294
 1295
 1296
 1297
 1298
 1299
 1300
 1301
 1302
 1303
 1304

Two-way coupled models have been applied in US and Europe extensively and then in Asia due to frequent occurrences of severe air pollution events accompanied with rapid economic growth in the region. Until now, no comprehensive study is conducted to elucidate the recent advances in two-way coupled models' applications in Asia. This paper provides a critical overview of current status and research focuses of related modeling studies using two-way coupled models in Asia between 2010 and 2019, and summarizes the effects of aerosol feedbacks on meteorological and air quality variables from these studies.

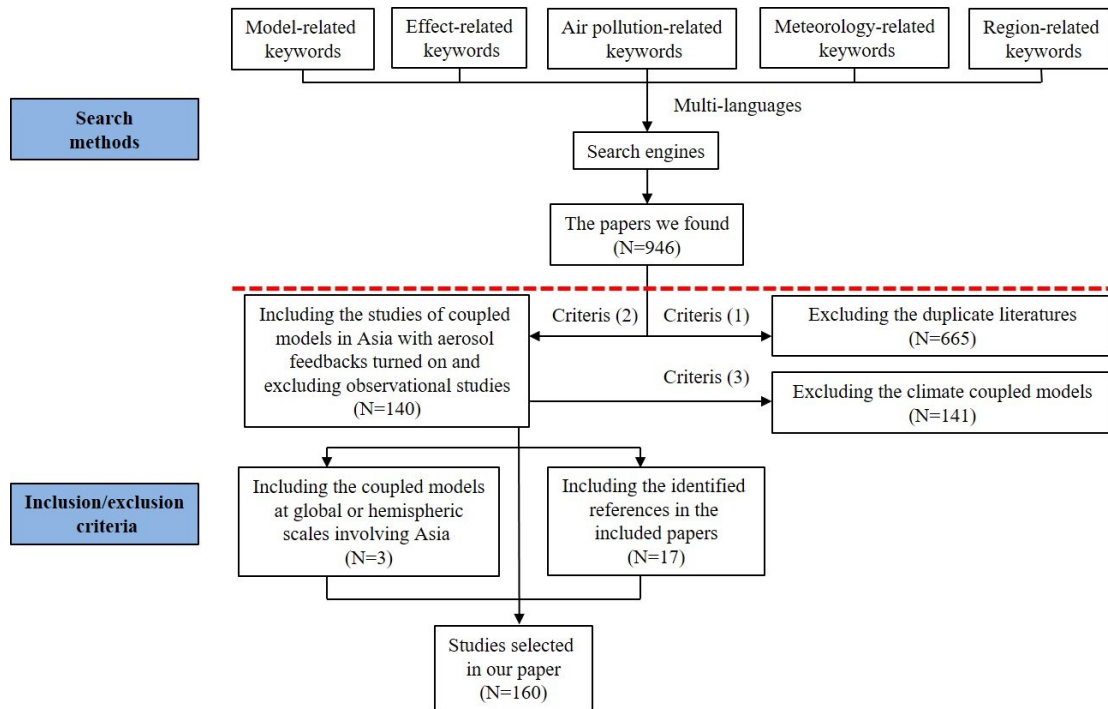
Through systematically searching peer-reviewed publications with several scientific-based search engines and a variety of key word combinations and applying certain selection criteria, 160 relevant papers were identified. Our bibliometric analysis results (as schematically illustrated in Fig. 9) showed that in Asia, the research activities with two-way coupled models had increased gradually in the past decade and the five two-way coupled models (WRF-Chem, WRF-CMAQ, WRF-NAQPMS, GRAPES-CUACE and GATOR-GCMOM) were extensively utilized to explore the ARI or/and ACI effects in Asia with focusing on several high aerosol loading areas (e.g., EA, India, China and NCP) during wintertime or/and severe pollution events, with less investigations looking into other areas and seasons with low pollution levels. Among the 160 papers, nearly 82 % of them focused on ARI (72 papers) and both ARI and ACI effects (60 papers), but papers that only considering ACI effects were relatively limited. The ARI or/and ACI effects of natural mineral dust, BC and BrC from anthropogenic sources and BC from ARB were mostly investigated, while a few studies quantitatively assessed the health impacts induced by aerosol effects.

Meta-analysis results revealed that enabling aerosol effects in two-way coupled models could improve their simulation/forecast capabilities of meteorology and air quality in Asia, but a wide range of differences occurred among the previous studies perhaps due to various model configurations (selections of model versions and parameterization schemes) and largest uncertainties related to ACI processes and their treatments in models. Compared to US and Europe, the aerosol-induced decrease of the shortwave radiative forcing was larger because of higher air pollution levels in Asia. The overall decrease (increase) of T2, WS10, PBLH and O₃ (RH2, PM_{2.5} and other gaseous pollutant concentrations) caused by ARI or/and ACI effects were reported from the modeling studies using two-way coupled models in Asia. The ranges of aerosol-induced variations of T2, PBLH, PM_{2.5} and O₃ concentrations were larger than other meteorological and air quality variables. For variables of CO, SO₂, NO₂, and NH₃, reliable estimates could not be obtained due to insufficient numbers of samples in past studies.

1305 Even though noticeable progresses toward the application of two-way coupled meteorology
 1306 and air quality models have been made in Asia and the world during the last decade, several
 1307 limitations are still presented. Enabling aerosol feedbacks lead to higher computational cost
 1308 compared to offline models, but this shortcoming can be overcome with the new developments of
 1309 cluster computing technology (i.e., Graphics Processing Unit (GPU)-accelerated computing and
 1310 cloud computing). The latest advances in the measurements and research of cloud properties,
 1311 precipitation characteristics, and physiochemical characteristics of aerosols that play pivotal roles
 1312 in CCN or IN activation mechanisms can guide the improvements and enhancements in two-way
 1313 coupled models, especially to abate the uncertainties in simulating ACI effects. Special attention
 1314 needs to be paid to assess the accuracies of different methodologies in terms of ARI and ACI
 1315 calculations in two-way coupled models in Asia and other regions. Besides the five two-way coupled
 1316 models mentioned in this paper, more models capable of simulating aerosol feedbacks (such as
 1317 WRF-CHIMERE and WRF-GEOS-Chem) have become available and projects covering more
 1318 comprehensive intercomparisons of these coupled models should be conducted in Asia. Future
 1319 assessments of the ARI or/and ACI effects should pay extra attention to their impacts on dry and
 1320 wet depositions simulated by two-way coupled models. So far, the majority of two-way coupled
 1321 models' simulations and evaluations focuses on episodic air pollution events occurring in certain
 1322 areas, therefore their long-term applications and evaluations are necessary and their real-time
 1323 forecasting capabilities should be explored as well.

1324
 1325

Appendix A



1326
 1327
 1328
 1329
 1330

Figure A1. Flowchart of literature search and identification

Appendix B

1331

Table B1. Lists of abbreviations and acronyms

ACI	Aerosol-cloud interactions
AOD	Aerosol optical depth
AQCHEM	the CMAQ's standard aqueous chemistry module
ARB	Agriculture residue burning
ARB_BC	BC emitted from agriculture residue burning
ARB_CAs	Carbonaceous aerosols emitted from agriculture residue burning
ARI	Aerosol-radiation interactions
ATM	In the atmosphere
BB	Biomass burning
BC	Black carbon
BCs	Boundary conditions
BOT	At the bottom

BrC	Brown carbon
CA	Central Asia
CAMx	Comprehensive Air quality Model with extensions
CAs	Carbonaceous aerosols
CC	Central China
CCN	Cloud condensation nuclei
CDNC	Cloud droplet number concentration
CHIMERE	A multi-scale chemistry-transport model for atmospheric composition analysis and forecast
CMAQ	Community Multiscale Air Quality model
CO	Carbon monoxide
CRFs	Concentration-response functions
DRF	Direct radiative forcing
EA	East Asia
EC	East China
EQUISOLV II	the EQUilibrium SOLVer version 2
GATOR-GCMOM	Gas, aerosol, transport, radiation, general circulation, mesoscale, and ocean Model
GOCART	The Global Ozone Chemistry Aerosol Radiation and Transport
	Global-regional assimilation and prediction system coupled with the Chinese Unified Atmospheric Chemistry
GPRAPES-CUACE	Environment forecasting system
GSI	Gridpoint Statistical Interpolation
H ₂ O ₂	Hydrogen peroxide
HNO ₃	Nitric acid
HO ₂	Hydroperoxyl
ICs	Initial conditions
IN	Ice nuclei
INPs	Ice nucleation parameterizations
IPCC	Intergovernmental Panel on Climate Change
IPR	Ice particle radius
IWP	Ice water path
LWP	Liquid water path
LWRF	Longwave radiative forcing
MARS-A	the Model for an Aerosol Reacting System-version A
MB	Mean bias
ME	Middle East
MESA-MTEM	the Multicomponent Equilibrium Solver for Aerosols with the Multicomponent Taylor Expansion Method
MICS-Asia	Model Inter-Comparison Study for Asia
MOZART	Model for Ozone and Related Chemical Tracer
MRYR	Middle reaches of the Yangtze River
N	Nitrate
N ₂ O ₅	Nitrogen pentoxide
NAQPMS	Nested Air Quality Prediction Modeling System
NC	North China
NCP	North China Plain
NEA	Northeast Asia
NME	Normalized mean error
NO ₂	Nitrogen dioxide
NU-WRF	National aeronautics and space administration Unified Weather Research and Forecasting model
NWC	Northwest China
O ₃	Ozone
OA	Organic aerosols
OC	Organic carbon
·OH	Hydroxyl radical
OPAC	Optical Properties of Aerosols and Clouds
PBL	Planetary boundary layer
PBLH	Planetary boundary layer height
PM _{2.5}	Fine particulate matter
PRD	Pearl River Delta
PSI	Papers with statistical indices
R	Correlation coefficient
RADM	the Regional Acid Deposition Mode
RH2	Relative humidity at 2 meters above the surface
RMSE	Root mean square error
RRTM	The Rapid Radiative Transfer Model
RRTMG	The Rapid Radiative Transfer Model for General Circulation Models
S	Sulfate
SA	South Asia
SC	South China
SEA	Southeast Asia
SEC	Southeast China
SH2	Specific humidity at 2 meters above the surface
SI	Statistical indices
SO ₂	Sulfur dioxide
SOA	Secondary organic aerosol
SWC	Southwest China
SWRF	Shortwave radiative forcing
T2	Air temperature at 2 meters above the surface
TOA	At the top of atmosphere
TP	Tibetan Plateau
US	the United States
VBS	Volatility basis set

WA	West Asia
WRF	Weather Research and Forecasting model
WRF-Chem	Weather Research and Forecasting model coupled with Chemistry
WRF-CHIMERE	Weather Research and Forecasting model coupled with a multi-scale Chemistry-Transport Model (CTM) for air quality forecasting and simulation
WRF-CMAQ	Weather Research and Forecasting model coupled with Community Multiscale Air Quality model
WRF-NAQPMS	Weather Research and Forecasting model coupled with the Nested Air Quality Prediction Modeling System
WS10	Wind speed at 10 meters above the surface
YRD	Yangtze River Delta

1332

1333

1334 Table B2. The compiled number of publications (NP) and number of samples (NS) for papers that providing
1335 statistical indices (SI) of meteorological variables.

No.*	Meteorological variables															
	T2				RH2				SH2				WS10			
	NS				NS				NS				NS			
	NP	R	MB	RMSE	NP	R	MB	RMSE	NP	R	MB	RMSE	NP	R	MB	RMSE
4	1	5	5 (4↑, 1↓)	5	1	5	5 (1↑, 4↓)	5								
5					1		3 (2↑, 1↓)	3								
7	1	4	4 (3↑, 1↓)													
13	1		1 (1↓)		1		1 (1↑)									
15	1	1			1	1						1	2			
16	1	1														
20	1	2	2 (1↑, 1↓)	2	1	2	2 (1↑, 1↓)	2				1	1	1 (1↑)		1
21	1	0	2 (2↓)	2								1		2 (1↑, 1↓)		2
22	1	1	1 (1↓)	1	1	1	1 (1↑)	1				1	1	1 (1↓)		1
23	1	1	1 (1↑)		1	1	1 (1↓)					1	1	1 (1↑)		
24	1	1	1 (1↑)		1	1	1 (1↓)					1	1	1 (1↑)		
25	1	1	1 (1↓)													
28	1		1 (1↑)	1	1		1 (1↓)	1				1		1 (1↑)		1
29	1	9	9 (6↑, 3↓)	9	1	8		9				1	9	9 (9↑)		9
33	1	6	6 (4↑, 2↓)	6												
34	1	2	2 (2↑)	2								1	2	2 (2↓)		2
35	1	2		2	1	1		1				1	1			1
38	1		4 (4↓)	4	1		4 (3↑, 1↓)	4								
50	1		8 (8↓)	8												
56	1	1	1 (1↓)	1	1	1	1 (1↓)	1				1	1	1 (1↑)		1
57	1	1			1	1						1	1			
61	1	4	4 (4↓)	4	1	4	4 (4↑)	4				1	4	4 (4↑)		4
62	1		5 (5↓)	5								1		5 (4↑, 1↓)		5
63	1	1														
71	1	1														
72	1	4	4 (3↑, 1↓)	4	1	4	4 (3↑, 1↓)	4								
73	1	1	1 (1↓)	1					1	1	1 (1↑)	1	1	1 (1↑)		1
75	1	4	4 (4↑)		1	4	4 (4↑)				0	1	4	4 (1↑, 3↓)		
77	1	4	4 (2↑, 2↓)						1	4	3 (3↑)	4	1	4 (4↑)		4
79	1		8 (6↑, 2↓)	8												
80	1	8	8 (8↑)	8	1	8	8 (8↓)	8				1	8	8 (6↑, 2↓)		8
85	1		4 (1↑, 3↓)	4	1		4 (2↑, 2↓)	4				1		4 (4↑)		4
87	1		3 (2↑, 1↓)	3								1		3 (2↑, 1↓)		3
88	1	3	3 (1↑, 2↓)	3	1	3	3 (2↑, 1↓)	3				1	3	3 (2↑, 1↓)		3
90	1	4	4 (1↑, 3↓)						1	4	4 (4↑)		4	4 (4↑)		
91	1	1	1 (1↓)	1					1	1	1 (1↑)	1	1	1 (1↑)		1
94	1	6	6 (4↑, 2↓)	6	1	6	6 (2↑, 4↓)	6				1	6	6 (6↑)		6
96	1	16	16 (11↑, 5↓)						1	16		1	16	16 (11↑, 5↓)		
97	1	1	1 (1↓)	1	1	1	1 (1↑)	1				1	1	1 (1↑)		1
106	1	6	6 (6↓)						1	6	5 (2↑, 3↓)		6	6 (6↑)		
109	1	2	2 (2↓)	2	1	3	3 (3↑)	3				1	2	2 (2↑)		2
112	1		2 (2↓)	2					1		2 (2↓)	2	1	2 (2↑)		2
116	1	2	2 (1↑, 1↓)	0	1	2	2 (1↑, 1↓)						1	1	1 (1↑)	1
121	1	1	1 (1↓)	1									1	1	1 (1↑)	1
122	1		2 (2↓)	2	1		2 (2↑)	2				1		2 (2↑)		2
125	1	4	4 (4↓)	4	1	4	4 (4↑)	4				1	4	4 (4↓)		4
126	1	4	4 (4↓)	4					1	4	4 (2↑, 2↓)	4	1	4 (4↑)		4
127	1		2 (2↓)	2								1		2 (2↑)		2
128	1	8	8 (8↓)	8					1	8	8 (5↑, 3↓)	8	1	8 (8↑)		8
129	1	1	1 (1↓)	1	1	1	1 (1↑)	1				1	1	1 (1↑)		1
133	1		1 (1↓)	0	1		4 (4↑)					1		4 (3↑, 1↓)		
143	1	4		4	1	4		4				1	4			4
147	1	2		2	1	2		2				1	2			2
151	1	7	7 (7↓)	7					1	7	7 (3↑, 4↓)	7	1	7 (7↑)		7
Total	53	137	167 (67↑, 100↓)	130	30	68	70 (42↑, 28↓)	73	9	35	35 (21↑, 14↓)	27	40	111	126 (104↑, 22↓)	97

1336

1337

1338

1339

1340

Note that the No.* is consistent with the No. in Table 1, and ↑ and ↓ mark over- and underestimations of variables, respectively, along with their number of samples.

Table B3. The compiled number of publications (NP) and number of samples (NS) for papers that providing statistical indices (SI) of air quality variables.

No.*	Air quality variables							
	PM _{2.5}				O ₃			
	NP	R	MB	RMSE	NP	R	MB	RMSE
4	1	5	5 (5↓)	5				
5	1		1 (1↑)	1	1		1 (1↓)	1
11	1	60						
15	1	1						
21	1		2 (1↑, 1↓)					
22	1	1	1 (1↑)	1				
23	1	1	1 (1↑)		1	1	1 (1↓)	
24	1	1	1 (1↓)		1		1 (1↓)	
25	1	1	1 (1↑)		1	1	1 (1↑)	
29	1	9	9 (6↑, 3↓)	9				

33	1	4	4 (4↓)	4	1	4	4 (3↑, 1↓)	4
34	1	2	2 (1↑, 1↓)	2				
35					1	1		1
50	1		4 (1↑, 3↓)	4				
56	1	1	1 (1↑)	1				
57	1	1						
59	1	6	6 (6↓)	6	1	6	6 (6↑)	6
61	1	12	12 (12↑)	12				
67	1	10	2 (2↓)	10				
71	1	1						
73	1	2	2 (1↑, 1↓)		1	4	4 (4↑)	
77	1	4						
85	1	3	3 (3↓)					
86	1	4	4 (2↑, 2↓)	4				
88	1	3	3 (1↑, 2↓)	3				
90	1	8	8 (2↑, 6↓)		1	14	14 (14↑)	
91	1	4	4 (1↑, 3↓)	4	1	6	6 (4↑, 2↓)	6
94	1	4	4 (3↑, 1↓)	4				
97	1	1	1 (1↓)	1				
100	1	1			1	1		
106	1	6	6 (2↑, 4↓)		1	8	8 (4↑, 4↓)	
112	1				1			
121					1			5
122	1	4	4 (1↑, 3↓)					
125	1	4	4 (2↑, 2↓)	4	1	4	4 (4↑)	4
126	1	4	4 (2↑, 2↓)	4	1	4	4 (4↑)	4
127	1		1 (1↑)	1				
128	1	8	8 (3↑, 5↓)	8				
129	1	3	3 (2↑, 1↓)	3	1	2	2 (1↑, 1↓)	2
133					1	4	4 (3↑, 1↓)	4
136	1	5	5 (5↓)					
146	1	1			1	20		20
147	1	2			2			
149	1	6			6			
150						21		21
151	1	12	6 (6↑)	6	1	24	12 (7↑, 5↓)	12
Total	42	205	122 (55↑, 67↓)	105	21	125	72 (55↑, 17↓)	90

1341 Note that the No.* is consistent with the No. in Table 1, and ↑ and ↓ mark over- and underestimations of variables, respectively, along with
1342 their number of samples.

1343

1344 Table B4. The compiled number of publications (NP) and number of samples (NS) for papers that simultaneously
1345 providing the statistical indices (SI) of meteorological variables simulated by coupled models (WRF-Chem, WRF-
1346 CMAQ, GRAPES-CUACE, WRF-NAQPMS and GATOR-GCMOM) with/out ARI.

No.*	Meteorological variables															
	T2				RH2				SH2				WS10			
	NP	NS			NP	NS			NP	NS			NP	NS		
	R	MB	RMSE	R	MB	RMSE	R	MB	RMSE	R	MB	RMSE	R	MB	RMSE	
32	1	3	3 (2↑, 1↓)	3												
78	1		4 (3↑, 1↓)	4												
124	1	2	2 (2↓)	2	1	2	2 (2↑)	2					1	2	2 (2↓)	2
125	1	2	2 (2↓)	2					1	2	2 (1↑, 1↓)	2	1	2	2 (2↑)	2
126	1		1 (1↓)	1									1		1 (1↑)	1
127	1	4	4 (4↓)	4					1	4	4 (3↑, 1↓)	4	1	4	4 (4↑)	4
146	1	1		1	1	1		1					1	1		1
Total	7	12	16 (5↑, 11↓)	17	2	3	2 (2↑)	3	2	6	6 (4↑, 2↓)	6	5	9	9 (7↑, 2↓)	10

1347 Note that the No.* is consistent with the No. in Table 1, and ↑ and ↓ mark over- and underestimations of variables, respectively, along with
1348 their number of samples.

1349

1350 Table B5. The compiled number of publications (NP) and number of samples (NS) for papers that simultaneously
1351 providing the statistical indices (SI) of air quality variables simulated by coupled models (WRF-Chem, WRF-CMAQ,
1352 GRAPES-CUACE, WRF-NAQPMS and GATOR-GCMOM) with/out ARI.

No.*	Air quality variables										
	PM _{2.5}				O ₃						
	NP	NS			NP	NS					
	R	MB	RMSE	R	MB	RMSE	R	MB	RMSE		
49	1			2 (1↑, 1↓)	2			1	10	10	
60	1			4 (4↑)	4						
124	1			2 (1↑, 1↓)	2			1	2	2 (2↑)	2
125	1			2 (1↑, 1↓)	2			1	2	2 (2↑)	2
127	1			4 (2↑, 2↓)	4						
146	1				1						
Total	5			14 (9↑, 5↓)	15			3	14	4 (4↑)	14

1353 Note that the No.* is consistent with the No. in Table 1, and ↑ and ↓ mark over- and underestimations of variables, respectively, along with
1354 their number of samples.

1355

1356 Table B6. Description of refractive indices and radiation schemes used in the WRF-Chem and WRF-CMAQ in Asia.

Model	Refractive indices of aerosol species groups		Radiation scheme	
	SW	LW	SW scheme (Spectral intervals)	LW scheme (Spectral intervals)
WRF-Chem	1. Water (1.35+1.524 ^λ),	1. Water (1.532+0.336i),	GODDARD (0.175-0.225, 0.225-0.245, 0.245-	RRTMG (10-350, 350-500, 500-630, 630-700,

4. Insoluble (1.272+1.165[±]_i,
1.168+1.073[±]_i, 1.208+8.650[±]_i, 1.253+8.092[±]_i,
1.329+8.000[±]_i, 1.418+8.000[±]_i, 1.456+8.000[±]_i,
1.518+8.000[±]_i, 1.530+8.000[±]_i, 1.530+8.000[±]_i,
1.530+3.000[±]_i, 1.470+9.000[±]_i)
5. Sea-salt (1.480+1.758[±]_i,
1.534+7.462[±]_i, 1.437+2.950[±]_i, 1.448+1.276[±]_i,
1.450+7.944[±]_i, 1.462+5.382[±]_i, 1.469+3.754[±]_i,
1.470+1.498[±]_i, 1.490+2.050[±]_i, 1.500+1.184[±]_i,
1.502+9.938[±]_i, 1.510+2.060[±]_i, 1.510+5.000[±]_i,
1.510+1.000[±]_i) in term of 14
wavelengths at 3.4615,
2.7885, 2.325, 2.046, 1.784,
1.4625, 1.2705, 1.0101,
0.7016, 0.53325, 0.38815,
0.299, 0.2316, 8.24 μm

1357
1358
1359

Table B7. Summary of normalized mean error (NME) (%) of surface meteorological and air quality variables using two-way coupled models (WRF-Chem and WRF-CMAQ).

T2	SH2	RH2	WS10	PM _{2.5}	O ₃	PM _{2.5} with ARI (ARI) or without ARI (NO)	O ₃ with ARI (ARI) or without ARI (NO)	Model	Region	Reference
					23.60, 38.50, 55.70, 39.80			WRF-Chem	EA	Liu X. et al. (2016)
0.80, 0.60, 0.60, 0.60		19.10, 16.50, 10.00, 10.10	58.90, 41.60, 44.90, 49.50	37.31, 37.61, 35.77, 34.69, 35.34, 35.41, 45.22, 44.33, 43.09, 39.29, 39.49, 39.07		37.61, 35.34, 44.33, 39.49 (ARI) 35.77, 35.41, 43.09, 39.07 (NO)		WRF-Chem	China	Zhang et al. (2018)
270.20, 22.30, 12.50, 17.60				44.99, 29.55, 37.28				WRF-Chem	EA	Zhang Yang et al. (2016a)
								WRF-Chem	NCP	Yang et al. (2015)
15.50, 15.80, 13.90, 9.90	10.40, 10.40, 9.90, 9.90		31.30, 31.30, 32.50, 32.50	49.80, 65.30, 49.80, 65.60, 88.30, 56.90, 88.40, 57.00	127.00, 32.20, 25.40, 126.10, 32.10, 25.00, 79.90, 25.80, 21.40, 45.80, 77.90, 25.60, 21.10, 39.50			WRF-Chem	EA	Zhang Y. et al. (2015a)
14	11		32	52.70, 58.00, 104.70, 62.00	87.50, 28.60, 23.30, 52.90, 32.40, 28.20			WRF-Chem	EA	Chen Y. et al. (2015)
-0.48, 0.19, 0.21, 0.05, 0.08, 0.13, 0.05, 0.04, 0.04, 0.05, 0.02, 0.02, 0.06, 0.05, 0.04, 0.02, 16.60, 10.50, 8.90, 12.90, 10.50, 10.20, 6.52, 6.58			0.33, 1.92, 0.71, 0.78, 0.28, 1.72, 0.61, 0.64, 0.24, 1.76, 0.00, 0.45, 0.34, 1.29, 0.44, 0.56					WRF-Chem	NCP	Chen D. et al. (2015)
		15.76, 12.15	112.28, 97.26					WRF-Chem	EA	Wang K. et al. (2018)
				36.00, 33.00	31.00, 22.00			WRF-Chem	NEA	Park et al. (2018)
				44.00, 44.60, 40.10, 54.30				WRF-Chem	China	Zhao et al. (2017)
				41.48, 41.00, 51.77, 55.70	26.68, 26.71, 34.43, 34.64	41.00, 55.70 (ARI) 41.48, 51.77 (NO)	26.71, 34.64 (ARI) 26.68, 34.43 (NO)	WRF-Chem	NCP	Gao M. et al. (2015)
				37.99, 35.06, 38.59, 35.44, 34.39				WRF-CMAQ	SEA	Nguyen et al. (2019b)
								WRF-CMAQ	China	Chang (2018)

1360
1361

Appendix C

1362

C1 Comparisons of SI at different temporal scales for meteorology

1363

To probe the model performance of simulated T2, RH2, SH2 and WS2 at different temporal scales, the SI of these meteorological variables from PSI were grouped according to the simulation time (yearly, seasonal, monthly and daily) and plotted in Figure C1. Note that the seasonal results contained SI values from simulations lasting more than one month and less than or equal to 3 months. Here in Figure C1, NP and NS were the number of PSI and samples with SI at different time scales, respectively, and also their total values were the same as the ones listed in Table S2. The correlation between simulated and observed T2 (Figure C1a) at the seasonal (mean R= 0.97 with the smallest sample size), yearly (0.91) and monthly (0.90) scales were stronger than that at the daily scale (0.87), indicating that long-term simulations of T2 were well reproduced by coupled models. As shown in Figure C1e, T2 underestimation mentioned above (Fig. 3a) appeared also in the seasonal, monthly and yearly simulations (average MB = -0.87 °C, -0.15 °C and -0.34 °C, respectively), but the daily

1373

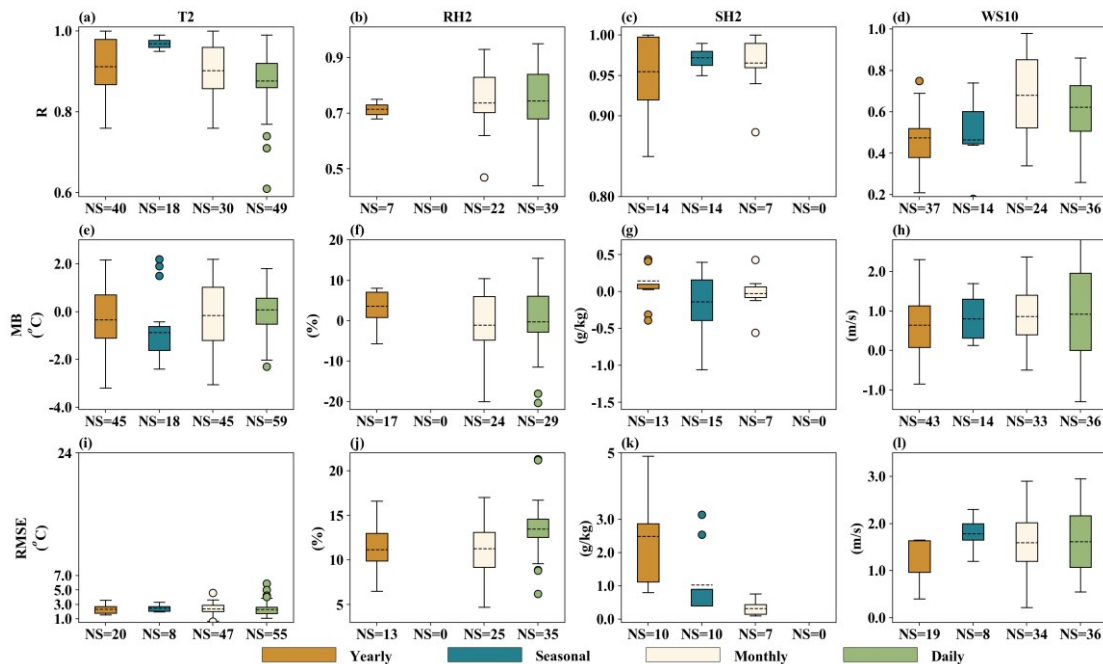
1374 T2 were overestimated (average MB = 0.07 °C). It should be noted that T2 at the monthly scale was
 1375 underpredicted mainly during winter months (16 samples). Regarding the mean RMSE, its value
 1376 (Figure C1i) at the daily scale was the largest (0.97 °C) in comparison with that at the other temporal
 1377 scales.

1378 Given that no SI was available for RH2 at the seasonal scale, results at other time scales were
 1379 discussed here. Figure C1b presented that simulated RH2 at the daily scale had the best correlation
 1380 coefficient (mean R = 0.74), followed by those at the monthly (0.73) and yearly (0.71) scales. Except
 1381 overestimation (average MB = 3.6 %) at the yearly scale (Figure C1f), modeled RH2 were
 1382 underestimated at the monthly (average MB = -1.1 %) and daily (average MB = -0.2 %) scales,
 1383 respectively. Therefore, coupled models calculated RH2 reasonably well in short-term simulations.
 1384 However, at the daily scale, RMSE of modeled RH2 (Figure C1j) was relatively large fluctuation
 1385 ranging from 6.2 % to 21.3 %.

1386 Lacking of SI for SH2 at the daily scale, only those at other time scales were compared. Even
 1387 though NP and NS were very limited, the modeled SH2 (Figure C1c) exhibited especially good
 1388 correlation with observations with the mean R values exceeding 0.95 at the yearly, seasonal and
 1389 monthly scales (0.99, 0.97 and 0.96, respectively) but had the largest mean RMSE (2.09 g·kg⁻¹) at
 1390 the yearly scale (Figure C1k). Also, both over- and under-estimations of modeled SH2 (Fig. C1g)
 1391 were reported at different time scales with average MB values as 0.15 g·kg⁻¹, -0.02 g·kg⁻¹, and -0.14
 1392 g·kg⁻¹ for yearly, seasonal and monthly simulations, respectively. Generally, the long-term
 1393 simulations of SH2 agreed better with observations than the short-term ones.

1394 As seen in Figure C1d, the modeled WS10 at the monthly scale (mean R = 0.68) correlated
 1395 with observations better than that at the daily, yearly and seasonal scales (mean R = 0.62, 0.48 and
 1396 0.46, respectively). The simulations at all temporal scales tended to overestimate WS10 comparing
 1397 against observations (Figure C1h) and their average MB were 0.80 m·s⁻¹ (seasonal), 0.86 m·s⁻¹
 1398 (monthly), 0.64 m·s⁻¹ (yearly) and 0.62 m·s⁻¹ (daily), respectively. The short-term simulations of
 1399 WS10 better matched with observations compared to the long-term ones. At the same time, the
 1400 largest mean RMSE (1.79 m·s⁻¹) of simulated WS10 (Figure C1l) appeared at the seasonal scale.

1401



1402
 1403
 1404
 1405

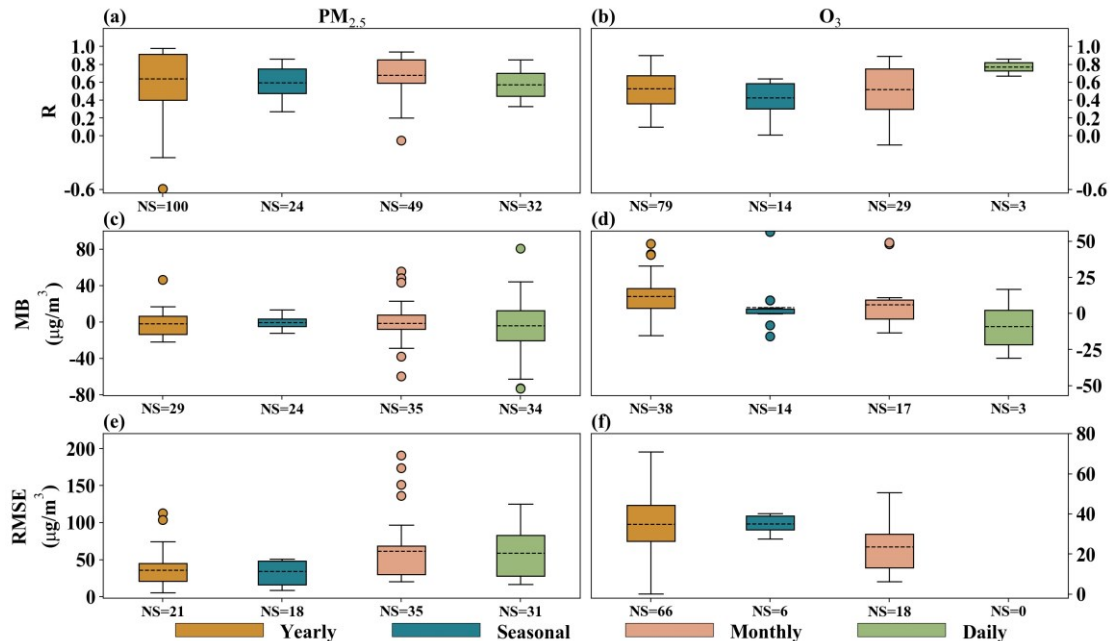
Figure C1. The statistical indices of modeled meteorological variables at different temporal scales (Yearly, Seasonal, Monthly and Daily) from past studies in Asia.

1406 C2 Comparisons of SI at different temporal scales for air quality

1407 Figure C2 depicted the SI of simulated PM_{2.5} and O₃ at yearly, seasonal, monthly and daily
 1408 scales. The correlation between simulated and observed PM_{2.5} (Figure C2a) at the monthly scale
 1409 (mean R = 0.68) was largest compared to those at the yearly (0.64), seasonal (0.59), daily (0.57)
 1410 scales. All the simulated PM_{2.5} were underestimated, with the average daily, monthly, seasonal, and

1411 yearly MB as -4.13 , -1.46 , -0.28 , and $-1.89 \mu\text{g}\cdot\text{m}^{-3}$, respectively (Figure C2c). As displayed in Figure
 1412 C2e, the mean RMSE at the monthly scale was the largest ($61.57 \mu\text{g}\cdot\text{m}^{-3}$).

1413 Regarding to correlation between simulated and observed O_3 (Figure C2b), it was the best at
 1414 the daily scale (mean $R= 0.77$). Modeled O_3 were overestimated at the seasonal (average MB =
 1415 $+4.12 \mu\text{g}\cdot\text{m}^{-3}$), monthly (average MB = $+6.11 \mu\text{g}\cdot\text{m}^{-3}$) and yearly (average MB = $+11.71 \mu\text{g}\cdot\text{m}^{-3}$)
 1416 scales, but underestimated at the daily scale (average MB = $-8.89 \mu\text{g}\cdot\text{m}^{-3}$) (Figure C2d). Note that no
 1417 RMSE for O_3 simulation was available at the daily scale, and the RMSE at the yearly scale (Figure
 1418 C2f) had relatively large fluctuation ranging from 0.21 to $71 \mu\text{g}\cdot\text{m}^{-3}$. Therefore, coupled models
 1419 calculated O_3 matched well with observation in short-term simulations.



1420 Figure C2. The quantile distributions of simulated $\text{PM}_{2.5}$ and O_3 performance metrics at different temporal scales
 1421 from past studies in Asia.
 1422
 1423

1424 **Data availability**

1425 The related dataset can be downloaded from <https://doi.org/10.5281/zenodo.5571076> (Gao et
 1426 al., 2021), and this dataset includes basic information (Table S1), performance metrics (Table S2),
 1427 quantitative effects of aerosol feedbacks on meteorological and air quality variables (Table S3),
 1428 model configuration and setup (Table S4) and aerosol-induced variations of simulated shortwave
 1429 and longwave radiative forcing (Table S5) extracted from collected studies of applications of two-
 1430 way coupled meteorology and air quality models in Asia.

1431

1432 **Author contribution**

1433 Chao Gao, Aijun Xiu, Xuelei Zhang and Qingqing Tong carried out the data collection, related
 1434 analysis, figure plotting, and manuscript writing; Hongmei Zhao, Shichun Zhang, Guangyi Yang
 1435 and Mengduo Zhang involved with the original research plan and made suggestions to the
 1436 manuscript writing.

1437

1438 **Competing interest**

1439 The authors declare that they have no conflict of interest.

1440

1441 **Acknowledgement**

1442 This study was financially sponsored by National Key Research and Development Program of

1443 China (No. 2017YFC0212304 and No. 2019YFE0194500), Talent Program of Chinese Academy of
1444 Sciences, and National Natural Science Foundation of China (No. 42171142, No. 41771071 and No.
1445 41571063). The authors are very grateful to many researchers who provided detailed information
1446 on the two-way coupled models and related research work. The list includes but is not limited to
1447 Xueshun Chen, Zifa Wang, Yi Gao, Meigen Zhang and Baozhu Ge (Institute of Atmospheric Physics,
1448 Chinese Academy of Sciences), Chunhong Zhou (Chinese Academy of Meteorological Sciences),
1449 Yang Zhang (Northeastern University), Mark Zachary Jacobson (Stanford University), Tianliang
1450 Zhao (Nanjing University of Information Science & Technology), Xin Huang (Nanjing University),
1451 Chun Zhao (University of Science and Technology of China), Junhua Yang and Shichang Kang
1452 (Northwest Institute of Eco-Environment and Resources, Chinese Academy of Sciences), Sachin
1453 Ghude (Ministry of Earth Sciences Government of India) and Luke Conibear (University of Leeds).
1454 We would also like to express our deepest appreciation to the editor James Allan and two anonymous
1455 reviewers for their constructive comments and suggestions, which helped to improve the quality and
1456 readability of this article.

1457

1458 Reference

- 1459 Ackerman, A. S., Toon, O. B., Stevens, D. E., Heymsfield, A. J., Ramanathan, V., and Welton, E. J.:
1460 Reduction of tropical cloudiness by soot, *Science* (80-.), 288, 1042–1047,
1461 <https://doi.org/10.1126/science.288.5468.1042>, 2000.
- 1462 Ahmadov, R., McKeen, S. A., Robinson, A. L., Bahreini, R., Middlebrook, A. M., De Gouw, J. A.,
1463 Meagher, J., Hsie, E., Edgerton, E., and Shaw, S.: A volatility basis set model for summertime
1464 secondary organic aerosols over the eastern United States in 2006, *J. Geophys. Res. Atmos.*, 117,
1465 <https://doi.org/10.1029/2011JD016831>, 2012.
- 1466 Albrecht, B. A.: Aerosols, cloud microphysics, and fractional cloudiness, *Science* (80-.), 245, 1227–
1467 1230, <https://doi.org/10.1126/science.245.4923.1227>, 1989.
- 1468 An, Z., Huang, R.-J., Zhang, R., Tie, X., Li, G., Cao, J., Zhou, W., Shi, Z., Han, Y., and Gu, Z.: Severe
1469 haze in northern China: A synergy of anthropogenic emissions and atmospheric processes, *Proc.*
1470 *Natl. Acad. Sci.*, 116, 8657–8666, <https://doi.org/10.1073/pnas.1900125116>, 2019.
- 1471 Andreae, M. O. and Rosenfeld, D.: Aerosol-cloud-precipitation interactions. Part 1. The nature and
1472 sources of cloud-active aerosols, *Earth-Science Rev.*, 89, 13–41,
1473 <https://doi.org/10.1016/j.earscirev.2008.03.001>, 2008.
- 1474 Appel, K. W., Pouliot, G. A., Simon, H., Sarwar, G., Pye, H. O. T., Napelenok, S. L., Akhtar, F., and
1475 Roselle, S. J.: Evaluation of dust and trace metal estimates from the Community Multiscale Air
1476 Quality (CMAQ) model version 5.0, *Geosci. Model Dev.*, 6, 883–899, <https://doi.org/10.5194/gmd-6-883-2013>, 2013.
- 1478 Appel, K. W., Napelenok, S. L., Foley, K. M., Pye, H. O. T., Hogrefe, C., Luecken, D. J., Bash, J. O.,
1479 Roselle, S. J., Pleim, J. E., Foroutan, H., Hutzell, W. T., Pouliot, G. A., Sarwar, G., Fahey, K. M.,
1480 Gantt, B., Gilliam, R. C., Heath, N. K., Kang, D., Mathur, R., Schwede, D. B., Spero, T. L., Wong,
1481 D. C., and Young, J. O.: Description and evaluation of the Community Multiscale Air Quality
1482 (CMAQ) modeling system version 5.1, *Geosci. Model Dev.*, 10, 1703–1732,
1483 <https://doi.org/10.5194/gmd-10-1703-2017>, 2017.
- 1484 Appel, K. W., Bash, J. O., Fahey, K. M., Foley, K. M., Gilliam, R. C., Hogrefe, C., Hutzell, W. T., Kang,
1485 D., Mathur, R., and Murphy, B. N.: The Community Multiscale Air Quality (CMAQ) model
1486 versions 5.3 and 5.3.1: system updates and evaluation, *Geosci. Model Dev.*, 14, 2867–2897,
1487 <https://doi.org/10.5194/gmd-14-2867-2021>, 2021.
- 1488 Archer-Nicholls, S., Lowe, D., Lacey, F., Kumar, R., Xiao, Q., Liu, Y., Carter, E., Baumgartner, J., and
1489 Wiedinmyer, C.: Radiative effects of residential sector emissions in China: sensitivity to uncertainty
1490 in black carbon emissions, *J. Geophys. Res. Atmos.*, 124, 5029–5044,
1491 <https://doi.org/10.1029/2018JD030120>, 2019.
- 1492 Ashrafi, K., Motlagh, M. S., and Neyestani, S. E.: Dust storms modeling and their impacts on air quality
1493 and radiation budget over Iran using WRF-Chem, *Air Qual. Atmos. Heal.*, 10, 1059–1076,
1494 <https://doi.org/10.1007/s11869-017-0494-8>, 2017.
- 1495 Bai, Y., Qi, H., Zhao, T., Zhou, Y., Liu, L., Xiong, J., Zhou, Z., and Cui, C.: Simulation of the responses
1496 of rainstorm in the Yangtze River Middle Reaches to changes in anthropogenic aerosol emissions,
1497 *Atmos. Environ.*, 220, 117081, <https://doi.org/10.1016/j.atmosenv.2019.117081>, 2020.
- 1498 Baklanov, A., Schlünzen, K., Suppan, P., Baldasano, J., Brunner, D., Aksoyoglu, S., Carmichael, G.,
1499 Douros, J., Flemming, J., and Forkel, R.: Online coupled regional meteorology chemistry models in
1500 Europe: current status and prospects, *Atmos. Chem. Phys.*, 14, 317–398,
1501 <https://doi.org/10.5194/acp-14-317-2014>, 2014.
- 1502 Baró, R., Jiménez-Guerrero, P., Balzarini, A., Curci, G., Forkel, R., Grell, G., Hirtl, M., Honzak, L.,
1503 Langer, M., and Pérez, J. L.: Sensitivity analysis of the microphysics scheme in WRF-Chem
1504 contributions to AQMEII phase 2, *Atmos. Environ.*, 115, 620–629,
1505 <https://doi.org/10.1016/j.atmosenv.2015.01.047>, 2015.
- 1506 Barth, M. C., Rasch, P. J., Kiehl, J. T., Benkovitz, C. M., and Schwartz, S. E.: Sulfur chemistry in the
1507 NCAR CCM: Description, evaluation, features and sensitivity to aqueous chemistry, *J. Geophys.*
1508 *Res.*, 105, 1387–1415, <https://doi.org/10.1029/1999JD900773>, 2000.

1509 Bauer, P., Thorpe, A., and Brunet, G.: The quiet revolution of numerical weather prediction, *Nature*, 525,
1510 47–55, <https://doi.org/10.1038/nature14956>, 2015.

1511 Beard, K. V.: Terminal velocity and shape of cloud and precipitation drops aloft, *J. Atmos. Sci.*, 33, 851–
1512 864, [https://doi.org/10.1175/1520-0469\(1976\)033<0851:TVASOC>2.0.CO;2](https://doi.org/10.1175/1520-0469(1976)033<0851:TVASOC>2.0.CO;2), 1976.

1513 Bei, N., Wu, J., Elser, M., Tian, F., Cao, J., El-Haddad, I., Li, X., Huang, R., Li, Z., and Long, X.: Impacts
1514 of meteorological uncertainties on the haze formation in Beijing-Tianjin-Hebei (BTH) during
1515 wintertime: a case study, *Atmos. Chem. Phys.*, 17, 14579, [https://doi.org/10.5194/acp-17-14579-](https://doi.org/10.5194/acp-17-14579-2017)
1516 2017, 2017.

1517 Beig, G., Chate, D. M., Ghude, S. D., Mahajan, A. S., Srinivas, R., Ali, K., Sahu, S. K., Parkhi, N.,
1518 Surendran, D., and Trimbake, H. R.: Quantifying the effect of air quality control measures during
1519 the 2010 Commonwealth Games at Delhi, India, *Atmos. Environ.*, 80, 455–463,
1520 <https://doi.org/10.1016/j.atmosenv.2013.08.012>, 2013.

1521 Bellouin, N., Jones, A., Haywood, J., and Christopher, S. A.: Updated estimate of aerosol direct radiative
1522 forcing from satellite observations and comparison against the Hadley Centre climate model, *J.*
1523 *Geophys. Res. Atmos.*, 113, <https://doi.org/10.1029/2007JD009385>, 2008.

1524 Benas, N., Meirink, J. F., Karlsson, K.-G., Stengel, M., and Stammes, P.: Satellite observations of
1525 aerosols and clouds over southern China from 2006 to 2015: analysis of changes and possible
1526 interaction mechanisms, *Atmos. Chem. Phys.*, 20, 457–474, [https://doi.org/10.5194/acp-20-457-](https://doi.org/10.5194/acp-20-457-2020)
1527 2020, 2020.

1528 Bennartz, R., Fan, J., Rausch, J., Leung, L. R., and Heidinger, A. K.: Pollution from China increases
1529 cloud droplet number, suppresses rain over the East China Sea, *Geophys. Res. Lett.*, 38,
1530 <https://doi.org/10.1029/2011GL047235>, 2011.

1531 Bharali, C., Nair, V. S., Chutia, L., and Babu, S. S.: Modeling of the effects of wintertime aerosols on
1532 boundary layer properties over the Indo Gangetic Plain, *J. Geophys. Res. Atmos.*, 124, 4141–4157,
1533 <https://doi.org/10.1029/2018JD029758>, 2019.

1534 Bhattacharya, A., Chakraborty, A., and Venugopal, V.: Role of aerosols in modulating cloud properties
1535 during active–break cycle of Indian summer monsoon, *Clim. Dyn.*, 49, 2131–2145,
1536 <https://doi.org/10.1007/s00382-016-3437-4>, 2017.

1537 Binkowski, F. S. and Roselle, S. J.: Models-3 Community Multiscale Air Quality (CMAQ) model aerosol
1538 component 1. Model description, *J. Geophys. Res. Atmos.*, 108,
1539 <https://doi.org/10.1029/2001JD001409>, 2003.

1540 Binkowski, F. S. and Shankar, U.: The regional particulate matter model: 1. Model description and
1541 preliminary results, *J. Geophys. Res. Atmos.*, 100, 26191–26209,
1542 <https://doi.org/10.1029/95JD02093>, 1995.

1543 Bollasina, M. A., Ming, Y., and Ramaswamy, V.: Anthropogenic aerosols and the weakening of the
1544 South Asian summer monsoon, *Science (80-.)*, 334, 502–505,
1545 <https://doi.org/10.1126/science.1204994>, 2011.

1546 Bran, S. H., Jose, S., and Srivastava, R.: Investigation of optical and radiative properties of aerosols
1547 during an intense dust storm: A regional climate modeling approach, *J. Atmos. Solar-Terrestrial*
1548 *Phys.*, 168, 21–31, <https://doi.org/10.1016/j.jastp.2018.01.003>, 2018.

1549 Briant, R., Tuccella, P., Deroubaix, A., Khvorostyanov, D., Menut, L., Mailler, S., and Turquety, S.:
1550 Aerosol-radiation interaction modelling using online coupling between the WRF 3.7.1
1551 meteorological model and the CHIMERE 2016 chemistry-transport model, through the OASIS3-
1552 MCT coupler, *Geosci. Model Dev.*, 10, 927–944, <https://doi.org/10.5194/gmd-10-927-2017>, 2017.

1553 Brunekreef, B. and Holgate, S. T.: Air pollution and health, *Lancet*, 360, 1233–1242,
1554 [https://doi.org/10.1016/S0140-6736\(02\)11274-8](https://doi.org/10.1016/S0140-6736(02)11274-8), 2002.

1555 Brunner, D., Savage, N., Jorba, O., Eder, B., Giordano, L., Badia, A., Balzarini, A., Baro, R., Bianconi,
1556 R., and Chemel, C.: Comparative analysis of meteorological performance of coupled chemistry-
1557 meteorology models in the context of AQMEII phase 2, *Atmos. Environ.*, 115, 470–498,
1558 <https://doi.org/10.1016/j.atmosenv.2014.12.032>, 2015.

1559 Byun, D. and Schere, K. L.: Review of the governing equations, computational algorithms, and other
1560 components of the Models-3 Community Multiscale Air Quality (CMAQ) modeling system, *Appl.*
1561 *Mech. Rev.*, 59, 51–77, <https://doi.org/10.1115/1.2128636>, 2006.

1562 Campbell, P., Zhang, Y., Yahya, K., Wang, K., Hogrefe, C., Pouliot, G., Knote, C., Hodzic, A., San Jose,
1563 R., and Perez, J. L.: A multi-model assessment for the 2006 and 2010 simulations under the Air
1564 Quality Model Evaluation International Initiative (AQMEII) phase 2 over North America: Part I.
1565 Indicators of the sensitivity of O₃ and PM_{2.5} formation regimes, *Atmos. Environ.*, 115, 569–586,
1566 <https://doi.org/10.1016/j.atmosenv.2014.12.026>, 2015.

1567 Campbell, P., Zhang, Y., Wang, K., Leung, R., Fan, J., Zheng, B., Zhang, Q., and He, K.: Evaluation of
1568 a multi-scale WRF-CAM5 simulation during the 2010 East Asian Summer Monsoon, *Atmos.*
1569 *Environ.*, 169, 204–217, <https://doi.org/10.1016/j.atmosenv.2017.09.008>, 2017.

1570 Carlton, A. G., Bhave, P. V., Napelenok, S. L., Edney, E. O., Sarwar, G., Pinder, R. W., Pouliot, G. A.,
1571 and Houyoux, M.: Model representation of secondary organic aerosol in CMAQv4.7, *Environ. Sci.*
1572 *Technol.*, 44, 8553–8560, <https://doi.org/10.1021/es100636q>, 2010.

1573 Casazza, M., Lega, M., Liu, G., Ulgiati, S., and Endrey, T. A.: Aerosol pollution, including eroded soils,
1574 intensifies cloud growth, precipitation, and soil erosion: A review, *J. Clean. Prod.*, 189, 135–144,
1575 <https://doi.org/10.1016/j.jclepro.2018.04.004>, 2018.

1576 Chang, S.: Characteristics of aerosols and cloud condensation nuclei (CCN) over China investigated by
1577 the two-way coupled WRF-CMAQ air quality model, 2018.

1578 Chapman, E. G., Jr, W. I. G., Easter, R. C., Barnard, J. C., Ghan, S. J., Pekour, M. S., and Fast, J. D.: and
1579 Physics Coupling aerosol-cloud-radiative processes in the WRF-Chem model : Investigating the
1580 radiative impact of elevated point sources, 945–964, <https://doi.org/10.5194/acp-9-945-2009>, 2009.

1581 Chen, D.-S., Ma, X., Xie, X., Wei, P., Wen, W., Xu, T., Yang, N., Gao, Q., Shi, H., and Guo, X.:
1582 Modelling the effect of aerosol feedbacks on the regional meteorology factors over China, *Aerosol*.
1583 *Air. Qual. Res.*, 15, 1559–1579, <https://doi.org/10.4209/aaqr.2014.11.0272>, 2015a.

1584 Chen, J., Li, C., Ristovski, Z., Milic, A., Gu, Y., Islam, M. S., Wang, S., Hao, J., Zhang, H., and He, C.:
1585 A review of biomass burning: Emissions and impacts on air quality, health and climate in China,
1586 *Sci. Total Environ.*, 579, 1000–1034, <https://doi.org/10.1016/j.scitotenv.2016.11.025>, 2017a.

1587 Chen, L., Zhu, J., Liao, H., Gao, Y., Qiu, Y., Zhang, M., Liu, Z., Li, N., and Wang, Y.: Assessing the
1588 formation and evolution mechanisms of severe haze pollution in the Beijing-Tianjin-Hebei region
1589 using process analysis, *Atmos. Chem. Phys.*, 19, 10845–10864, <https://doi.org/10.5194/acp-19-10845-2019>, 2019a.

1591 Chen, L., Gao, Y., Zhang, M., Fu, J. S., Zhu, J., Liao, H., Li, J., Huang, K., Ge, B., and Wang, X.: MICS-
1592 Asia III: Multi-model comparison and evaluation of aerosol over East Asia, *Atmos. Chem. Phys.*,
1593 19, 11911–11937, <https://doi.org/10.5194/acp-19-11911-2019>, 2019b.

1594 Chen, S., Huang, J., Zhao, C., Qian, Y., Leung, L. R., and Yang, B.: Modeling the transport and radiative
1595 forcing of Taklimakan dust over the Tibetan Plateau: A case study in the summer of 2006, *J.*
1596 *Geophys. Res. Atmos.*, 118, 797–812, <https://doi.org/10.1002/jgrd.50122>, 2013.

1597 Chen, S., Zhao, C., Qian, Y., Leung, L. R., Huang, J., Huang, Z., Bi, J., Zhang, W., Shi, J., and Yang, L.:
1598 Regional modeling of dust mass balance and radiative forcing over East Asia using WRF-Chem,
1599 *Atmos. Chem. Phys.*, 15, 15–30, <https://doi.org/10.1016/j.atmosenv.2014.02.001>, 2014.

1600 Chen, S., Huang, J., Qian, Y., Zhao, C., Kang, L., Yang, B., Wang, Y., Liu, Y., Yuan, T., and Wang, T.:
1601 An overview of mineral dust modeling over East Asia, *J. Meteorol. Res.*, 31, 633–653,
1602 <https://doi.org/10.1007/s13351-017-6142-2>, 2017b.

1603 Chen, S., Huang, J., Kang, L., Wang, H., Ma, X., He, Y., Yuan, T., Yang, B., Huang, Z., and Zhang, G.:
1604 Emission, transport, and radiative effects of mineral dust from the Taklimakan and Gobi deserts:
1605 comparison of measurements and model results., *Atmos. Chem. Phys.*, 17, 2401–2421,
1606 <https://doi.org/10.5194/acp-17-2401-2017>, 2017c.

1607 Chen, X., Wang, Z., Yu, F., Pan, X., Li, J., Ge, B., Wang, Z., Hu, M., Yang, W., and Chen, H.: Estimation
1608 of atmospheric aging time of black carbon particles in the polluted atmosphere over central-eastern
1609 China using microphysical process analysis in regional chemical transport model, *Atmos. Environ.*,
1610 163, 44–56, <https://doi.org/j.atmosenv.2017.05.016>, 2017d.

1611 Chen, X., Yang, W., Wang, Z., Li, J., Hu, M., An, J., Wu, Q., Wang, Z., Chen, H., and Wei, Y.: Improving
1612 new particle formation simulation by coupling a volatility-basis set (VBS) organic aerosol module
1613 in NAQPMS+APM, *Atmos. Environ.*, 204, 1–11, <https://doi.org/j.atmosenv.2019.01.053>, 2019c.

1614 Chen, X., Yu, F., Yang, W., Sun, Y., Chen, H., Du, W., Zhao, J., Wei, Y., Wei, L., and Du, H.: Global-
1615 regional nested simulation of particle number concentration by combing microphysical processes
1616 with an evolving organic aerosol module, *Atmos. Chem. Phys.*, 21, 9343–9366,
1617 <https://doi.org/10.5194/acp-21-9343-2021>, 2021.

1618 Chen, Y., Zhang, Y., Fan, J., Leung, L.-Y. R., Zhang, Q., and He, K.: Application of an online-coupled
1619 regional climate model, WRF-CAM5, over East Asia for examination of ice nucleation schemes:
1620 Part I. Comprehensive model evaluation and trend analysis for 2006 and 2011, 3, 627–667,
1621 <https://doi.org/10.3390/cli3030627>, 2015b.

1622 Choobari, O. A., Zawar-Reza, P., and Sturman, A.: The global distribution of mineral dust and its impacts
1623 on the climate system: A review, *Atmos. Res.*, 138, 152–165,
1624 <https://doi.org/10.1016/j.atmosres.2013.11.007>, 2014.

1625 Conibear, L., Butt, E. W., Knote, C., Arnold, S. R., and Spracklen, D. V.: Residential energy use
1626 emissions dominate health impacts from exposure to ambient particulate matter in India, *Nat.*
1627 *Commun.*, 9, 1–9, <https://doi.org/10.1038/s41467-018-02986-7>, 2018a.

1628 Conibear, L., Butt, E. W., Knote, C., Arnold, S. R., and Spracklen, D. V.: Stringent Emission Control
1629 Policies Can Provide Large Improvements in Air Quality and Public Health in India, 2, 196–211,
1630 <https://doi.org/10.1029/2018gh000139>, 2018b.

1631 Conti, G. O., Heibati, B., Kloog, I., Fiore, M., and Ferrante, M.: A review of AirQ Models and their
1632 applications for forecasting the air pollution health outcomes, *Environ. Sci. Pollut. Res.*, 24, 6426–
1633 6445, <https://doi.org/10.1007/s11356-016-8180-1>, 2017.

1634 Craig, A., Valcke, S., and Coquart, L.: Development and performance of a new version of the OASIS
1635 coupler, OASIS3-MCT_3.0, *Geosci. Model Dev.*, 10, 3297, <https://doi.org/10.5194/gmd-10-3297-2017>, 2017.

1637 Cuchiara, G. C., Li, X., Carvalho, J., and Rappenglück, B.: Intercomparison of planetary boundary layer
1638 parameterization and its impacts on surface ozone concentration in the WRF/Chem model for a case
1639 study in Houston/Texas, *Atmos. Environ.*, 96, 175–185,
1640 <https://doi.org/10.1016/j.atmosenv.2014.07.013>, 2014.

1641 Dahutia, P., Pathak, B., and Bhuyan, P. K.: Vertical distribution of aerosols and clouds over north-eastern
1642 South Asia: Aerosol-cloud interactions, *Atmos. Environ.*, 215, 116882,
1643 <https://doi.org/10.1016/j.atmosenv.2019.116882>, 2019.

1644 Ding, A. J., Huang, X., Nie, W., Sun, J. N., Kerminen, V., Petäjä, T., Su, H., Cheng, Y. F., Yang, X., and
1645 Wang, M. H.: Enhanced haze pollution by black carbon in megacities in China, *Geophys. Res. Lett.*,
1646 43, 2873–2879, <https://doi.org/10.1002/2016GL067745>, 2016.

1647 Ding, Q. J., Sun, J., Huang, X., Ding, A., Zou, J., Yang, X., and Fu, C.: Impacts of black carbon on the
1648 formation of advection–radiation fog during a haze pollution episode in eastern China, *Atmos.*
1649 *Chem. Phys.*, 19, 7759–7774, <https://doi.org/10.5194/acp-19-7759-2019>, 2019.

1650 Dipu, S., Prabha, T. V., Pandithurai, G., Dudhia, J., Pfister, G., Rajesh, K., and Goswami, B. N.: Impact
1651 of elevated aerosol layer on the cloud macrophysical properties prior to monsoon onset, *Atmos.*
1652 *Environ.*, 70, 454–467, <https://doi.org/10.1016/j.atmosenv.2012.12.036>, 2013.

1653 Donat, M. G., Lowry, A. L., Alexander, L. V., O’Gorman, P. A., and Maher, N.: More extreme
1654 precipitation in the world’s dry and wet regions, *Nat. Clim. Chang.*, 6, 508–513,
1655 <https://doi.org/10.1038/nclimate2941>, 2016.

1656 Dong, X., Fu, J. S., Huang, K., Zhu, Q., and Tipton, M.: Regional Climate Effects of Biomass Burning
1657 and Dust in East Asia: Evidence From Modeling and Observation, *Geophys. Res. Lett.*, 46, 11490–
1658 11499, <https://doi.org/10.1029/2019GL083894>, 2019.

1659 Easter, R. C., Ghan, S. J., Zhang, Y., Saylor, R. D., Chapman, E. G., Laulainen, N. S., Abdul-Razzak,
1660 H., Leung, L. R., Bian, X., and Zaveri, R. A.: MIRAGE: Model description and evaluation of
1661 aerosols and trace gases, *J. Geophys. Res. Atmos.*, 109, <https://doi.org/10.1029/2004JD004571>,
1662 2004.

1663 Eck, T. F., Holben, B. N., Reid, J. S., Xian, P., Giles, D. M., Sinyuk, A., Smirnov, A., Schafer, J. S.,
1664 Slutsker, I., and Kim, J.: Observations of the interaction and transport of fine mode aerosols with
1665 cloud and/or fog in Northeast Asia from Aerosol Robotic Network and satellite remote sensing, *J.*
1666 *Geophys. Res. Atmos.*, 123, 5560–5587, <https://doi.org/10.1029/2018JD028313>, 2018.

1667 El-Harbawi, M.: Air quality modelling, simulation, and computational methods: a review, *Environ. Rev.*,
1668 21, 149–179, <https://doi.org/10.1139/er-2012-0056>, 2013.

1669 ENVIRON, U. G.: Comprehensive Air Quality Model with Extensions (CAMx). Version 4.50, Env. Int.
1670 Corp. Novato, 2008.

1671 EPA: Meteorological Model Performance for Annual 2016 Simulation WRF v3.8, United States Environ.
1672 Prot. Agency, 2018.

1673 Fahey, K. M. and Pandis, S. N.: Optimizing model performance: variable size resolution in cloud
1674 chemistry modeling, *Atmos. Environ.*, 35, 4471–4478, [https://doi.org/10.1016/S1352-2310\(01\)00224-2](https://doi.org/10.1016/S1352-2310(01)00224-2), 2001.

1675 Fahey, K. M., Carlton, A. G., Pye, H. O. T., Baek, J., Hutzell, W. T., Stanier, C. O., Baker, K. R., Appel,
1676 K. W., Jaoui, M., and Offenberg, J. H.: A framework for expanding aqueous chemistry in the
1677 Community Multiscale Air Quality (CMAQ) model version 5.1, *Geosci. Model Dev.*, 10, 1587–
1678 1605, <https://doi.org/10.5194/gmd-10-1587-2017>, 2017.

1679 Fan, J., Rosenfeld, D., Yang, Y., Zhao, C., Leung, L. R., and Li, Z.: Substantial contribution of
1680 anthropogenic air pollution to catastrophic floods in Southwest China, *Geophys. Res. Lett.*, 42,
1681 6066–6075, <https://doi.org/10.1002/2015GL064479>, 2015.

1682 Fan, J., Wang, Y., Rosenfeld, D., and Liu, X.: Review of aerosol-cloud interactions: Mechanisms,
1683 significance, and challenges, *J. Atmos. Sci.*, 73, 4221–4252, <https://doi.org/10.1175/JAS-D-16-0037.1>, 2016.

1684 Fan, J., Rosenfeld, D., Zhang, Y., Giangrande, S. E., Li, Z., Machado, L. A. T., Martin, S. T., Yang, Y.,
1685 Wang, J., and Artaxo, P.: Substantial convection and precipitation enhancements by ultrafine
1686 aerosol particles, *Science (80-.)*, 359, 411–418, <https://doi.org/10.1126/science.aan8461>, 2018.

1687 Fast, J. D., Gustafson Jr, W. I., Easter, R. C., Zaveri, R. A., Barnard, J. C., Chapman, E. G., Grell, G. A.,
1688 and Peckham, S. E.: Evolution of ozone, particulates, and aerosol direct radiative forcing in the
1689 vicinity of Houston using a fully coupled meteorology-chemistry-aerosol model, *J. Geophys. Res.*
1690 *Atmos.*, 111, <https://doi.org/10.1029/2005JD006721>, 2006.

1691 Feingold, G., Eberhard, W. L., Veron, D. E., and Previdi, M.: First measurements of the Twomey indirect
1692 effect using ground-based remote sensors, *Geophys. Res. Lett.*, 30,
1693 <https://doi.org/10.1029/2002GL016633>, 2003.

1694 Feng, Y., Kotamarthi, V. R., Coulter, R., Zhao, C., and Cadetdu, M.: Radiative and thermodynamic
1695 responses to aerosol extinction profiles during the pre-monsoon month over South Asia., *Atmos.*
1696 *Chem. Phys.*, 16, <https://doi.org/10.5194/acp-16-247-2016>, 2016.

1697 Foley, K. M., Roselle, S. J., Appel, K. W., Bhawe, P. V., Pleim, J. E., Otte, T. L., Mathur, R., Sarwar, G.,
1698 Young, J. O., and Gilliam, R. C.: Incremental testing of the Community Multiscale Air Quality
1699 (CMAQ) modeling system version 4.7, *Geosci. Model Dev.*, 3, 205–226,
1700 <https://doi.org/10.5194/gmd-3-205-2010>.

1701 Forkel, R., Brunner, D., Baklanov, A., Balzarini, A., Hirtl, M., Honzak, L., Jiménez-Guerrero, P., Jorba,
1702 O., Pérez, J. L., and San José, R.: A multi-model case study on aerosol feedbacks in online coupled
1703 chemistry-meteorology models within the cost action ES1004 EuMetChem, in: Air pollution
1704 modeling and its application XXIV, Springer, 23–28, https://doi.org/10.1007/978-3-319-24478-5_4,
1705 2016.

1706 Fu, P., Aggarwal, S. G., Chen, J., Li, J., Sun, Y., Wang, Z., Chen, H., Liao, H., Ding, A., and Umarji, G.
1707 S.: Molecular markers of secondary organic aerosol in Mumbai, India, *Environ. Sci. Technol.*, 50,
1708 4659–4667, <https://doi.org/10.1021/acs.est.6b00372>, 2016.

1709 Gao, C., Zhang, X., Xiu, A., Huang, L., Zhao, H., Wang, K., and Tong, Q.: Spatiotemporal distribution
1710 of biogenic volatile organic compounds emissions in China, *Acta Sci. Circumstantiae*, 39, 4140–
1711 4151, <https://doi.org/10.13671/j.hjkxxb.2019.0243>, 2019.

1712 Gao, J., Zhu, B., Xiao, H., Kang, H., Pan, C., Wang, D., and Wang, H.: Effects of black carbon and
1713 boundary layer interaction on surface ozone in Nanjing, China., *Atmos. Chem. Phys.*, 18, 7081–
1714 7091, <https://doi.org/10.5194/acp-18-7081-2018>, 2018.

1716 7094, <https://doi.org/10.5194/acp-18-7081-2018>, 2018a.

1717 Gao, M., Guttikunda, S. K., Carmichael, G. R., Wang, Y., Liu, Z., Stanier, C. O., Saide, P. E., and Yu,

1718 M.: Health impacts and economic losses assessment of the 2013 severe haze event in Beijing area,

1719 *Sci. Total Environ.*, 511, 553–561, <https://doi.org/10.1016/j.scitotenv.2015.01.005>, 2015a.

1720 Gao, M., Carmichael, G. R., Wang, Y., Saide, P. E., Yu, M., Xin, J., Liu, Z., and Wang, Z.: Modeling

1721 study of the 2010 regional haze event in the North China Plain, *Atmos. Chem. Phys.*, 16, 1673–

1722 1691, <https://doi.org/10.5194/acp-16-1673-2016>, 2016a.

1723 Gao, M., Carmichael, G. R., Saide, P. E., Lu, Z., Yu, M., Streets, D. G., and Wang, Z.: Response of

1724 winter fine particulate matter concentrations to emission and meteorology changes in North China,

1725 *Atmos. Chem. Phys.*, 16, 11837–11851, <https://doi.org/10.5194/acp-16-11837-2016>, 2016b.

1726 Gao, M., Carmichael, G. R., Wang, Y., Saide, P. E., Liu, Z., Xin, J., Shan, Y., and Wang, Z.: Chemical

1727 and Meteorological Feedbacks in the Formation of Intense Haze Events, in: *Air Pollution in Eastern*

1728 *Asia: An Integrated Perspective*, Springer, 437–452, [https://doi.org/10.1007/978-3-319-59489-](https://doi.org/10.1007/978-3-319-59489-7_21)

1729 *7_21*, 2017a.

1730 Gao, M., Liu, Z., Wang, Y., Lu, X., Ji, D., Wang, L., Li, M., Wang, Z., Zhang, Q., and Carmichael, G.

1731 R.: Distinguishing the roles of meteorology, emission control measures, regional transport, and co-

1732 benefits of reduced aerosol feedbacks in “APEC Blue,” *Atmos. Environ.*, 167, 476–486,

1733 <https://doi.org/10.1016/j.atmosenv.2017.08.054>, 2017b.

1734 Gao, M., Saide, P. E., Xin, J., Wang, Y., Liu, Z., Wang, Y., Wang, Z., Pagowski, M., Guttikunda, S. K.,

1735 and Carmichael, G. R.: Estimates of health impacts and radiative forcing in winter haze in eastern

1736 China through constraints of surface PM_{2.5} predictions, *Environ. Sci. Technol.*, 51, 2178–2185,

1737 <https://doi.org/10.1021/acs.est.6b03745>, 2017c.

1738 Gao, M., Han, Z., Liu, Z., Li, M., Xin, J., Tao, Z., Li, J., Kang, J. E., Huang, K., Dong, X., Zhuang, B.,

1739 Li, S., Ge, B., Wu, Q., Cheng, Y., Wang, Y., Lee, H. J., Kim, C. H., Fu, J. S., Wang, T., Chin, M.,

1740 Woo, J. H., Zhang, Q., Wang, Z., and Carmichael, G. R.: Air quality and climate change, Topic 3

1741 of the Model Inter-Comparison Study for Asia Phase III (MICS-Asia III)- Part 1: Overview and

1742 model evaluation, *Atmos. Chem. Phys.*, 18, 4859–4884, <https://doi.org/10.5194/acp-18-4859-2018>,

1743 2018b.

1744 Gao, M., Ji, D., Liang, F., and Liu, Y.: Attribution of aerosol direct radiative forcing in China and India

1745 to emitting sectors, *Atmos. Environ.*, 190, 35–42, <https://doi.org/10.1016/j.atmosenv.2018.07.011>,

1746 2018c.

1747 Gao, Y. and Zhang, M.: Changes in the diurnal variations of clouds and precipitation induced by

1748 anthropogenic aerosols over East China in August 2008, *Atmos. Pollut. Res.*, 9, 513–525,

1749 <https://doi.org/10.1016/j.apr.2017.11.013>, 2018.

1750 Gao, Y., Zhang, M., Liu, X., and Zhao, C.: Model Analysis of the Anthropogenic Aerosol Effect on

1751 Clouds over East Asia, *Atmos. Ocean. Sci. Lett.*, 5, 1–7,

1752 <https://doi.org/10.1080/16742834.2012.11446968>, 2012.

1753 Gao, Y., Zhao, C., Liu, X., Zhang, M., and Leung, L. R.: WRF-Chem simulations of aerosols and

1754 anthropogenic aerosol radiative forcing in East Asia, *Atmos. Environ.*, 92, 250–266,

1755 <https://doi.org/10.1016/j.atmosenv.2014.04.038>, 2014.

1756 Gao, Y., Zhang, M., Liu, Z., Wang, L., Wang, P., Xia, X., Tao, M., and Zhu, L.: Modeling the feedback

1757 between aerosol and meteorological variables in the atmospheric boundary layer during a severe

1758 fog-haze event over the North China Plain., *Atmos. Chem. Phys.*, 15, 4279–4295,

1759 <https://doi.org/10.5194/acp-15-4279-2015>, 2015b.

1760 Gao, Y., Zhang, M., Liu, X., and Wang, L.: Change in diurnal variations of meteorological variables

1761 induced by anthropogenic aerosols over the North China Plain in summer 2008, *Theor. Appl.*

1762 *Climatol.*, 124, 103–118, <https://doi.org/10.1007/s00704-015-1403-4>, 2016c.

1763 García-Díez, M., Fernández, J., Fita, L., and Yagüe, C.: Seasonal dependence of WRF model biases and

1764 sensitivity to PBL schemes over Europe, *Q. J. R. Meteorol. Soc.*, 139, 501–514,

1765 <https://doi.org/10.1002/qj.1976>, 2013.

1766 Ge, C., Wang, J., and Reid, J. S.: Mesoscale modeling of smoke transport over the Southeast Asian

1767 Maritime Continent: coupling of smoke direct radiative effect below and above the low-level clouds,

1768 *Atmos. Chem. Phys.*, 14, 159–174, <https://doi.org/10.5194/acp-14-159-2014>, 2014.

1769 Georgiou, G. K., Christoudias, T., Proestos, Y., Kushta, J., Hadjinicolaou, P., and Lelieveld, J.: Air

1770 quality modelling in the summer over the eastern Mediterranean using WRF-Chem: chemistry and

1771 aerosol mechanism intercomparison, *Atmos. Chem. Phys.*, 18, 1555–1571,

1772 <https://doi.org/10.5194/acp-18-1555-2018>, 2018.

1773 Gery, M. W., Whitten, G. Z., Killus, J. P., and Dodge, M. C.: A photochemical kinetics mechanism for

1774 urban and regional scale computer modeling, *J. Geophys. Res. Atmos.*, 94, 12925–12956,

1775 <https://doi.org/10.1029/JD094iD10p12925>, 1989.

1776 Ghan, S. J. and Zaveri, R. A.: Parameterization of optical properties for hydrated internally mixed aerosol,

1777 *J. Geophys. Res. Atmos.*, 112, <https://doi.org/10.1029/2006JD007927>, 2007.

1778 Ghude, S. D., Chate, D. M., Jena, C., Beig, G., Kumar, R., Barth, M. C., Pfister, G. G., Fadnavis, S., and

1779 Pithani, P.: Premature mortality in India due to PM_{2.5} and ozone exposure, *Geophys. Res. Lett.*, 43,

1780 4650–4658, <https://doi.org/10.1002/2016GL068949>, 2016.

1781 Giglio, L., Randerson, J. T., Van der Werf, G. R., Kasibhatla, P. S., Collatz, G. J., Morton, D. C., and

1782 DeFries, R. S.: Assessing variability and long-term trends in burned area by merging multiple

1783 satellite fire products, 7, 1171–1186, <https://doi.org/10.5194/bg-7-1171-2010>, 2010.

1784 Ginoux, P., Chin, M., Tegen, I., Prospero, J. M., Holben, B., Dubovik, O., and Lin, S.: Sources and

1785 distributions of dust aerosols simulated with the GOCART model, *J. Geophys. Res. Atmos.*, 106,
1786 20255–20273, <https://doi.org/10.1029/2000JD000053>, 2001.

1787 Giorgi, F. and Chameides, W. L.: Rainout lifetimes of highly soluble aerosols and gases as inferred from
1788 simulations with a general circulation model, *J. Geophys. Res. Atmos.*, 91, 14367–14376,
1789 <https://doi.org/10.1029/JD091iD13p14367>, 1986.

1790 Gong, S. L., Barrie, L. A., and Blanchet, J.: Modeling sea-salt aerosols in the atmosphere: 1. Model
1791 development, *J. Geophys. Res. Atmos.*, 102, 3805–3818, <https://doi.org/10.1029/96JD02953>, 1997.

1792 Gong, S. L., Barrie, L. A., Blanchet, J., Von Salzen, K., Lohmann, U., Lesins, G., Spacek, L., Zhang, L.
1793 M., Girard, E., and Lin, H.: Canadian Aerosol Module: A size-segregated simulation of atmospheric
1794 aerosol processes for climate and air quality models 1. Module development, *J. Geophys. Res.*
1795 *Atmos.*, 108, AAC-3, <https://doi.org/10.1029/2001JD002002>, 2003a.

1796 Gong, S. L., Zhang, X. Y., Zhao, T. L., McKendry, I. G., Jaffe, D. A., and Lu, N. M.: Characterization
1797 of soil dust aerosol in China and its transport and distribution during 2001 ACE-Asia: 2. Model
1798 simulation and validation, *J. Geophys. Res. Atmos.*, 108, <https://doi.org/10.1029/2002JD002633>,
1799 2003b.

1800 Goren, T. and Rosenfeld, D.: Decomposing aerosol cloud radiative effects into cloud cover, liquid water
1801 path and Twomey components in marine stratocumulus, *Atmos. Res.*, 138, 378–393,
1802 <https://doi.org/10.1016/j.atmosres.2013.12.008>, 2014.

1803 Govardhan, G., Nanjundiah, R. S., Satheesh, S. K., Krishnamoorthy, K., and Kotamarthi, V. R.:
1804 Performance of WRF-Chem over Indian region: Comparison with measurements, *J. Earth Syst. Sci.*,
1805 124, 875–896, <https://doi.org/10.1007/s12040-015-0576-7>, 2015.

1806 Govardhan, G. R., Nanjundiah, R. S., Satheesh, S. K., Moorthy, K. K., and Takemura, T.: Inter-
1807 comparison and performance evaluation of chemistry transport models over Indian region, *Atmos.*
1808 *Environ.*, 125, 486–504, <https://doi.org/10.1016/j.atmosenv.2015.10.065>, 2016.

1809 Gray, L. J., Beer, J., Geller, M., Haigh, J. D., Lockwood, M., Matthes, K., Cubasch, U., Fleitmann, D.,
1810 Harrison, G., and Hood, L.: Solar influences on climate, *Rev. Geophys.*, 48,
1811 <https://doi.org/10.1029/2009RG000282>, 2010.

1812 Grell, G., Freitas, S. R., Stuefer, M., and Fast, J.: Inclusion of biomass burning in WRF-Chem: impact
1813 of wildfires on weather forecasts, *Atmos. Chem. Phys.*, 11, 5289–5303, <https://doi.org/10.5194/acp-11-5289-2011>, 2011.

1814 Grell, G. A., Peckham, S. E., Schmitz, R., McKeen, S. A., Frost, G., Skamarock, W. C., and Eder, B.:
1815 Fully coupled “online” chemistry within the WRF model, *Atmos. Environ.*, 39, 6957–6975,
1816 <https://doi.org/10.1016/j.atmosenv.2005.04.027>, 2005.

1817 Griffin, R. J., Cocker III, D. R., Seinfeld, J. H., and Dabdub, D.: Estimate of global atmospheric organic
1818 aerosol from oxidation of biogenic hydrocarbons, *Geophys. Res. Lett.*, 26, 2721–2724,
1819 <https://doi.org/10.1029/1999GL900476>, 1999.

1820 Groß, S., Esselborn, M., Weinzierl, B., Wirth, M., Fix, A., and Petzold, A.: Aerosol classification by
1821 airborne high spectral resolution lidar observations, *Atmos. Chem. Phys.*, 13, 2487–2505,
1822 <https://doi.org/10.5194/acp-13-2487-2013>, 2013.

1823 Guenther, A., Karl, T., Harley, P., Wiedinmyer, C., Palmer, P. I., and Geron, C.: Estimates of global
1824 terrestrial isoprene emissions using MEGAN (Model of Emissions of Gases and Aerosols from
1825 Nature), *Atmos. Chem. Phys.*, 6, 3181–3210, 2006.

1826 Guo, J., Deng, M., Fan, J., Li, Z., Chen, Q., Zhai, P., Dai, Z., and Li, X.: Precipitation and air pollution
1827 at mountain and plain stations in northern China: Insights gained from observations and modeling,
1828 *J. Geophys. Res. Atmos.*, 119, 4793–4807, <https://doi.org/10.1002/2013JD021161>, 2014.

1829 Guo, J., Liu, H., Li, Z., Rosenfeld, D., Jiang, M., Xu, W., and Jiang, J. H.: Aerosol-induced changes in
1830 the vertical structure of precipitation: a perspective of TRMM precipitation radar, 18, 13329–13343,
1831 <https://doi.org/10.5194/acp-18-13329-2018>, 2018.

1832 Gurjar, B. R., Ravindra, K., and Nagpure, A. S.: Air pollution trends over Indian megacities and their
1833 local-to-global implications, *Atmos. Environ.*, 142, 475–495,
1834 <https://doi.org/10.1016/j.atmosenv.2016.06.030>, 2016.

1835 Haywood, J. and Boucher, O.: Estimates of the direct and indirect radiative forcing due to tropospheric
1836 aerosols: A review, *Rev. Geophys.*, 38, 513–543, <https://doi.org/10.1029/1999RG000078>, 2000.

1837 He, J. and Zhang, Y.: Improvement and further development in CESM/CAM5: gas-phase chemistry and
1838 inorganic aerosol treatments, *Atmos. Chem. Phys.*, 14, 9171–9200, <https://doi.org/10.5194/acp-14-9171-2014>, 2014.

1839 He, J., Zhang, Y., Wang, K., Chen, Y., Leung, L. R., Fan, J., Li, M., Zheng, B., Zhang, Q., and Duan, F.:
1840 Multi-year application of WRF-CAM5 over East Asia-Part I: Comprehensive evaluation and
1841 formation regimes of O₃ and PM_{2.5}, *Atmos. Environ.*, 165, 122–142,
1842 <https://doi.org/10.1016/j.atmosenv.2017.06.015>, 2017.

1843 Hodshire, A. L., Akherati, A., Alvarado, M. J., Brown-Steiner, B., Jathar, S. H., Jimenez, J. L.,
1844 Kreidenweis, S. M., Lonsdale, C. R., Onasch, T. B., and Ortega, A. M.: Aging effects on biomass
1845 burning aerosol mass and composition: A critical review of field and laboratory studies, *Environ.*
1846 *Sci. Technol.*, 53, 10007–10022, <https://doi.org/10.1021/acs.est.9b02588>, 2019.

1847 Hodzic, A. and Jimenez, J. L.: Modeling anthropogenically controlled secondary organic aerosols in a
1848 megacity: A simplified framework for global and climate models, *Geosci. Model Dev.*, 4, 901–917,
1849 <https://doi.org/10.5194/gmd-4-901-2011>, 2011.

1850 Ten Hoeve, J. E. and Jacobson, M. Z.: Worldwide health effects of the Fukushima Daiichi nuclear
1851 accident, *Energy Environ. Sci.*, 5, 8743–8757, <https://doi.org/10.1039/c2ee22019a>, 2012.

1854 Hong, C., Zhang, Q., Zhang, Y., Tang, Y., Tong, D., and He, K.: Multi-year downscaling application of
1855 two-way coupled WRF v3.4 and CMAQ v5.0.2 over east Asia for regional climate and air quality
1856 modeling: model evaluation and aerosol direct effects., *Geosci. Model Dev.*, 10, 2447–2470,
1857 <https://doi.org/10.5194/gmd-10-2447-2017>, 2017.

1858 Hong, C., Zhang, Q., Zhang, Y., Davis, S. J., Tong, D., Zheng, Y., Liu, Z., Guan, D., He, K., and
1859 Schellnhuber, H. J.: Impacts of climate change on future air quality and human health in China,
1860 *Proc. Natl. Acad. Sci.*, 116, 17193–17200, <https://doi.org/10.1073/pnas.1812881116>, 2019.

1861 Hu, X., Klein, P. M., and Xue, M.: Evaluation of the updated YSU planetary boundary layer scheme
1862 within WRF for wind resource and air quality assessments, *J. Geophys. Res. Atmos.*, 118, 10–490,
1863 <https://doi.org/10.1002/jgrd.50823>, 2013.

1864 Huang, J., Wang, T., Wang, W., Li, Z., and Yan, H.: Climate effects of dust aerosols over East Asian
1865 arid and semiarid regions, *J. Geophys. Res. Atmos.*, 119, 11–398,
1866 <https://doi.org/10.1002/2014JD021796>, 2014.

1867 Huang, L., Lin, W., Li, F., Wang, Y., and Jiang, B.: Climate impacts of the biomass burning in Indochina
1868 on atmospheric conditions over southern China, *Aerosol Air Qual. Res.*, 19, 2707–2720,
1869 <https://doi.org/10.4209/aaqr.2019.01.0028>, 2019.

1870 Huang, X., Song, Y., Zhao, C., Cai, X., Zhang, H., and Zhu, T.: Direct radiative effect by multicomponent
1871 aerosol over China, *J. Clim.*, 28, 3472–3495, <https://doi.org/10.1175/JCLI-D-14-00365.1>, 2015.

1872 Huang, X., Ding, A., Liu, L., Liu, Q., Ding, K., Niu, X., Nie, W., Xu, Z., Chi, X., and Wang, M.: Effects
1873 of aerosol-radiation interaction on precipitation during biomass-burning season in East China.,
1874 *Atmos. Chem. Phys.*, 16, 10063–10082, <https://doi.org/10.5194/acp-16-10063-2016>, 2016.

1875 Illingworth, A. J., Barker, H. W., Beljaars, A., Ceccaldi, M., Chepfer, H., Clerbaux, N., Cole, J., Delanoë,
1876 J., Domenech, C., and Donovan, D. P.: The EarthCARE satellite: The next step forward in global
1877 measurements of clouds, aerosols, precipitation, and radiation, *Bull. Am. Meteorol. Soc.*, 96, 1311–
1878 1332, <https://doi.org/10.1175/BAMS-D-12-00227.1>, 2015.

1879 Im, U., Bianconi, R., Solazzo, E., Kioutsioukis, I., Badia, A., Balzarini, A., Baró, R., Bellasio, R.,
1880 Brunner, D., and Chemel, C.: Evaluation of operational on-line-coupled regional air quality models
1881 over Europe and North America in the context of AQMEII phase 2. Part I: Ozone, *Atmos. Environ.*,
1882 115, 404–420, <https://doi.org/10.1016/j.atmosenv.2014.09.042>, 2015a.

1883 Im, U., Bianconi, R., Solazzo, E., Kioutsioukis, I., Badia, A., Balzarini, A., Baró, R., Bellasio, R.,
1884 Brunner, D., and Chemel, C.: Evaluation of operational online-coupled regional air quality models
1885 over Europe and North America in the context of AQMEII phase 2. Part II: Particulate matter,
1886 *Atmos. Environ.*, 115, 421–441, <https://doi.org/10.1016/j.atmosenv.2014.08.072>, 2015b.

1887 IPCC: Climate change 2007: Synthesis Report. Contribution of Working Groups I, II and III to the Fourth
1888 Assessment Report of the Intergovernmental Panel on Climate Change, 2007.

1889 IPCC: Climate change 2014: Synthesis Report. Contribution of Working Groups I, II and III to the Fifth
1890 Assessment Report of the Intergovernmental Panel on Climate Change., 2014.

1891 IPCC: Climate change 2021: Synthesis Report. Contribution of Working Groups I, II and III to the Sixth
1892 Assessment Report of the Intergovernmental Panel on Climate Change., 2021.

1893 Jacobson, M. Z.: Developing, coupling, and applying a gas, aerosol, transport, and radiation model to
1894 study urban and regional air pollution, 1994.

1895 Jacobson, M. Z.: Development and application of a new air pollution modeling system—Part III.
1896 Aerosol-phase simulations, *Atmos. Environ.*, 31, 587–608, [https://doi.org/10.1016/S1352-2310\(96\)00201-4](https://doi.org/10.1016/S1352-2310(96)00201-4), 1997a.

1898 Jacobson, M. Z.: Numerical techniques to solve condensational and dissolutional growth equations when
1899 growth is coupled to reversible reactions, *Aerosol Sci. Technol.*, 27, 491–498,
1900 <https://doi.org/10.1080/02786829708965489>, 1997b.

1901 Jacobson, M. Z.: Fundamentals of atmospheric modeling, Cambridge university press, 1999.

1902 Jacobson, M. Z.: Strong radiative heating due to the mixing state of black carbon in atmospheric aerosols,
1903 409, 695–697, <https://doi.org/10.1038/35055518>, 2001.

1904 Jacobson, M. Z.: Analysis of aerosol interactions with numerical techniques for solving coagulation,
1905 nucleation, condensation, dissolution, and reversible chemistry among multiple size distributions, *J.*
1906 *Geophys. Res. Atmos.*, 107, AAC-2, <https://doi.org/10.1029/2001JD002044>, 2002.

1907 Jacobson, M. Z.: Development of mixed-phase clouds from multiple aerosol size distributions and the
1908 effect of the clouds on aerosol removal, *J. Geophys. Res. Atmos.*, 108,
1909 <https://doi.org/10.1029/2002JD002691>, 2003.

1910 Jacobson, M. Z.: History of, processes in, and numerical techniques in GATOR-GCMOM, 2012a.

1911 Jacobson, M. Z.: Investigating cloud absorption effects: Global absorption properties of black carbon, tar
1912 balls, and soil dust in clouds and aerosols, *J. Geophys. Res. Atmos.*, 117,
1913 <https://doi.org/10.1029/2011JD017218>, 2012b.

1914 Jacobson, M. Z. and Jadhav, V.: World estimates of PV optimal tilt angles and ratios of sunlight incident
1915 upon tilted and tracked PV panels relative to horizontal panels, *Sol. Energy*, 169, 55–66,
1916 <https://doi.org/10.1016/j.solener.2018.04.030>, 2018.

1917 Jacobson, M. Z. and Turco, R. P.: Simulating condensational growth, evaporation, and coagulation of
1918 aerosols using a combined moving and stationary size grid, *Aerosol Sci. Technol.*, 22, 73–92,
1919 <https://doi.org/10.1080/02786829408959729>, 1995.

1920 Jacobson, M. Z., Turco, R. P., Jensen, E. J., and Toon, O. B.: Modeling coagulation among particles of
1921 different composition and size, *Atmos. Environ.*, 28, 1327–1338, [https://doi.org/10.1016/1352-2310\(94\)90280-1](https://doi.org/10.1016/1352-2310(94)90280-1), 1994.

- 1923 Jacobson, M. Z., Lu, R., Turco, R. P., and Toon, O. B.: Development and application of a new air
 1924 pollution modeling system-part I: Gas-phase simulations, *Atmos. Environ.*, 30, 1939–1963,
 1925 [https://doi.org/10.1016/1352-2310\(95\)00139-5](https://doi.org/10.1016/1352-2310(95)00139-5), 1996a.
- 1926 Jacobson, M. Z., Tabazadeh, A., and Turco, R. P.: Simulating equilibrium within aerosols and
 1927 nonequilibrium between gases and aerosols, *J. Geophys. Res. Atmos.*, 101, 9079–9091,
 1928 <https://doi.org/10.1029/96JD00348>, 1996b.
- 1929 Jacobson, M. Z., Kaufman, Y. J., and Rudich, Y.: Examining feedbacks of aerosols to urban climate with
 1930 a model that treats 3-D clouds with aerosol inclusions, *J. Geophys. Res. Atmos.*, 112,
 1931 <https://doi.org/10.1029/2007JD008922>, 2007.
- 1932 Jacobson, M. Z., Nghiem, S. V., Sorichetta, A., and Whitney, N.: Ring of impact from the mega-
 1933 urbanization of Beijing between 2000 and 2009, *J. Geophys. Res. Atmos.*, 120, 5740–5756,
 1934 <https://doi.org/10.1002/2014JD023008>, 2015.
- 1935 Jacobson, M. Z., Nghiem, S. V., and Sorichetta, A.: Short-term impacts of the megaurbanizations of New
 1936 Delhi and Los Angeles between 2000 and 2009, *J. Geophys. Res. Atmos.*, 124, 35–56,
 1937 <https://doi.org/10.1029/2018JD029310>, 2019.
- 1938 Jena, C., Ghude, S. D., Pfister, G. G., Chate, D. M., Kumar, R., Beig, G., Surendran, D. E., Fadnavis, S.,
 1939 and Lal, D. M.: Influence of springtime biomass burning in South Asia on regional ozone (O₃): A
 1940 model based case study, *Atmos. Environ.*, 100, 37–47,
 1941 <https://doi.org/10.1016/j.atmosenv.2014.10.027>, 2015.
- 1942 Jeong, J. I. and Park, R. J.: Winter monsoon variability and its impact on aerosol concentrations in East
 1943 Asia, *Environ. Pollut.*, 221, 285–292, <https://doi.org/10.1016/j.envpol.2016.11.075>, 2017.
- 1944 Jia, X. and Guo, X.: Impacts of Anthropogenic Atmospheric Pollutant on Formation and Development
 1945 of a Winter Heavy Fog Event, *Chinese J. Atmos. Sci.*, 36, 995–1008,
 1946 <https://doi.org/10.1007/s11783-011-0280-z>, 2012.
- 1947 Jia, X., Quan, J., Zheng, Z., Liu, X., Liu, Q., He, H., and Liu, Y.: Impacts of Anthropogenic Aerosols on
 1948 Fog in North China Plain, *J. Geophys. Res. Atmos.*, 124, 252–265,
 1949 <https://doi.org/10.1029/2018JD029437>, 2019.
- 1950 Jiang, B., Huang, B., Lin, W., and Xu, S.: Investigation of the effects of anthropogenic pollution on
 1951 typhoon precipitation and microphysical processes using WRF-Chem, *J. Atmos. Sci.*, 73, 1593–
 1952 1610, <https://doi.org/10.1175/JAS-D-15-0202.1>, 2016.
- 1953 Jiang, B., Lin, W., Li, F., and Chen, J.: Sea-salt aerosol effects on the simulated microphysics and
 1954 precipitation in a tropical cyclone, *J. Meteorol. Res.*, 33, 115–125, <https://doi.org/10.1007/s13351-019-8108-z>, 2019a.
- 1955 Jiang, B., Lin, W., Li, F., and Chen, B.: Simulation of the effects of sea-salt aerosols on cloud ice and
 1956 precipitation of a tropical cyclone, *Atmos. Sci. Lett.*, 20, e936, <https://doi.org/10.1002/asl.936>,
 1957 2019b.
- 1959 Jimenez, P. A., Hacker, J. P., Dudhia, J., Haupt, S. E., Ruiz-Arias, J. A., Gueymard, C. A., Thompson,
 1960 G., Eidhammer, T., and Deng, A.: WRF-Solar: Description and clear-sky assessment of an
 1961 augmented NWP model for solar power prediction, *Bull. Am. Meteorol. Soc.*, 97, 1249–1264,
 1962 <https://doi.org/10.1175/BAMS-D-14-00279.1>, 2016.
- 1963 Jin, Q., Wei, J., Yang, Z.-L., Pu, B., and Huang, J.: Consistent response of Indian summer monsoon to
 1964 Middle East dust in observations and simulations, *Atmos. Chem. Phys.*, 15, 9897–9915,
 1965 <https://doi.org/10.5194/acp-15-9897-2015>, 2015.
- 1966 Jin, Q., Yang, Z.-L., and Wei, J.: High sensitivity of Indian summer monsoon to Middle East dust
 1967 absorptive properties, *Sci. Rep.*, 6, 1–8, <https://doi.org/10.1038/srep30690>, 2016a.
- 1968 Jin, Q., Yang, Z.-L., and Wei, J.: Seasonal responses of Indian summer monsoon to dust aerosols in the
 1969 Middle East, India, and China, *J. Clim.*, 29, 6329–6349, <https://doi.org/10.1175/JCLI-D-15-0622.1>,
 1970 2016b.
- 1971 Jung, J., Souri, A. H., Wong, D. C., Lee, S., Jeon, W., Kim, J., and Choi, Y.: The Impact of the Direct
 1972 Effect of Aerosols on Meteorology and Air Quality Using Aerosol Optical Depth Assimilation
 1973 During the KORUS-AQ Campaign, *J. Geophys. Res. Atmos.*, 124, 8303–8319,
 1974 <https://doi.org/10.1029/2019JD030641>, 2019.
- 1975 Kajino, M., Ueda, H., Han, Z., Kudo, R., Inomata, Y., and Kaku, H.: Synergy between air pollution and
 1976 urban meteorological changes through aerosol-radiation-diffusion feedback—A case study of
 1977 Beijing in January 2013, *Atmos. Environ.*, 171, 98–110,
 1978 <https://doi.org/10.1016/j.atmosenv.2017.10.018>, 2017.
- 1979 Kant, S., Panda, J., and Gautam, R.: A seasonal analysis of aerosol-cloud-radiation interaction over
 1980 Indian region during 2000–2017, *Atmos. Environ.*, 201, 212–222,
 1981 <https://doi.org/10.1016/j.atmosenv.2018.12.044>, 2019.
- 1982 Kedia, S., Cherian, R., Islam, S., Das, S. K., and Kaginalkar, A.: Regional simulation of aerosol radiative
 1983 effects and their influence on rainfall over India using WRFChem model, *Atmos. Res.*, 182, 232–
 1984 242, <https://doi.org/10.1016/j.atmosres.2016.07.008>, 2016.
- 1985 Kedia, S., Vellore, R. K., Islam, S., and Kaginalkar, A.: A study of Himalayan extreme rainfall events
 1986 using WRF-Chem, *Meteorol. Atmos. Phys.*, 131, 1133–1143, <https://doi.org/10.1007/s00703-018-0626-1>, 2019a.
- 1987 Kedia, S., Kumar, S., Islam, S., Hazra, A., and Kumar, N.: Aerosols impact on the convective and non-
 1988 convective rain distribution over the Indian region : Results from WRF-Chem simulation, *Atmos.*
 1989 *Environ.*, 202, 64–74, <https://doi.org/10.1016/j.atmosenv.2019.01.020>, 2019b.
- 1990 Keita, S. A., Girard, E., Raut, J.-C., Leriche, M., Blanchet, J.-P., Pelon, J., Onishi, T., and Cirisan, A.: A

1992 new parameterization of ice heterogeneous nucleation coupled to aerosol chemistry in WRF-Chem
1993 model version 3.5.1: evaluation through ISDAC measurements, *Geosci. Model Dev.*, 13, 5737–
1994 5755, <https://doi.org/10.5194/gmd-13-5737-2020>, 2020.

1995 Kim, B., Schwartz, S. E., Miller, M. A., and Min, Q.: Effective radius of cloud droplets by ground-based
1996 remote sensing: Relationship to aerosol, *J. Geophys. Res. Atmos.*, 108,
1997 <https://doi.org/10.1029/2003JD003721>, 2003.

1998 Knote, C., Hodzic, A., Jimenez, J. L., Volkamer, R., Orlando, J. J., Baidar, S., Brioude, J., Fast, J.,
1999 Gentner, D. R., and Goldstein, A. H.: Simulation of semi-explicit mechanisms of SOA formation
2000 from glyoxal in aerosol in a 3-D model, *Atmos. Chem. Phys.*, 14, 6213–6239,
2001 <https://doi.org/10.5194/acp-14-6213-2014>, 2014.

2002 Koch, D. and Del Genio, A. D.: Black carbon semi-direct effects on cloud cover: review and synthesis.,
2003 *Atmos. Chem. Phys.*, 10, 7685–7696, <https://doi.org/10.5194/acp-10-7685-2010>, 2010.

2004 Kong, X., Forkel, R., Sokhi, R. S., Suppan, P., Baklanov, A., Gauss, M., Brunner, D., Barò, R., Balzarini,
2005 A., Chemel, C., Curci, G., Jiménez-Guerrero, P., Hirtl, M., Honzak, L., Im, U., Pérez, J. L., Pirovano,
2006 G., San Jose, R., Schlünzen, K. H., Tsegas, G., Tuccella, P., Werhahn, J., Zbakar, R., and Galmarini,
2007 S.: Analysis of meteorology-chemistry interactions during air pollution episodes using online
2008 coupled models within AQMEII phase-2, *Atmos. Environ.*, 115, 527–540,
2009 <https://doi.org/10.1016/j.atmosenv.2014.09.020>, 2015.

2010 Kuik, F., Lauer, A., Churkina, G., Denier van der Gon, H., Fenner, D., Mar, K., and Butler, T.: Air quality
2011 modelling in the Berlin-Brandenburg region using WRF-Chem v3.7.1: sensitivity to resolution of
2012 model grid and input data, *Geosci. Model Dev.*, 9, 4339–4363, <https://doi.org/10.5194/gmd-9-4339-2016>, 2016.

2013 Kulmala, M., Laaksonen, A., and Pirjola, L.: Parameterizations for sulfuric acid/water nucleation rates,
2014 *J. Geophys. Res. Atmos.*, 103, 8301–8307, <https://doi.org/10.1029/97JD03718>, 1998.

2015 Kumar, P., Sokolik, I. N., and Nenes, A.: Parameterization of cloud droplet formation for global and
2016 regional models: including adsorption activation from insoluble CCN., *Atmos. Chem. Phys.*, 9,
2017 2517–2532, <https://doi.org/10.5194/acp-9-2517-2009>, 2009.

2018 Kumar, R., Naja, M., Pfister, G. G., Barth, M. C., Wiedinmyer, C., and Brasseur, G. P.: Simulations over
2019 South Asia using the Weather Research and Forecasting model with Chemistry (WRF-Chem):
2020 chemistry evaluation and initial results, *Geosci. Model Dev.*, 5, 619–648,
2021 <https://doi.org/10.5194/gmd-5-619-2012>, 2012a.

2022 Kumar, R., Naja, M., Pfister, G. G., Barth, M. C., and Brasseur, G. P.: Simulations over South Asia using
2023 the Weather Research and Forecasting model with Chemistry (WRF-Chem): set-up and
2024 meteorological evaluation, *Geosci. Model Dev.*, 5, 321–343, <https://doi.org/10.5194/gmd-5-321-2012>, 2012b.

2025 Kumar, R., Barth, M. C., Pfister, G. G., Naja, M., and Brasseur, G. P.: WRF-Chem simulations of a
2026 typical pre-monsoon dust storm in northern India: influences on aerosol optical properties and
2027 radiation budget, *Atmos. Chem. Phys.*, 14, 2431–2446, <https://doi.org/10.5194/acp-14-2431-2014>,
2028 2014.

2029 Kuniyal, J. C. and Guleria, R. P.: The current state of aerosol-radiation interactions: a mini review, *J.*
2030 *Aerosol Sci.*, 130, 45–54, <https://doi.org/10.1016/j.jaerosci.2018.12.010>, 2019.

2031 Lau, W. K. M., Kim, K.-M., Shi, J.-J., Matsui, T., Chin, M., Tan, Q., Peters-Lidard, C., and Tao, W.-K.:
2032 Impacts of aerosol–monsoon interaction on rainfall and circulation over Northern India and the
2033 Himalaya Foothills, *Clim. Dyn.*, 49, 1945–1960, <https://doi.org/10.1007/s00382-016-3430-y>, 2017.

2034 Lee, H.-H., Chen, S.-H., Kumar, A., Zhang, H., and Kleeman, M. J.: Improvement of aerosol
2035 activation/ice nucleation in a source-oriented WRF-Chem model to study a winter Storm in
2036 California, *Atmos. Res.*, 235, 104790, <https://doi.org/10.1016/j.atmosres.2019.104790>, 2020.

2037 Lee, Y. C., Yang, X., and Wenig, M.: Transport of dusts from East Asian and non-East Asian sources to
2038 Hong Kong during dust storm related events 1996–2007, *Atmos. Environ.*, 44, 3728–3738,
2039 <https://doi.org/10.1016/j.atmosenv.2010.03.034>, 2010.

2040 Lelieveld, J., Evans, J. S., Fnais, M., Giannadaki, D., and Pozzer, A.: The contribution of outdoor air
2041 pollution sources to premature mortality on a global scale, *Nature*, 525, 367,
2042 <https://doi.org/10.1038/nature15371>, 2015.

2043 Lelieveld, J., Bourtsoukidis, E., Brühl, C., Fischer, H., Fuchs, H., Harder, H., Hofzumahaus, A., Holland,
2044 F., Marno, D., and Neumaier, M.: The South Asian monsoon-pollution pump and purifier, *Science*
2045 (80-.), 361, 270–273, <https://doi.org/10.1126/science.aar2501>, 2018.

2046 Li, J., Wang, Z., Wang, X., Yamaji, K., Takigawa, M., Kanaya, Y., Pochanart, P., Liu, Y., Irie, H., and
2047 Hu, B.: Impacts of aerosols on summertime tropospheric photolysis frequencies and photochemistry
2048 over Central Eastern China, *Atmos. Environ.*, 45, 1817–1829,
2049 <https://doi.org/10.1016/j.atmosenv.2011.01.016>, 2011a.

2050 Li, J., Chen, X., Wang, Z., Du, H., Yang, W., Sun, Y., Hu, B., Li, J., Wang, W., and Wang, T.: Radiative
2051 and heterogeneous chemical effects of aerosols on ozone and inorganic aerosols over East Asia, *Sci.*
2052 *Total Environ.*, 622, 1327–1342, <https://doi.org/10.1016/j.scitotenv.2017.12.041>, 2018a.

2053 Li, J., Nagashima, T., Kong, L., Ge, B., Yamaji, K., Fu, J. S., Wang, X., Fan, Q., Itahashi, S., and Hyo-
2054 Jung, L.: Model evaluation and intercomparison of surface-level ozone and relevant species in East
2055 Asia in the context of MICS-Asia Phase III–Part 1: Overview, *Atmos. Chem. Phys.*, 19, 12993–
2056 13015, <https://doi.org/10.5194/acp-19-12993-2019>, 2019a.

2057 Li, L. and Liao, H.: Role of the Radiative Effect of Black Carbon in Simulated PM_{2.5} Concentrations
2058 during a Haze Event in China, *Atmos. Ocean. Sci. Lett.*, 7, 434–440,
2059 2010.

2061 <https://doi.org/10.3878/j.issn.1674-2834.14.0023>, 2014.
 2062 Li, L. and Sokolik, I. N.: The Dust Direct Radiative Impact and Its Sensitivity to the Land Surface State
 2063 and Key Minerals in the WRF-Chem-DuMo Model: A Case Study of Dust Storms in Central Asia,
 2064 *J. Geophys. Res. Atmos.*, 123, 4564–4582, <https://doi.org/10.1029/2017JD027667>, 2018.
 2065 Li, M., Zhang, Q., Kurokawa, J., and Woo, J.-H.: MIX: a mosaic Asian anthropogenic emission inventory
 2066 under the international collaboration framework of the MICS-Asia and HTAP, *Atmos. Chem. Phys.*,
 2067 17, 935–963, <https://doi.org/10.5194/acp-17-935-2017>, 2017a.
 2068 Li, M., Wang, T., Xie, M., Li, S., Zhuang, B., Chen, P., Huang, X., and Han, Y.: Agricultural fire impacts
 2069 on ozone photochemistry over the Yangtze River Delta region, East China, *J. Geophys. Res. Atmos.*,
 2070 123, 6605–6623, <https://doi.org/10.1029/2018JD028582>, 2018b.
 2071 Li, M., Wang, T., Xie, M., Li, S., Zhuang, B., Huang, X., Chen, P., Zhao, M., and Liu, J.: Formation and
 2072 evolution mechanisms for two extreme haze episodes in the Yangtze River Delta region of China
 2073 during winter 2016, *J. Geophys. Res. Atmos.*, 124, 3607–3623,
 2074 <https://doi.org/10.1029/2019JD030535>, 2019b.
 2075 Li, M. M., Wang, T., Xie, M., Zhuang, B., Li, S., Han, Y., and Chen, P.: Impacts of aerosol-radiation
 2076 feedback on local air quality during a severe haze episode in Nanjing megacity, eastern China,
 2077 *Tellus, Ser. B Chem. Phys. Meteorol.*, 69, 1–16, <https://doi.org/10.1080/16000889.2017.1339548>,
 2078 2017b.
 2079 Li, M. M., Wang, T., Han, Y., Xie, M., Li, S., Zhuang, B., and Chen, P.: Modeling of a severe dust event
 2080 and its impacts on ozone photochemistry over the downstream Nanjing megacity of eastern China,
 2081 *Atmos. Environ.*, 160, 107–123, <https://doi.org/10.1016/j.atmosenv.2017.04.010>, 2017c.
 2082 Li, Z., Niu, F., Fan, J., Liu, Y., Rosenfeld, D., and Ding, Y.: Long-term impacts of aerosols on the vertical
 2083 development of clouds and precipitation, *Nat. Geosci.*, 4, 888–894,
 2084 <https://doi.org/10.1038/ngeo1313>, 2011b.
 2085 Li, Z., Lau, W. K. M., Ramanathan, V., Wu, G., Ding, Y., Manoj, M. G., Liu, J., Qian, Y., Li, J., Zhou,
 2086 T., Fan, J., Rosenfeld, D., Ming, Y., Wang, Y., Huang, J., Wang, B., Xu, X., Lee, S. S., Cribb, M.,
 2087 Zhang, F., Yang, X., Zhao, C., Takemura, T., Wang, K., Xia, X., Yin, Y., Zhang, H., Guo, J., Zhai,
 2088 P. M., Sugimoto, N., Babu, S. S., and Brasseur, G. P.: Aerosol and monsoon climate interactions
 2089 over Asia, *Rev. Geophys.*, 54, 866–929, <https://doi.org/10.1002/2015RG000500>, 2016.
 2090 Li, Z., Wang, Y., Guo, J., Zhao, C., Cribb, M. C., Dong, X., Fan, J., Gong, D., Huang, J., and Jiang, M.:
 2091 East Asian study of tropospheric aerosols and their impact on regional clouds, precipitation, and
 2092 climate (EAST-AIRCPC), *J. Geophys. Res. Atmos.*, 124, 13026–13054,
 2093 <https://doi.org/10.1029/2019JD030758>, 2019c.
 2094 Liao, J., Wang, T., Wang, X., Xie, M., Jiang, Z., Huang, X., and Zhu, J.: Impacts of different urban
 2095 canopy schemes in WRF/Chem on regional climate and air quality in Yangtze River Delta, China,
 2096 *Atmos. Res.*, 145, 226–243, <https://doi.org/10.1016/j.atmosres.2014.04.005>, 2014.
 2097 Lin, C.-Y., Zhao, C., Liu, X., Lin, N.-H., and Chen, W.-N.: Modelling of long-range transport of
 2098 Southeast Asia biomass-burning aerosols to Taiwan and their radiative forcings over East Asia,
 2099 *Tellus B Chem. Phys. Meteorol.*, 66, 23733, <https://doi.org/10.3402/tellusb.v66.23733>, 2014a.
 2100 Lin, N.-H., Sayer, A. M., Wang, S.-H., Loftus, A. M., Hsiao, T.-C., Sheu, G.-R., Hsu, N. C., Tsay, S.-C.,
 2101 and Chantara, S.: Interactions between biomass-burning aerosols and clouds over Southeast Asia:
 2102 Current status, challenges, and perspectives, *Environ. Pollut.*, 195, 292–307,
 2103 <https://doi.org/10.1016/j.envpol.2014.06.036>, 2014b.
 2104 Liu, C., Wang, T., Chen, P., Li, M., Zhao, M., Zhao, K., Wang, M., and Yang, X.: Effects of Aerosols
 2105 on the Precipitation of Convective Clouds: A Case Study in the Yangtze River Delta of China, *J.*
 2106 *Geophys. Res. Atmos.*, 124, 7868–7885, <https://doi.org/10.1029/2018JD029924>, 2019.
 2107 Liu, G., Shao, H., Coakley Jr, J. A., Curry, J. A., Haggerty, J. A., and Tschudi, M. A.: Retrieval of cloud
 2108 droplet size from visible and microwave radiometric measurements during INDOEX: Implication
 2109 to aerosols' indirect radiative effect, *J. Geophys. Res. Atmos.*, 108, AAC 2-1-AAC 2-10,
 2110 <https://doi.org/10.1029/2001JD001395>, 2003.
 2111 Liu, L., Huang, X., Ding, A., and Fu, C.: Dust-induced radiative feedbacks in north China : A dust storm
 2112 episode modeling study using WRF-Chem, *Atmos. Environ.*, 129, 43–54,
 2113 <https://doi.org/10.1016/j.atmosenv.2016.01.019>, 2016a.
 2114 Liu, L., Bai, Y., Lin, C., and Yang, H.: Evaluation of Regional Air Quality Numerical Forecasting System
 2115 in Central China and Its Application for Aerosol Radiative Effect, *Meteorol. Mon.*, 44, 1179–1190,
 2116 <https://doi.org/10.7519/j.issn.1000-0526.2018.09.006>, 2018a.
 2117 Liu, Q., Jia, X., Quan, J., Li, J., Li, X., Wu, Y., Chen, D., Wang, Z., and Liu, Y.: New positive feedback
 2118 mechanism between boundary layer meteorology and secondary aerosol formation during severe
 2119 haze events, *Sci. Rep.*, 8, 1–8, <https://doi.org/10.1038/s41598-018-24366-3>, 2018b.
 2120 Liu, X., Easter, R. C., Ghan, S. J., Zaveri, R., Rasch, P., Shi, X., Lamarque, J.-F., Gettelman, A., Morrison,
 2121 H., and Vitt, F.: Toward a minimal representation of aerosols in climate models: Description and
 2122 evaluation in the Community Atmosphere Model CAM5, *Geosci. Model Dev.*, 5, 709–739,
 2123 <https://doi.org/10.5194/gmd-5-709-2012>, 2012.
 2124 Liu, X., Zhang, Y., Zhang, Q., and He, K.: Application of online-coupled WRF/Chem-MADRID in East
 2125 Asia : Model evaluation and climatic effects of anthropogenic aerosols, *Atmos. Environ.*, 124, 321–
 2126 336, <https://doi.org/10.1016/j.atmosenv.2015.03.052>, 2016b.
 2127 Liu, Z., Yim, S. H. L., Wang, C., and Lau, N. C.: The Impact of the Aerosol Direct Radiative Forcing on
 2128 Deep Convection and Air Quality in the Pearl River Delta Region, *Geophys. Res. Lett.*, 45, 4410–
 2129 4418, <https://doi.org/10.1029/2018GL077517>, 2018c.

- 2130 Liu, Z., Yi, M., Zhao, C., Lau, N. C., Guo, J., Bollasina, M., and Yim, S. H. L.: Contribution of local and
2131 remote anthropogenic aerosols to a record-breaking torrential rainfall event in Guangdong Province,
2132 China, *Atmos. Chem. Phys.*, 20, 223–241, <https://doi.org/10.5194/acp-20-223-2020>, 2020.
- 2133 Lohmann, U. and Diehl, K.: Sensitivity studies of the importance of dust ice nuclei for the indirect aerosol
2134 effect on stratiform mixed-phase clouds, *J. Atmos. Sci.*, 63, 968–982,
2135 <https://doi.org/10.1175/JAS3662.1>, 2006.
- 2136 Lohmann, U. and Feichter, J.: Global indirect aerosol effects: a review, *Atmos. Chem. Phys.*, 5, 715–737,
2137 <https://doi.org/10.5194/acp-5-715-2005>, 2005.
- 2138 Ma, X. and Wen, W.: Modelling the Effect of Black Carbon and Sulfate Aerosol on the Regional
2139 Meteorology Factors, in: IOP Conf. Ser. Earth Environ. Sci., 12002, <https://doi.org/10.1088/1755-1315/78/1/012002>, 2017.
- 2140 Ma, X., Chen, D., Wen, W., Sheng, L., Hu, J., Tong, H., and Wei, P.: Effect of Particle Pollution on
2141 Regional Meteorological Factors in China, *J. Beijing Univ. Technol.*, 285–295,
2142 <https://doi.org/10.11936/bjutxb2015040075>, 2016.
- 2143 Mailler, S., Menut, L., Khvorostyanov, D., Valari, M., Couvidat, F., Siour, G., Turquety, S., Briant, R.,
2144 Tuccella, P., and Bessagnet, B.: CHIMERE-2017: from urban to hemispheric chemistry-transport
2145 modeling, *Geosci. Model Dev.*, 10, 2397–2423, <https://doi.org/10.5194/gmd-10-2397-2017>, 2017.
- 2146 Makar, P. A., Gong, W., Milbrandt, J., Hogrefe, C., Zhang, Y., Curci, G., Žabkar, R., Im, U., Balzarini,
2147 A., Baró, R., Bianconi, R., Cheung, P., Forkel, R., Gravel, S., Hirtl, M., Honzak, L., Hou, A.,
2148 Jiménez-Guerrero, P., Langer, M., Moran, M. D., Pabla, B., Pérez, J. L., Pirovano, G., San José, R.,
2149 Tuccella, P., Werhahn, J., Zhang, J., and Galmarini, S.: Feedbacks between air pollution and weather,
2150 Part 1: Effects on weather, *Atmos. Environ.*, 115, 442–469,
2151 <https://doi.org/10.1016/j.atmosenv.2014.12.003>, 2015a.
- 2152 Makar, P. A., Gong, W., Hogrefe, C., Zhang, Y., Curci, G., Žabkar, R., Milbrandt, J., Im, U., Balzarini,
2153 A., Baró, R., Bianconi, R., Cheung, P., Forkel, R., Gravel, S., Hirtl, M., Honzak, L., Hou, A.,
2154 Jiménez-Guerrero, P., Langer, M., Moran, M. D., Pabla, B., Pérez, J. L., Pirovano, G., San José, R.,
2155 Tuccella, P., Werhahn, J., Zhang, J., and Galmarini, S.: Feedbacks between air pollution and weather,
2156 part 2: Effects on chemistry, *Atmos. Environ.*, 115, 499–526,
2157 <https://doi.org/10.1016/j.atmosenv.2014.10.021>, 2015b.
- 2158 Manisalidis, I., Stavropoulou, E., Stavropoulos, A., and Bezirtzoglou, E.: Environmental and health
2159 impacts of air pollution: A review, *Front. public Heal.*, 8, <https://doi.org/10.3389/fpubh.2020.00014>,
2160 2020.
- 2161 Marelle, L., Raut, J.-C., Law, K. S., Berg, L. K., Fast, J. D., Easter, R. C., Shrivastava, M., and Thomas,
2162 J. L.: Improvements to the WRF-Chem 3.5. 1 model for quasi-hemispheric simulations of aerosols
2163 and ozone in the Arctic, *Geosci. Model Dev.*, 10, 3661–3677, <https://doi.org/10.5194/gmd-10-3661-2017>, 2017.
- 2164 Martin, D. E. and Leight, W. G.: Objective temperature estimates from mean circulation patterns, *Mon.*
2165 *Weather Rev.*, 77, 275–283, [https://doi.org/10.1175/1520-0493\(1949\)077<0275:OTEFMC>2.0.CO;2](https://doi.org/10.1175/1520-0493(1949)077<0275:OTEFMC>2.0.CO;2), 1949.
- 2166 Martin, S. T., Schlenker, J. C., Malinowski, A., Hung, H., and Rudich, Y.: Crystallization of atmospheric
2167 sulfate-nitrate-ammonium particles, *Geophys. Res. Lett.*, 30,
2168 <https://doi.org/10.1029/2003GL017930>, 2003.
- 2169 Mass, C. and Ovens, D.: Fixing WRF's high speed wind bias: A new subgrid scale drag parameterization
2170 and the role of detailed verification, in: 24th conference on weather and forecasting and 20th
2171 conference on numerical weather prediction, preprints, 91st American meteorological society
2172 annual meeting, 2011.
- 2173 McCormick, R. A. and Ludwig, J. H.: Climate modification by atmospheric aerosols, *Science (80-.)*,
2174 156, 1358–1359, <https://doi.org/10.1126/science.156.3780.1358>, 1967.
- 2175 McMurphy, P. H. and Friedlander, S. K.: New particle formation in the presence of an aerosol, *Atmos.*
2176 *Environ.*, 13, 1635–1651, [https://doi.org/10.1016/0004-6981\(79\)90322-6](https://doi.org/10.1016/0004-6981(79)90322-6), 1979.
- 2177 Miao, Y., Liu, S., Zheng, Y., and Wang, S.: Modeling the feedback between aerosol and boundary layer
2178 processes: a case study in Beijing, China, *Environ. Sci. Pollut. Res.*, 23, 3342–3357,
2179 <https://doi.org/10.1007/s11356-015-5562-8>, 2016.
- 2180 Miao, Y., Guo, J., Liu, S., Zhao, C., Li, X., Zhang, G., Wei, W., and Ma, Y.: Impacts of synoptic condition
2181 and planetary boundary layer structure on the trans-boundary aerosol transport from Beijing-
2182 Tianjin-Hebei region to northeast China, *Atmos. Environ.*, 181, 1–11,
2183 <https://doi.org/10.1016/j.atmosenv.2018.03.005>, 2018.
- 2184 Napari, I., Noppel, M., Vehkamäki, H., and Kulmala, M.: Parametrization of ternary nucleation rates for
2185 H₂SO₄-NH₃-H₂O vapors, *J. Geophys. Res. Atmos.*, 107, AAC 6-1-AAC 6-6,
2186 <https://doi.org/10.1029/2002JD002132>, 2002.
- 2187 Nenes, A., Pandis, S. N., and Pilinis, C.: ISORROPIA: A new thermodynamic equilibrium model for
2188 multiphase multicomponent inorganic aerosols, *Aquat. geochemistry*, 4, 123–152,
2189 <https://doi.org/10.1023/A:1009604003981>, 1998.
- 2190 Nguyen, G. T. H., Shimadera, H., Sekiguchi, A., Matsuo, T., and Kondo, A.: Investigation of aerosol
2191 direct effects on meteorology and air quality in East Asia by using an online coupled modeling
2192 system, *Atmos. Environ.*, 207, 182–196, <https://doi.org/10.1016/j.atmosenv.2019.03.017>, 2019a.
- 2193 Nguyen, G. T. H., Shimadera, H., Uranishi, K., Matsuo, T., Kondo, A., and Thepanondh, S.: Numerical
2194 assessment of PM_{2.5} and O₃ air quality in continental Southeast Asia: Baseline simulation and
2195 aerosol direct effects investigation, *Atmos. Environ.*, 219, 117054,
2196

2199 <https://doi.org/10.1016/j.atmosenv.2019.117054>, 2019b.

2200 North, G. R., Pyle, J. A., and Zhang, F.: Encyclopedia of atmospheric sciences, Elsevier, 2014.

2201 Odum, J. R., Jungkamp, T. P. W., Griffin, R. J., Flagan, R. C., and Seinfeld, J. H.: The atmospheric

2202 aerosol-forming potential of whole gasoline vapor, *Science* (80-.), 276, 96–99,

2203 <https://doi.org/10.1126/science.276.5309.96>, 1997.

2204 Park, S.-Y., Lee, H.-J., Kang, J.-E., Lee, T., and Kim, C.-H.: Aerosol radiative effects on mesoscale

2205 cloud-precipitation variables over Northeast Asia during the MAPS-Seoul 2015 campaign, *Atmos.*

2206 *Environ.*, 172, 109–123, <https://doi.org/10.1016/j.atmosenv.2017.10.044>, 2018.

2207 Penner, J. E., Dong, X., and Chen, Y.: Observational evidence of a change in radiative forcing due to the

2208 indirect aerosol effect, *Nature*, 427, 231–234, <https://doi.org/10.1038/nature02234>, 2004.

2209 Qiu, Y., Liao, H., Zhang, R., and Hu, J.: Simulated impacts of direct radiative effects of scattering and

2210 absorbing aerosols on surface layer aerosol concentrations in China during a heavily polluted event

2211 in february 2014, *J. Geophys. Res.*, 122, 5955–5975, <https://doi.org/10.1002/2016JD026309>, 2017.

2212 Quaas, J., Boucher, O., Bellouin, N., and Kinne, S.: Satellite-based estimate of the direct and indirect

2213 aerosol climate forcing, *J. Geophys. Res. Atmos.*, 113, <https://doi.org/10.1029/2007JD008962>,

2214 2008.

2215 Reid, J. S., Koppmann, R., Eck, T. F., and Eleuterio, D. P.: A review of biomass burning emissions part

2216 II: intensive physical properties of biomass burning particles, *Atmos. Chem. Phys.*, 5, 799–825,

2217 <https://doi.org/10.5194/acp-5-799-2005>, 2005.

2218 Rohde, R. A. and Muller, R. A.: Air pollution in China: mapping of concentrations and sources, *PLoS*

2219 *One*, 10, e0135749, <https://doi.org/10.1371/journal.pone.0135749>, 2015.

2220 Rosenfeld, D.: Suppression of rain and snow by urban and industrial air pollution, *Science* (80-.), 287,

2221 1793–1796, <https://doi.org/10.1126/science.287.5459.1793>, 2000.

2222 Rosenfeld, D., Lohmann, U., Raga, G. B., O’Dowd, C. D., Kulmala, M., Fuzzi, S., Reissell, A., and

2223 Andreae, M. O.: Flood or drought: How do aerosols affect precipitation?, *Science* (80-.), 321,

2224 1309–1313, <https://doi.org/10.1126/science.1160606>, 2008.

2225 Rosenfeld, D., Andreae, M. O., Asmi, A., Chin, M., de Leeuw, G., Donovan, D. P., Kahn, R., Kinne, S.,

2226 Kivekäs, N., and Kulmala, M.: Global observations of aerosol-cloud-precipitation-climate

2227 interactions, *Rev. Geophys.*, 52, 750–808, <https://doi.org/10.1002/2013RG000441>, 2014.

2228 Rosenfeld, D., Zhu, Y., Wang, M., Zheng, Y., Goren, T., and Yu, S.: Aerosol-driven droplet

2229 concentrations dominate coverage and water of oceanic low-level clouds, *Science* (80-.), 363,

2230 <https://doi.org/10.1126/science.aav0566>, 2019.

2231 Saleh, R., Robinson, E. S., Tkacik, D. S., Ahern, A. T., Liu, S., Aiken, A. C., Sullivan, R. C., Presto, A.

2232 A., Dubey, M. K., and Yokelson, R. J.: Brownness of organics in aerosols from biomass burning

2233 linked to their black carbon content, *Nat. Geosci.*, 7, 647–650, <https://doi.org/10.1038/ngeo2220>,

2234 2014.

2235 Sarangi, C., Tripathi, S. N., Tripathi, S., and Barth, M. C.: Aerosol-cloud associations over Gangetic

2236 Basin during a typical monsoon depression event using WRF-Chem simulation, *J. Geophys. Res.*

2237 *Atmos.*, 120, 10–974, <https://doi.org/10.1002/2015JD023634>, 2015.

2238 Satheesh, S. K. and Moorthy, K. K.: Radiative effects of natural aerosols: A review, *Atmos. Environ.*,

2239 39, 2089–2110, <https://doi.org/10.1016/j.atmosenv.2004.12.029>, 2005.

2240 Sato, Y. and Suzuki, K.: How do aerosols affect cloudiness?, *Science* (80-.), 363, 580–581,

2241 <https://doi.org/10.1126/science.aaw3720>, 2019.

2242 Saylor, R. D., Baker, B. D., Lee, P., Tong, D., Pan, L., and Hicks, B. B.: The particle dry deposition

2243 component of total deposition from air quality models: right, wrong or uncertain?, *Tellus B Chem.*

2244 *Phys. Meteorol.*, 71, 1550324, <https://doi.org/10.1080/16000889.2018.1550324>, 2019.

2245 Seaman, N. L.: Meteorological modeling for air-quality assessments, *Atmos. Environ.*, 34, 2231–2259,

2246 [https://doi.org/10.1016/S1352-2310\(99\)00466-5](https://doi.org/10.1016/S1352-2310(99)00466-5), 2000.

2247 Seethala, C., Pandithurai, G., Fast, J. D., Polade, S. D., Reddy, M. S., and Peckham, S. E.: Evaluating

2248 WRF-Chem multi-scale model in simulating aerosol radiative properties over the tropics-a case

2249 study over India, 26, 269–284, <https://doi.org/10.1007/s12647-011-0025-2>, 2011.

2250 Seinfeld, J. and Pandis, S.: Atmospheric chemistry and physics: atmospheric chemistry and physics, 1998.

2251 Sekiguchi, A., Shimadera, H., and Kondo, A.: Impact of aerosol direct effect on wintertime PM_{2.5}

2252 simulated by an online coupled meteorology-air quality model over east asia, *Aerosol Air Qual.*

2253 *Res.*, 18, 1068–1079, <https://doi.org/10.4209/aaqr.2016.06.0282>, 2018.

2254 Sekiguchi, M., Nakajima, T., Suzuki, K., Kawamoto, K., Higurashi, A., Rosenfeld, D., Sano, I., and

2255 Mukai, S.: A study of the direct and indirect effects of aerosols using global satellite data sets of

2256 aerosol and cloud parameters, *J. Geophys. Res. Atmos.*, 108, <https://doi.org/10.1029/2002JD003359>,

2257 2003.

2258 Shahid, M. Z., Shahid, I., Chishtie, F., Shahzad, M. I., and Bulbul, G.: Analysis of a dense haze event

2259 over North-eastern Pakistan using WRF-Chem model and remote sensing, *J. Atmos. Solar-*

2260 *Terrestrial Phys.*, 182, 229–241, <https://doi.org/10.1016/j.jastp.2018.12.007>, 2019.

2261 Shao, Y.: Simplification of a dust emission scheme and comparison with data, *J. Geophys. Res. Atmos.*,

2262 109, <https://doi.org/10.1029/2003JD004372>, 2004.

2263 Shao, Y. and Dong, C. H.: A review on East Asian dust storm climate, modelling and monitoring, *Glob.*

2264 *Planet. Change*, 52, 1–22, <https://doi.org/10.1016/j.gloplacha.2006.02.011>, 2006.

2265 Shen, H., Shi, H., Shi, H., and Ma, X.: Simulation Study of Influence of Aerosol Pollution on Regional

2266 Meteorological Factors in Beijing-Tianjin-Hebei Region, *J. Anhui Agric. Sci.*, 43, 207–210,

2267 <https://doi.org/10.13989/j.cnki.0517-6611.2015.25.217>, 2015.

2268 Shen, X., Jiang, X., Liu, D., Zu, F., and Fan, S.: Simulations of Anthropogenic Aerosols Effects on the
2269 Intensity and Precipitation of Typhoon Fitow (1323) Using WRF-Chem Model, *Chinese J. Atmos.*
2270 *Sci.*, 41, 960–974, <https://doi.org/10.3878/j.issn.1006-9895.1703.16216>, 2017.

2271 Singh, P., Sarawade, P., and Adhikary, B.: Carbonaceous Aerosol from Open Burning and its Impact on
2272 Regional Weather in South Asia, *Aerosol Air Qual. Res.*, 20, 419–431,
2273 <https://doi.org/10.4209/aaqr.2019.03.0146>, 2020.

2274 Slinn, W. G. N.: Precipitation scavenging, in *atmospheric sciences and power production-1979*, Div.
2275 Biomed. Environ. Res. US Dep. Energy, Washingt. DC, 1984.

2276 Soni, P., Tripathi, S. N., and Srivastava, R.: Radiative effects of black carbon aerosols on Indian monsoon:
2277 a study using WRF-Chem model, *Theor. Appl. Climatol.*, 132, 115–134,
2278 <https://doi.org/10.1007/s00704-017-2057-1>, 2018.

2279 Srinivas, R., Panicker, A. S., Parkhi, N. S., Peshin, S. K., and Beig, G.: Sensitivity of online coupled
2280 model to extreme pollution event over a mega city Delhi, *Atmos. Pollut. Res.*, 7, 25–30,
2281 <https://doi.org/10.1016/j.apr.2015.07.001>, 2016.

2282 Su, L. and Fung, J. C. H.: Investigating the role of dust in ice nucleation within clouds and further effects
2283 on the regional weather system over East Asia--Part 1: model development and validation., *Atmos.*
2284 *Chem. Phys.*, 18, 8707–8725, <https://doi.org/10.5194/acp-18-8707-2018>, 2018a.

2285 Su, L. and Fung, J. C. H.: Investigating the role of dust in ice nucleation within clouds and further effects
2286 on the regional weather system over East Asia--Part 2: modification of the weather system., *Atmos.*
2287 *Chem. Phys.*, 18, 11529–11545, <https://doi.org/10.5194/acp-18-11529-2018>, 2018b.

2288 Sud, Y. C. and Walker, G. K.: A review of recent research on improvement of physical parameterizations
2289 in the GLA GCM, 1990.

2290 Sun, K., Liu, H., Wang, X., Peng, Z., and Xiong, Z.: The aerosol radiative effect on a severe haze episode
2291 in the Yangtze River Delta, *J. Meteorol. Res.*, 31, 865–873, [https://doi.org/10.1007/s13351-017-](https://doi.org/10.1007/s13351-017-7007-4)
2292 [7007-4](https://doi.org/10.1007/s13351-017-7007-4), 2017.

2293 Takemura, T., Nakajima, T., Higurashi, A., Ohta, S., and Sugimoto, N.: Aerosol distributions and
2294 radiative forcing over the Asian Pacific region simulated by Spectral Radiation-Transport Model
2295 for Aerosol Species (SPRINTARS), *J. Geophys. Res. Atmos.*, 108,
2296 <https://doi.org/10.1029/2002JD003210>, 2003.

2297 Tang, Y., Han, Y., Ma, X., and Liu, Z.: Elevated heat pump effects of dust aerosol over Northwestern
2298 China during summer, *Atmos. Res.*, 203, 95–104, <https://doi.org/10.1016/j.atmosres.2017.12.004>,
2299 2018.

2300 Thompson, G. and Eidhammer, T.: A study of aerosol impacts on clouds and precipitation development
2301 in a large winter cyclone, *J. Atmos. Sci.*, 71, 3636–3658, <https://doi.org/10.1175/JAS-D-13-0305.1>,
2302 2014.

2303 Toon, O. B., McKay, C. P., Ackerman, T. P., and Santhanam, K.: Rapid calculation of radiative heating
2304 rates and photodissociation rates in inhomogeneous multiple scattering atmospheres, *J. Geophys.*
2305 *Res. Atmos.*, 94, 16287–16301, <https://doi.org/10.1029/JD094iD13p16287>, 1989.

2306 Treback, C., Tripoli, G., Arritt, R., Cotton, W. R., and Pielke, R. A.: The regional atmospheric modeling
2307 system, in: *Proceedings of an International Conference on Development Applications of Computer*
2308 *Techniques Environmental Studies*, 601–607, 1986.

2309 Tsay, S.-C., Hsu, N. C., Lau, W. K.-M., Li, C., Gabriel, P. M., Ji, Q., Holben, B. N., Welton, E. J.,
2310 Nguyen, A. X., and Janjai, S.: From BASE-ASIA toward 7-SEAS: A satellite-surface perspective
2311 of boreal spring biomass-burning aerosols and clouds in Southeast Asia, *Atmos. Environ.*, 78, 20–
2312 34, <https://doi.org/10.1016/j.atmosenv.2012.12.013>, 2013.

2313 Twomey, S.: The influence of pollution on the shortwave albedo of clouds, *J. Atmos. Sci.*, 34, 1149–
2314 1152, [https://doi.org/10.1175/1520-0469\(1977\)034<1149:TlOPOT>2.0.CO;2](https://doi.org/10.1175/1520-0469(1977)034<1149:TlOPOT>2.0.CO;2), 1977.

2315 Uno, I., Wang, Z., Chiba, M., Chun, Y. S., Gong, S. L., Hara, Y., Jung, E., Lee, S., Liu, M., and Mikami,
2316 M.: Dust model intercomparison (DMIP) study over Asia: Overview, *J. Geophys. Res. Atmos.*, 111,
2317 <https://doi.org/10.1029/2005JD006575>, 2006.

2318 Vehkamäki, H., Kulmala, M., Napari, I., Lehtinen, K. E. J., Timmreck, C., Noppel, M., and Laaksonen,
2319 A.: An improved parameterization for sulfuric acid-water nucleation rates for tropospheric and
2320 stratospheric conditions, *J. Geophys. Res. Atmos.*, 107, AAC 3-1-AAC 3-10,
2321 <https://doi.org/10.1029/2002JD002184>, 2002.

2322 Wang, D., Jiang, B., Lin, W., and Gu, F.: Effects of aerosol-radiation feedback and topography during
2323 an air pollution event over the North China Plain during December 2017, *Atmos. Pollut. Res.*, 10,
2324 587–596, <https://doi.org/10.1016/j.apr.2018.10.006>, 2019a.

2325 Wang, H. and Niu, T.: Sensitivity studies of aerosol data assimilation and direct radiative feedbacks in
2326 modeling dust aerosols, *Atmos. Environ.*, 64, 208–218,
2327 <https://doi.org/10.1016/j.atmosenv.2012.09.066>, 2013.

2328 Wang, H., Zhang, X., Gong, S., Chen, Y., Shi, G., and Li, W.: Radiative feedback of dust aerosols on the
2329 East Asian dust storms, *J. Geophys. Res. Atmos.*, 115, <https://doi.org/10.1029/2009JD013430>, 2010.

2330 Wang, H., Shi, G., Zhu, J., Chen, B., Che, H., and Zhao, T.: Case study of longwave contribution to dust
2331 radiative effects over East Asia, *Chinese Sci. Bull.*, 58, 3673–3681, [https://doi.org/10.1007/s11434-](https://doi.org/10.1007/s11434-013-5752-z)
2332 [013-5752-z](https://doi.org/10.1007/s11434-013-5752-z), 2013.

2333 Wang, H., Shi, G. Y., Zhang, X. Y., Gong, S. L., Tan, S. C., Chen, B., Che, H. Z., and Li, T.: Mesoscale
2334 modelling study of the interactions between aerosols and PBL meteorology during a haze episode
2335 in China Jing-Jin-Ji and its near surrounding region--Part 2: Aerosols' radiative feedback effects,
2336 *Atmos. Chem. Phys.*, 15, 3277–3287, <https://doi.org/10.5194/acp-15-3277-2015>, 2015a.

- 2337 Wang, H., Peng, Y., Zhang, X., Liu, H., Zhang, M., Che, H., Cheng, Y., and Zheng, Y.: Contributions to
2338 the explosive growth of PM_{2.5} mass due to aerosol-radiation feedback and decrease in turbulent
2339 diffusion during a red alert heavy haze in Beijing–Tianjin–Hebei, China, *Atmos. Chem. Phys.*, 18,
2340 17717–17733, <https://doi.org/10.5194/acp-18-17717-2018>, 2018a.
- 2341 Wang, J., Wang, S., Jiang, J., Ding, A., Zheng, M., Zhao, B., Wong, D. C., Zhou, W., Zheng, G., Wang,
2342 L., Pleim, J. E., and Hao, J.: Impact of aerosol-meteorology interactions on fine particle pollution
2343 during China's severe haze episode in January 2013, *Environ. Res. Lett.*, 9,
2344 <https://doi.org/10.1088/1748-9326/9/9/094002>, 2014a.
- 2345 Wang, J., Allen, D. J., Pickering, K. E., Li, Z., and He, H.: Impact of aerosol direct effect on East Asian
2346 air quality during the EAST-AIRE campaign, *J. Geophys. Res. Atmos.*, 121, 6534–6554,
2347 <https://doi.org/10.1002/2016JD025108>, 2016.
- 2348 Wang, J., Xing, J., Mathur, R., Pleim, J. E., Wang, S., Hogrefe, C., Gan, C.-M., Wong, D. C., and Hao,
2349 J.: Historical trends in PM_{2.5}-related premature mortality during 1990–2010 across the northern
2350 hemisphere, *Environ. Health Perspect.*, 125, 400–408, <https://doi.org/10.1289/EHP298>, 2017.
- 2351 Wang, K., Yahya, K., Zhang, Y., Hogrefe, C., Pouliot, G., Knote, C., Hodzic, A., San Jose, R., Perez, J.
2352 L., and Jiménez-Guerrero, P.: A multi-model assessment for the 2006 and 2010 simulations under
2353 the Air Quality Model Evaluation International Initiative (AQMEII) Phase 2 over North America:
2354 Part II. Evaluation of column variable predictions using satellite data, *Atmos. Environ.*, 115, 587–
2355 603, <https://doi.org/10.1016/j.atmosenv.2014.07.044>, 2015b.
- 2356 Wang, K., Zhang, Y., Zhang, X., Fan, J., Leung, L. R., Zheng, B., Zhang, Q., and He, K.: Fine-scale
2357 application of WRF-CAM5 during a dust storm episode over East Asia: Sensitivity to grid
2358 resolutions and aerosol activation parameterizations, *Atmos. Environ.*, 176, 1–20,
2359 <https://doi.org/10.1016/j.atmosenv.2017.12.014>, 2018b.
- 2360 Wang, L., Fu, J. S., Wei, W., Wei, Z., Meng, C., Ma, S., and Wang, J.: How aerosol direct effects
2361 influence the source contributions to PM_{2.5} concentrations over Southern Hebei, China in severe
2362 winter haze episodes, *Front. Environ. Sci. Eng.*, 12, 13, <https://doi.org/10.1007/s11783-018-1014-2>, 2018c.
- 2364 Wang, Z., Wang, Z., Li, J., Zheng, H., Yan, P., and Li, J.: Development of a meteorology-chemistry two-
2365 way coupled numerical model (WRF-NAQPMS) and its application in a severe autumn haze
2366 simulation over the Beijing-Tianjin-Hebei area, China. *Clim. Environ. Res.*, 19, 153–163,
2367 <https://doi.org/10.3878/j.issn.1006-9585.2014.13231>, 2014b.
- 2368 Wang, Z., Huang, X., and Ding, A.: Dome effect of black carbon and its key influencing factors: a one-
2369 dimensional modelling study, *Atmos. Chem. Phys.*, 18, 2821–2834, <https://doi.org/10.5194/acp-18-2821-2018>, 2018d.
- 2371 Wang, Z., Huang, X., and Ding, A.: Optimization of vertical grid setting for air quality modelling in
2372 China considering the effect of aerosol-boundary layer interaction, *Atmos. Environ.*, 210, 1–13,
2373 <https://doi.org/10.1016/j.atmosenv.2019.04.042>, 2019b.
- 2374 Wang, Z. F., Li, J., Wang, Z., Yang, W., Tang, X., Ge, B., Yan, P., Zhu, L., Chen, X., and Chen, H.:
2375 Modeling study of regional severe hazes over mid-eastern China in January 2013 and its
2376 implications on pollution prevention and control, *Sci. China Earth Sci.*, 57, 3–13,
2377 <https://doi.org/10.1007/s11430-013-4793-0>, 2014c.
- 2378 Wendisch, M., Keil, A., Müller, D., Wandinger, U., Wendling, P., Stifter, A., Petzold, A., Fiebig, M.,
2379 Wiegner, M., and Freudenthaler, V.: Aerosol-radiation interaction in the cloudless atmosphere
2380 during LACE 98 1. Measured and calculated broadband solar and spectral surface insulations, *J.*
2381 *Geophys. Res. Atmos.*, 107, LAC 6-1-LAC 6-20, <https://doi.org/10.1029/2000JD000226>, 2002.
- 2382 Wexler, A. S., Lurmann, F. W., and Seinfeld, J. H.: Modelling urban and regional aerosols-I. Model
2383 development, *Atmos. Environ.*, 28, 531–546, [https://doi.org/10.1016/1352-2310\(94\)90129-5](https://doi.org/10.1016/1352-2310(94)90129-5), 1994.
- 2384 Whitby, K. T.: The physical characteristics of sulfur aerosols, in: *Sulfur in the Atmosphere*, Elsevier,
2385 135–159, <https://doi.org/10.1016/B978-0-08-022932-4.50018-5>, 1978.
- 2386 Wiedinmyer, C., Akagi, S. K., Yokelson, R. J., Emmons, L. K., Al-Saadi, J. A., Orlando, J. J., and Soja,
2387 A. J.: The Fire INventory from NCAR (FINN): A high resolution global model to estimate the
2388 emissions from open burning, *Geosci. Model Dev.*, 4, 625–641, <https://doi.org/10.5194/gmd-4-625-2011>, 2011.
- 2390 Wilcox, E. M.: Direct and semi-direct radiative forcing of smoke aerosols over clouds, *Atmos. Chem.*
2391 *Phys.*, 12, 139–149, <https://doi.org/10.5194/acp-12-139-2012>, 2012.
- 2392 Wong, D. C., Pleim, J., Mathur, R., Binkowski, F., Otte, T., Gilliam, R., Pouliot, G., Xiu, A., Young, J.
2393 O., and Kang, D.: WRF-CMAQ two-way coupled system with aerosol feedback: software
2394 development and preliminary results, *Geosci. Model Dev.*, 5, 299–312,
2395 <https://doi.org/10.5194/gmd-5-299-2012>, 2012.
- 2396 Wu, J., Bei, N., Hu, B., Liu, S., Zhou, M., Wang, Q., Li, X., Lang, L., Tian, F., and Liu, Z.: Aerosol-
2397 radiation feedback deteriorates the wintertime haze in the North China Plain, *Atmos. Chem. Phys.*,
2398 19, 8703–8719, <https://doi.org/10.5194/acp-19-8703-2019>, 2019a.
- 2399 Wu, J., Bei, N., Hu, B., Liu, S., Zhou, M., Wang, Q., Li, X., Liu, L., Feng, T., Liu, Z., Wang, Y., Cao, J.,
2400 Tie, X., Wang, J., Molina, L. T., and Li, G.: Is water vapor a key player of the wintertime haze in
2401 North China Plain?, *Atmos. Chem. Phys.*, 19, 8721–8739, <https://doi.org/10.5194/acp-19-8721-2019>, 2019b.
- 2403 Wu, L., Su, H., and Jiang, J. H.: Regional simulation of aerosol impacts on precipitation during the East
2404 Asian summer monsoon, *J. Geophys. Res. Atmos.*, 118, 6454–6467,
2405 <https://doi.org/10.1002/jgrd.50527>, 2013.

- 2406 Wu, W. and Zhang, Y.: Effects of particulate matter (PM_{2.5}) and associated acidity on ecosystem
2407 functioning: response of leaf litter breakdown, *Environ. Sci. Pollut. Res.*, 25, 30720–30727,
2408 <https://doi.org/10.1007/s11356-018-2922-1>, 2018.
- 2409 Wu, Y., Han, Y., Voulgarakis, A., Wang, T., Li, M., Wang, Y., Xie, M., Zhuang, B., and Li, S.: An
2410 agricultural biomass burning episode in eastern China: Transport, optical properties, and impacts on
2411 regional air quality, *J. Geophys. Res. Atmos.*, 122, 2304–2324,
2412 <https://doi.org/10.1002/2016JD025319>, 2017.
- 2413 Xie, M., Liao, J., Wang, T., Zhu, K., Zhuang, B., Han, Y., Li, M., and Li, S.: Modeling of the
2414 anthropogenic heat flux and its effect on regional meteorology and air quality over the Yangtze
2415 River Delta region, China, *Atmos. Chem. Phys.*, 16, 6071–6089, [https://doi.org/10.5194/acp-16-](https://doi.org/10.5194/acp-16-6071-2016)
2416 6071-2016, 2016.
- 2417 Xing, J., Mathur, R., Pleim, J., Hogrefe, C., Gan, C., Wong, D. C., Wei, C., and Wang, J.: Air pollution
2418 and climate response to aerosol direct radiative effects: A modeling study of decadal trends across
2419 the northern hemisphere, *J. Geophys. Res. Atmos.*, 120, 12–221,
2420 <https://doi.org/10.1002/2015JD023933>, 2015a.
- 2421 Xing, J., Mathur, R., Pleim, J., Hogrefe, C., Gan, C. M., Wong, D. C., and Wei, C.: Can a coupled
2422 meteorology-chemistry model reproduce the historical trend in aerosol direct radiative effects over
2423 the Northern Hemisphere?, *Atmos. Chem. Phys.*, 15, 9997–10018, [https://doi.org/10.5194/acp-15-](https://doi.org/10.5194/acp-15-9997-2015)
2424 9997-2015, 2015b.
- 2425 Xing, J., Mathur, R., Pleim, J., Hogrefe, C., Gan, C.-M., Wong, D.-C., Wei, C., Gilliam, R., and Pouliot,
2426 G.: Observations and modeling of air quality trends over 1990-2010 across the Northern
2427 Hemisphere: China, the United States and Europe., *Atmos. Chem. Phys.*, 15, 2723–2747,
2428 <https://doi.org/10.5194/acp-15-2723-2015>, 2015c.
- 2429 Xing, J., Wang, J., Mathur, R., Pleim, J., Wang, S., Hogrefe, C., Gan, C.-M., Wong, D. C., and Hao, J.:
2430 Unexpected benefits of reducing aerosol cooling effects, *Environ. Sci. Technol.*, 50, 7527–7534,
2431 <https://doi.org/10.1021/acs.est.6b00767>, 2016.
- 2432 Xing, J., Wang, J., Mathur, R., Wang, S., Sarwar, G., Pleim, J., Hogrefe, C., Zhang, Y., Jiang, J., and
2433 Wong, D. C.: Impacts of aerosol direct effects on tropospheric ozone through changes in
2434 atmospheric dynamics and photolysis rates, *Atmos. Chem. Phys.*, 17, 9869–9883,
2435 <https://doi.org/10.5194/acp-17-9869-2017>, 2017.
- 2436 Yahya, K., Wang, K., Gudoshava, M., Glotfelty, T., and Zhang, Y.: Application of WRF/Chem over
2437 North America under the AQMEII Phase 2: Part I. Comprehensive evaluation of 2006 simulation,
2438 *Atmos. Environ.*, 115, 733–755, <https://doi.org/10.1016/j.atmosenv.2014.08.063>, 2015.
- 2439 Yan, J., Wang, X., Gong, P., Wang, C., and Cong, Z.: Review of brown carbon aerosols: Recent progress
2440 and perspectives, *Sci. Total Environ.*, 634, 1475–1485,
2441 <https://doi.org/10.1016/j.scitotenv.2018.04.083>, 2018.
- 2442 Yang, J., Duan, K., Kang, S., Shi, P., and Ji, Z.: Potential feedback between aerosols and meteorological
2443 conditions in a heavy pollution event over the Tibetan Plateau and Indo-Gangetic Plain, *Clim. Dyn.*,
2444 48, 2901–2917, <https://doi.org/10.1007/s00382-016-3240-2>, 2017.
- 2445 Yang, J., Kang, S., Ji, Z., and Chen, D.: Modeling the origin of anthropogenic black carbon and its
2446 climatic effect over the Tibetan Plateau and surrounding regions, *J. Geophys. Res. Atmos.*, 123,
2447 671–692, <https://doi.org/10.1002/2017JD027282>, 2018.
- 2448 Yang, T. and Liu, Y.: Impact of anthropogenic pollution on “7.21” extreme heavy rainstorm, *J. Meteorol.*
2449 *Sci.*, 37, 742–752, <https://doi.org/10.3969/2016jms.0074>, 2017a.
- 2450 Yang, T. and Liu, Y.: Mechanism analysis of the impacts of aerosol direct effects on a rainstorm, *J. Trop.*
2451 *Meteorol.*, 33, 762–773, <https://doi.org/10.16032/j.issn.1004-4965.2017.05.019>, 2017b.
- 2452 Yang, Y., Tang, J., Sun, J., Wang, L., Wang, X., Zhang, Y., Qu, Q., and Zhao, W.: Synoptic Effect of a
2453 Heavy Haze Episode over North China, *Clim. Environ. Res.*, 20, 555–570,
2454 <https://doi.org/10.3878/j.issn.1006-9585.2015.15018>, 2015.
- 2455 Yang, Y., Fan, J., Leung, L. R., Zhao, C., Li, Z., and Rosenfeld, D.: Mechanisms contributing to
2456 suppressed precipitation in Mt. Hua of central China. Part I: Mountain valley circulation, *J. Atmos.*
2457 *Sci.*, 73, 1351–1366, <https://doi.org/10.1175/JAS-D-15-0233.1>, 2016.
- 2458 Yang, Y., Zhao, C., Dong, X., Fan, G., Zhou, Y., Wang, Y., Zhao, L., Lv, F., and Yan, F.: Toward
2459 understanding the process-level impacts of aerosols on microphysical properties of shallow cumulus
2460 cloud using aircraft observations, *Atmos. Res.*, 221, 27–33,
2461 <https://doi.org/10.1016/j.atmosres.2019.01.027>, 2019.
- 2462 Yao, H., Song, Y., Liu, M., Archer-Nicholls, S., Lowe, D., McFiggans, G., Xu, T., Du, P., Li, J., and Wu,
2463 Y.: Direct radiative effect of carbonaceous aerosols from crop residue burning during the summer
2464 harvest season in East China, *Atmos. Chem. Phys.*, 17, 5205–5219, [https://doi.org/10.5194/acp-17-](https://doi.org/10.5194/acp-17-5205-2017)
2465 5205-2017, 2017.
- 2466 Yasunari, T. J. and Yamazaki, K.: Impacts of Asian dust storm associated with the stratosphere-to-
2467 troposphere transport in the spring of 2001 and 2002 on dust and tritium variations in Mount
2468 Wrangell ice core, Alaska, *Atmos. Environ.*, 43, 2582–2590,
2469 <https://doi.org/10.1016/j.atmosenv.2009.02.025>, 2009.
- 2470 Yiğit, E., Knížová, P. K., Georgieva, K., and Ward, W.: A review of vertical coupling in the Atmosphere–
2471 Ionosphere system: Effects of waves, sudden stratospheric warmings, space weather, and of solar
2472 activity, *J. Atmos. Solar-Terrestrial Phys.*, 141, 1–12, <https://doi.org/10.1016/j.jastp.2016.02.011>,
2473 2016.
- 2474 Yoo, J.-W., Jeon, W., Park, S.-Y., Park, C., Jung, J., Lee, S.-H., and Lee, H. W.: Investigating the regional

2475 difference of aerosol feedback effects over South Korea using the WRF-CMAQ two-way coupled
2476 modeling system, *Atmos. Environ.*, 218, 116968, <https://doi.org/10.1016/j.atmosenv.2019.116968>,
2477 2019.

2478 Yoon, J., Chang, D. Y., Lelieveld, J., Pozzer, A., Kim, J., and Yum, S. S.: Empirical evidence of a positive
2479 climate forcing of aerosols at elevated albedo, *Atmos. Res.*, 229, 269–279,
2480 <https://doi.org/10.1016/j.atmosres.2019.07.001>, 2019.

2481 Yu, F.: Binary H₂SO₄-H₂O homogeneous nucleation based on kinetic quasi-unary nucleation model:
2482 Look-up tables, *J. Geophys. Res. Atmos.*, 111, <https://doi.org/10.1029/2005JD006358>, 2006.

2483 Yu, F. and Luo, G.: Simulation of particle size distribution with a global aerosol model: contribution of
2484 nucleation to aerosol and CCN number concentrations, *Atmos. Chem. Phys.*, 9, 7691–7710,
2485 <https://doi.org/10.5194/acp-9-7691-2009>, 2009.

2486 Yu, H., Kaufman, Y. J., Chin, M., Feingold, G., Remer, L. A., Anderson, T. L., Balkanski, Y., Bellouin,
2487 N., Boucher, O., and Christopher, S.: A review of measurement-based assessments of the aerosol
2488 direct radiative effect and forcing, *Atmos. Chem. Phys.*, 6, 613–666, <https://doi.org/10.5194/acp-6-613-2006>, 2006.

2490 Yuan, T., Chen, S., Huang, J., Wu, D., Lu, H., Zhang, G., Ma, X., Chen, Z., Luo, Y., and Ma, X.:
2491 Influence of dynamic and thermal forcing on the meridional transport of Taklimakan Desert dust in
2492 spring and summer, *J. Clim.*, 32, 749–767, <https://doi.org/10.1175/JCLI-D-18-0361.1>, 2019.

2493 Zaveri, R. A., Easter, R. C., Fast, J. D., and Peters, L. K.: Model for simulating aerosol interactions and
2494 chemistry (MOSAIC), *J. Geophys. Res. Atmos.*, 113, <https://doi.org/10.1029/2007JD008782>, 2008.

2495 Zhan, J., Chang, W., Li, W., Wang, Y., Chen, L., and Yan, J.: Impacts of meteorological conditions,
2496 aerosol radiative feedbacks, and emission reduction scenarios on the coastal haze episodes in
2497 southeastern China in December 2013, *J. Appl. Meteorol. Climatol.*, 56, 1209–1229,
2498 <https://doi.org/10.1175/JAMC-D-16-0229.1>, 2017.

2499 Zhang, B., Wang, Y., and Hao, J.: Simulating aerosol-radiation-cloud feedbacks on meteorology and air
2500 quality over eastern China under severe haze conditions in winter, *Atmos. Chem. Phys.*, 15, 2387–
2501 2404, <https://doi.org/10.5194/acp-15-2387-2015>, 2015a.

2502 Zhang, H., DeNero, S. P., Joe, D. K., Lee, H.-H., Chen, S.-H., Michalakes, J., and Kleeman, M. J.:
2503 Development of a source oriented version of the WRF/Chem model and its application to the
2504 California regional PM₁₀/PM_{2.5} air quality study, *Atmos. Chem. Phys.*, 14, 485–503,
2505 <https://doi.org/10.5194/acp-14-485-2014>, 2014a.

2506 Zhang, H., Cheng, S., Li, J., Yao, S., and Wang, X.: Investigating the aerosol mass and chemical
2507 components characteristics and feedback effects on the meteorological factors in the Beijing-
2508 Tianjin-Hebei region, China, *Environ. Pollut.*, 244, 495–502,
2509 <https://doi.org/10.1016/j.envpol.2018.10.087>, 2019.

2510 Zhang, L., Wang, T., Lv, M., and Zhang, Q.: On the severe haze in Beijing during January 2013:
2511 Unraveling the effects of meteorological anomalies with WRF-Chem, *Atmos. Environ.*, 104, 11–
2512 21, <https://doi.org/10.1016/j.atmosenv.2015.01.001>, 2015b.

2513 Zhang, L., Gong, S., Zhao, T., Zhou, C., Wang, Y., Li, J., Ji, D., He, J., Liu, H., and Gui, K.: Development
2514 of WRF/CUACE v1.0 model and its preliminary application in simulating air quality in China,
2515 *Geosci. Model Dev.*, 14, 703–718, <https://doi.org/10.5194/gmd-14-703-2021>, 2021.

2516 Zhang, X., Zhang, Q., Hong, C., Zheng, Y., Geng, G., Tong, D., Zhang, Y., and Zhang, X.: Enhancement
2517 of PM_{2.5} Concentrations by Aerosol-Meteorology Interactions Over China, *J. Geophys. Res. Atmos.*,
2518 123, 1179–1194, <https://doi.org/10.1002/2017JD027524>, 2018.

2519 Zhang, X. Y., Gong, S. L., Shen, Z. X., Mei, F. M., Xi, X. X., Liu, L. C., Zhou, Z. J., Wang, D., Wang,
2520 Y. Q., and Cheng, Y.: Characterization of soil dust aerosol in China and its transport and distribution
2521 during 2001 ACE-Asia: 1. Network observations, *J. Geophys. Res. Atmos.*, 108,
2522 <https://doi.org/10.1029/2002JD002632>, 2003a.

2523 Zhang, X. Y., Gong, S. L., Zhao, T. L., Arimoto, R., Wang, Y. Q., and Zhou, Z. J.: Sources of Asian dust
2524 and role of climate change versus desertification in Asian dust emission, *Geophys. Res. Lett.*, 30,
2525 <https://doi.org/10.1029/2003GL018206>, 2003b.

2526 Zhang, Y.: Online-coupled meteorology and chemistry models: history, current status, and outlook,
2527 *Atmos. Chem. Phys.*, 8, 2895–2932, <https://doi.org/10.5194/acp-8-2895-2008>, 2008.

2528 Zhang, Y., Pun, B., Vijayaraghavan, K., Wu, S., Seigneur, C., Pandis, S. N., Jacobson, M. Z., Nenes, A.,
2529 and Seinfeld, J. H.: Development and application of the model of aerosol dynamics, reaction,
2530 ionization, and dissolution (MADRID), *J. Geophys. Res. Atmos.*, 109,
2531 <https://doi.org/10.1029/2003JD003501>, 2004.

2532 Zhang, Y., Hu, X. M., Howell, G. W., Sills, E., Fast, J. D., Gustafson Jr, W. I., Zaveri, R. A., Grell, G.
2533 A., Peckham, S. E., and McKeen, S. A.: Modeling atmospheric aerosols in WRF/CHEM, in:
2534 WRF/MM5 Users's Workshop, 2005.

2535 Zhang, Y., Pan, Y., Wang, K., Fast, J. D., and Grell, G. A.: WRF/Chem-MADRID: Incorporation of an
2536 aerosol module into WRF/Chem and its initial application to the TexAQS2000 episode, *J. Geophys.
2537 Res. Atmos.*, 115, <https://doi.org/10.1029/2009JD013443>, 2010.

2538 Zhang, Y., Karamchandani, P., Glotfelty, T., Streets, D. G., Grell, G., Nenes, A., Yu, F., and Bennartz,
2539 R.: Development and initial application of the global-through-urban weather research and
2540 forecasting model with chemistry (GU-WRF/Chem), *J. Geophys. Res. Atmos.*, 117,
2541 <https://doi.org/10.1029/2012JD017966>, 2012.

2542 Zhang, Y., Zhang, X., Cai, C., Wang, K., and Wang, L.: Studying Aerosol-Cloud-Climate Interactions
2543 over East Asia Using WRF/Chem, in: *Air Pollution Modeling and its Application XXIII*, Springer,

2544 61–66, https://doi.org/10.1007/978-3-319-04379-1_10, 2014b.

2545 Zhang, Y., Chen, Y., Fan, J., and Leung, L.-Y. R.: Application of an online-coupled regional climate
2546 model, WRF-CAM5, over East Asia for examination of ice nucleation schemes: part II. Sensitivity
2547 to heterogeneous ice nucleation parameterizations and dust emissions, 3, 753–774,
2548 <https://doi.org/10.3390/cli3030753>, 2015c.

2549 Zhang, Y., Zhang, X., Wang, K., He, J., Leung, L. R., Fan, J., and Nenes, A.: Incorporating an advanced
2550 aerosol activation parameterization into WRF-CAM5: Model evaluation and parameterization
2551 intercomparison, *J. Geophys. Res. Atmos.*, 120, 6952–6979, <https://doi.org/10.1002/2014JD023051>,
2552 2015d.

2553 Zhang, Y., Zhang, X., Wang, L., Zhang, Q., Duan, F., and He, K.: Application of WRF/Chem over East
2554 Asia: Part I. Model evaluation and intercomparison with MM5/CMAQ, *Atmos. Environ.*, 124, 285–
2555 300, <https://doi.org/10.1016/j.atmosenv.2015.07.022>, 2016a.

2556 Zhang, Y., Zhang, X., Wang, K., Zhang, Q., Duan, F., and He, K.: Application of WRF/Chem over East
2557 Asia: Part II. Model improvement and sensitivity simulations, *Atmos. Environ.*, 124, 301–320,
2558 <https://doi.org/10.1016/j.atmosenv.2015.07.023>, 2016b.

2559 Zhang, Y., Fan Shuxian, Li Hao, and Kang Boshi: Effects of aerosol radiative feedback during a severe
2560 smog process over eastern China, *Acta Meteorol.*, 74, <https://doi.org/10.11676/qxxb2016.028>,
2561 2016c.

2562 Zhang, Y., He, J., Zhu, S., and Gantt, B.: Sensitivity of simulated chemical concentrations and aerosol-
2563 meteorology interactions to aerosol treatments and biogenic organic emissions in WRF/Chem, *J.*
2564 *Geophys. Res. Atmos.*, 121, 6014–6048, <https://doi.org/10.1002/2016JD024882>, 2016d.

2565 Zhang, Y., Wang, K., and He, J.: Multi-year application of WRF-CAM5 over East Asia-Part II:
2566 Interannual variability, trend analysis, and aerosol indirect effects, *Atmos. Environ.*, 165, 222–239,
2567 <https://doi.org/10.1016/j.atmosenv.2017.06.029>, 2017.

2568 Zhao, B., Liou, K., Gu, Y., Li, Q., Jiang, J. H., Su, H., He, C., Tseng, H.-L. R., Wang, S., and Liu, R.:
2569 Enhanced PM_{2.5} pollution in China due to aerosol-cloud interactions, *Sci. Rep.*, 7, 1–11,
2570 <https://doi.org/10.1038/s41598-017-04096-8>, 2017.

2571 Zhao, B., Wang, Y., Gu, Y., Liou, K.-N., Jiang, J. H., Fan, J., Liu, X., Huang, L., and Yung, Y. L.: Ice
2572 nucleation by aerosols from anthropogenic pollution, *Nat. Geosci.*, 12, 602–607,
2573 <https://doi.org/10.1038/s41561-019-0389-4>, 2019.

2574 Zhong, M., Saikawa, E., Liu, Y., Naik, V., Horowitz, L. W., Takigawa, M., Zhao, Y., Lin, N.-H., and
2575 Stone, E. A.: Air quality modeling with WRF-Chem v3.5 in East Asia: sensitivity to emissions and
2576 evaluation of simulated air quality, *Geosci. Model Dev.*, 9, 1201–1218,
2577 <https://doi.org/10.5194/gmd-9-1201-2016>, 2016.

2578 Zhong, M., Chen, F., and Saikawa, E.: Sensitivity of projected PM_{2.5}- and O₃-related health impacts to
2579 model inputs: A case study in mainland China, *Environ. Int.*, 123, 256–264,
2580 <https://doi.org/10.1016/j.envint.2018.12.002>, 2019.

2581 Zhong, S., Qian, Y., Zhao, C., Leung, R., and Yang, X.: A case study of urbanization impact on summer
2582 precipitation in the Greater Beijing Metropolitan Area: Urban heat island versus aerosol effects, *J.*
2583 *Geophys. Res. Atmos.*, 120, 10–903, <https://doi.org/10.1002/2015JD023753>, 2015.

2584 Zhong, S., Qian, Y., Zhao, C., Leung, R., Wang, H., Yang, B., Fan, J., Yan, H., Yang, X.-Q., and Liu,
2585 D.: Urbanization-induced urban heat island and aerosol effects on climate extremes in the Yangtze
2586 River Delta region of China., *Atmos. Chem. Phys.*, 17, 5439–5457, <https://doi.org/10.5194/acp-17-5439-2017>, 2017.

2588 Zhou, C., Gong, S. L., Zhang, X. Y., Wang, Y. Q., Niu, T., Liu, H. L., Zhao, T. L., Yang, Y. Q., and Hou,
2589 Q.: Development and evaluation of an operational SDS forecasting system for East Asia:
2590 CUACE/Dust, *Atmos. Chem. Phys.*, 8, 787–798, <https://doi.org/10.5194/acp-8-787-2008>, 2008.

2591 Zhou, C., Gong, S., Zhang, X., Liu, H., Xue, M., Cao, G., An, X., Che, H., Zhang, Y., and Niu, T.:
2592 Towards the improvements of simulating the chemical and optical properties of Chinese aerosols
2593 using an online coupled model-CUACE/Aero, *Tellus B Chem. Phys. Meteorol.*, 64, 18965,
2594 <https://doi.org/10.3402/tellusb.v64i0.18965>, 2012.

2595 Zhou, C., Zhang, X., Gong, S., Wang, Y., and Xue, M.: Improving aerosol interaction with clouds and
2596 precipitation in a regional chemical weather modeling system, 16, 145–160,
2597 <https://doi.org/10.5194/acp-16-145-2016>, 2016.

2598 Zhou, D., Ding, K., Huang, X., Liu, L., Liu, Q., Xu, Z., Jiang, F., Fu, C., and Ding, A.: Transport, mixing
2599 and feedback of dust, biomass burning and anthropogenic pollutants in eastern Asia: a case study,
2600 18, 16345–16361, <https://doi.org/10.5194/acp-18-16345-2018>, 2018.

2601 Zhou, M., Zhang, L., Chen, D., Gu, Y., Fu, T.-M., Gao, M., Zhao, Y., Lu, X., and Zhao, B.: The impact
2602 of aerosol-radiation interactions on the effectiveness of emission control measures, *Environ. Res.*
2603 *Lett.*, 14, 24002, <https://doi.org/10.1088/1748-9326/aaf27d>, 2019.

2604 Zhou, Y., Gong, S., Zhou, C., Zhang, L., He, J., Wang, Y., Ji, D., Feng, J., Mo, J., and Ke, H.: A new
2605 parameterization of uptake coefficients for heterogeneous reactions on multi-component
2606 atmospheric aerosols, *Sci. Total Environ.*, 781, 146372,
2607 <https://doi.org/10.1016/j.scitotenv.2021.146372>, 2021.

2608 Zhuang, B., Jiang, F., Wang, T., Li, S., and Zhu, B.: Investigation on the direct radiative effect of fossil
2609 fuel black-carbon aerosol over China, *Theor. Appl. Climatol.*, 104, 301–312,
2610 <https://doi.org/10.1007/s00704-010-0341-4>, 2011.

2611

2612

